December 2019

The Curious Case of NAD-Cleaving Nudix Hydrolases

Atreyei Ray
University of Wisconsin-Milwaukee

THE CURIOUS CASE OF NAD-CLEAVING NUDIX HYDROLASES

by

Atreyei Ray

A Dissertation Submitted in

Partial Fulfillment of the

Requirements for the Degree of

Doctor of Philosophy

in Chemistry

at

The University of Wisconsin-Milwaukee

December 2019

ABSTRACT

THE CURIOUS CASE OF NAD-CLEAVING NUDIX HYDROLASES

by

Atreyei Ray

The University of Wisconsin- Milwaukee, 2019
Under the Supervision of Professor David N. Frick

Nudix proteins are members of a large family of homologous enzymes that hydrolyze nucleoside diphosphates linked to other compounds (x). These enzymes have catalytic activity on a wide range of substrates such as dNTPs (both canonical and their oxidized forms), nucleotide sugars, alcohols, dinucleoside polyphosphates, dinucleotide cofactors, and nucleoside diphosphates linked to RNA. The bacterial genome encodes around 13, while the human genome encodes for 22 such nudix proteins.

The *E. coli* genome encodes for a mutT mutator gene, the progenitor of the family expressing the MutT pyrophosphohydrolase (NudA) protein (Treffers et al., 1954; Bhatnagar et al., 1988). The enzyme was found to hydrolyze both canonical and mutagenic nucleoside triphosphates, most commonly the toxic form of dGTP, 8-oxo-dGTP, preventing its misincorporation during DNA replication (Maki et al., 1992). Nudt1 is its functional homologue in humans and plays a vital role in removing mutagenic dNTPs to prevent A:T to C:G transversion, by hydrolyzing the 8-oxo dGTP to 8-oxo dGMP (Nakabeppu, 2001). The *E. coli* NudC and its functional homolog in humans, Nudt12 are members of the NADH diphosphatases of the Nudix hydrolase superfamily, cleaving the pyrophosphate bond in their nucleotide substrates, such as such as NADH, NADPH, $NADP^+$, ADP-ribose and AppA to yield two nucleoside monophosphates. Isomeric forms of NADH were discovered as a substrate for the enzyme,

renalase (Beaupre et al., 2015). For the first time, experiments in this thesis tests the 'housecleaning' activity of NudC and Nudt12 on these toxic isomers of their nascent substrate.

Since the early discovery of the Nudix hydrolase class of proteins, several members have been reported to have mRNA decapping activity. The *E. coli* RppH (NudH) nudix enzyme removes pyrophosphate from the 5'-end of RNA while the yeast Dcp2 (Nudt20) nudix protein was the first eukaryotic mRNA decapping enzyme discovered to remove m^7GDP from canonically capped mRNA (Wang et al., 2002). Nudt3 has also been demonstrated as an mRNA decapping enzyme (McLennan et al., 2006; Song et al., 2013; Kiledjian et al., 2016). Nudt16 has been reported to have 5'-end U8 snoRNA decapping activity (Grzela et al., 2018). With the recent discovery of the cofactor nicotinamide adenine dinucleotide (NAD^+) as a transcriptional modification of prokaryotic mRNA (Chen et al., 2009), it has been suggested that NudC is involved in RNA decapping, eventually triggering its decay (Cahová et al., 2014). Its functional homolog in mouse, Nudt12 has also been shown to decap both canonical and ncinRNA (non-canonical initiating nucleotide) *in vitro* (Grudzien-Nogalska et al., 2017). Evidence for direct interaction between these decapping Nudix hydrolases and their oligonucleotide substrates is yet to be shown. For the first time, we report binding between DNA/RNA and Nudix decapping proteins, and serendipitously discover that the human Nudt12 protein exclusively binds RNA and not DNA, preferring to bind *in vitro* transcribed NAD^+-capped RNA.

Although the decapping activity of NudC (Cahová et al., 2014) and Nudt12 (Grudzien-Nogalska et al., 2019) on NAD^+-capped RNA has previously been shown using TLC, we used a more analytical approach to confirm these results using LC/MS. The preference of these proteins to cleave NADH-capped RNA over NADH was also observed during these experiments.

It has been hypothesized that the NAD^+ on the terminal end of both prokaryotic and eukaryotic RNA stabilizes the nucleic acids as the ^{7}mG cap does for eukaryotic mRNAs. NAD^+/NADH are widely studied, important coenzymes, involved in many critical biological redox reactions. Oxidized NAD, NAD^+ accepts two electrons while its reduced form, NADH donates two electrons to a variety of substrates. Kinetics of NAD^+/NADH redox reactions can easily be measured because NADH absorbs light at 340 nm but NAD^+ does not. In this thesis, we explored the hypothesis that ncinRNA might play a more obvious chemical role in the cell, by participating in cellular redox reactions. To test if ncinRNA can be functional in redox reactions, T7 RNA polymerase was used to synthesize RNA *in vitro,* initiating with the ncin: NAD^+, NADH, $NADP^+$ and NADPH. After analyzing the nature of the RNA using agarose gel electrophoresis, gel extraction and LC/MS, we compared the ability of the RNAs to reduce pyruvate and oxidize lactate in reactions catalyzed by the *E. coli*, rabbit muscle and bovine heart L-lactate dehydrogenase (LDH). LDH is a well-characterized redox enzyme, with strict substrate specificity, discriminating between NADH and the very similar NADPH. As suspected, LDH did not oxidize either NADPH or NADPH-capped RNA. However, LDH oxidized both NADH and NADH-capped RNA and reduced NAD^+ and NAD^+-capped RNA. This is the first study to show a clear biochemical role for ncinRNA, suggesting that ncinRNAs may be participants in cellular chemical reactions. ncinRNAs might therefore form a new and interesting class of key ribonucleoproteins or even ribozymes capable of catalyzing redox reactions.

This thesis aims to the address the elusive physiological role of NADH-cleaving Nudix hydrolases. For the first time, we report a distinct biochemical purpose for the existence of ncinRNAs *in vivo* involved in redox reactions.

Dedicated to my father, Arunachal Ray

TABLE OF CONTENTS

LIST OF FIGURES

LIST OF TABLES

LIST OF ABBREVIATIONS

2DHNAD	2- dihydroNAD
6DHNAD	6- dihydroNAD
ADP	Adenosine Diphosphate
ADPr	ADP-ribose
ADPRC	ADP-ribosyl cyclase
AMP	Adenosine Monophosphate
AppA	Adenosine 5'-diphospho-5'-adenosine
ApppA	Adenosine 5'-triphospho-5'-adenosine
AppppA	Adenosine 5'-tetraphospho-5'-adenosine
ARCA	Anti-Reverse Cap Analog
ATP	Adenosine Triphosphate
AUF	AU-rich element RNA-binding protein
BSA	Bovine Serum Albumin
cADPR	cyclic ADP-ribose
CBP	Cap Binding Protein
cDNA	Complementary DNA
CIAP	Calf Intestinal Alkaline Phosphatase

CIAP	Calf Intestinal Alkaline Phosphatase
CoA	Coenzyme A
CTD	C-Terminal Domain
CTP	Cytidine Triphosphate
CuAAC	Copper-catalyzed azide alkyne cycloaddition
Dcp	Decapping enzyme
dCTP	Deoxycytidine Triphosphate
DEAE	Diethylaminoethyl
DLD	Lipoamide Dehydrogenase
DNA	Deoxyribonucleic Acid
DTT	Dithiothreitol
dTTP	Deoxythymidine Triphosphate
dUTP	Deoxyuridine Triphosphate
EDTA	Ethylenediaminetetraacetic acid
EGFP	Enhanced Green Fluorescent Protein
EMSA	Electrophoretic Mobility Shift Assay
FAD	Flavin Adenine Dinucleotide
FP	Fluorescence Polarization

FRET	Förster Energy Resonance Transfer
FR	Fluorescence Ratiometric
GAPDH	Glyceraldehydr-3-phosphate Dehydrogenase
GDP	Guanosine Diphosphate
GDPMH	GDP-mannose mannosyl hydrolase
GF	Gel Filtration
GMP	Guanosine Monophosphate
GTP	Guanosine Triphosphate
HIF	Hypoxia Inducible Factor
HPLC	High Pressure Liquid Chromatography
IC_{50}	Half maximal inhibitory concentration
IDH	Isocitrate Dehydrogenase
IMAC	Immobilized Metal Affinity Chromatography
IPTG	Isopropyl-β-D-thiogalactoside
ITP	Inosine Triphosphate
k_{cat}	Turnover number
k_{cat}/K_m	Catalytic efficiency

K_d	Dissociation constant
K_i	Inhibition constant
K_m	Michaelis constant
LC/MS	Liquid Chromatography Mass Spectrometry
LDH	Lactate Dehydrogenase
lncRNA	Long non-coding RNA
m^7G	7-methylguansine triphosphate
MDH	Malate Dehydrogenase
ME	Malic enzyme
MG	Malachite Green
mRNA	Messenger RNA
NAD	Nicotinamide Adenine Dinucleotide
NAD^+	Nicotinamide Adenine Dinucleotide (oxidized form)
NADH	Nicotinamide Adenine Dinucleotide (reduced form)
NADP	Nicotinamide Adenine Dinucleotide Phosphate
$NADP^+$	Nicotinamide Adenine Dinucleotide Phosphate (oxidized form)
NADPH	Nicotinamide Adenine Dinucleotide Phosphate (reduced form)
Nam	Nicotinamide

nCBC	nuclear cap binding complex
NCD	Nicotinamide Cytosine Dinucleotide
NCIN	Non Canonical Initiating Nucleotide
ncinRNA	Non canonical initiating nucleotide capped RNA
NGD	Nicotinamide Guanine Dinucleotide
NGS	Next-Generation Sequencing
NiNTA	Nickel Nitrilotriacetic Acid
NMN	Nicotinamide Mono Nucleotide (oxidized form)
NMNH	Nicotinamide Mono Nucleotide (reduced form)
NPY	NADH PYrophosphatase
NS3h	Non-structural protein 3 Helicase
NTA	Nitrilotriacetic acid
NTD	N-Terminal Domain
NUD	Nicotinamide Uracil Dinucleotide
NUDIX	Nucleoside Diphosphates linked to another moiety X
OD	Optical Density
PAGE	Polyacrylamide Gel Electrophoresis
PAR	ADP-ribose polymer

PARP	Poly (ADP-ribose) polymerase
PCR	Polymerase Chain Reaction
PGK	Phosphoglycerate kinase
PIFE	Protein Induced Fluorescence Enhancement
PTS	Peroxisomal Targeting Signal
RBP	RNA-binding protein
Ren	Renalase
RNA	Ribonucleic Acid
SDS	Sodium Dodecyl Sulfate
Sir	Silent Information Regulator
SMX	Sulfamethoxazole
snRNA	Small nuclear RNA
TMP	Trimethoprim
UV	Ultraviolet
XTP	Xanthosine Triphosphate

ACKNOWLEDGEMENTS

First and foremost, I would like to thank my supervisor, Dr. David N. Frick, without whom this thesis would not have been possible. His guidance and persistent help throughout my research program have been invaluable and he has taught me how to be a rigorous and critical scientist.

A special thank you to the rest of my committee as well. Each member of my committee has helped me in some way towards my research program and I am very grateful for their continued support. In alphabetical order: Dr. Madhusudan Dey, Dr. Shama Mirza, Dr. Xiaohua Peng and Dr. Nicholas Silvaggi. A special mention to Dr. Graham Moran as well for always pushing me to go that extra mile.

The members of the Frick lab, thank you, for always keeping it fun. I would also like to thank my parents for their continued love and support, both personally and professionally, from all the way across the world. My husband, Ayusman thank you for always being by my side, encouraging and believing in me and in our dreams, even more on the bad days.

Chapter 1 Introduction

The Nudix (nucleoside diphosphates linked to another moiety x) proteins are a superfamily of pyrophosphohydrolases characterized by the conserved amino acid sequence commonly referred to as the NUDIX box $GX_5EX_7REVXEEXGU$, where X is any amino acid and U is a hydrophobic residue. Since its discovery, the Nudix superfamily has been divided into classes based on their substrate specificity (Srouji *et al.*, 2017) having activity over a range of substrates such as deoxynucleotides, nucleotide sugars, dinucleoside polyphosphates and dinucleotide coenzymes.

The *E. coli* genome encodes for a *mut*T mutator gene, the progenitor of the Nudix family expressing the MutT pyrophosphohydrolase (or NudA) protein (Treffers et al., 1954; Bhatnagar et al., 1988). This enzyme can catalyze the hydrolysis of both canonical and mutagenic nucleoside triphosphates, most commonly the toxic form of dGTP: 8-oxo-dGTP, preventing its misincorporation during DNA replication (Maki et al., 1992). Soon after, the *E. coli* genome was discovered to encode for NudC (Frick & Bessman, 1995), its functional homolog in yeast NPY1 (AbdelRaheim et al., 2001) and Nudt12 in humans (Abdelraheim et al., 2003). These proteins were classified as members of one such subclass of the Nudix family, that cleave dinucleotides, such as NADH, NADPH, $NADP^+$, ADP-ribose and AppA to yield two nucleoside monophosphate. This subclass of Nudix proteins is found to have a marked preference for the reduced form of NAD^+, NADH. It should be noted that for the regeneration of NADH, the cell spends a couple of ATP molecules; first an AMP moiety is transferred from ATP to nicotinate ribonucleotide to form desamido-NAD^+ and then in the reduction of NAD^+ to NADH. Why the genome would express a

protein that hydrolyzes not only an important cofactor in cellular metabolism but also an energy rich molecule has been a concern.

Initially, it had been hypothesized that NudC may be a 'housecleaning enzyme', cleansing the cell of potentially deleterious metabolites (Bessman et al., 1996). With Beaupre BA et al.'s unique discovery in 2015, of the role that the human enzyme renalase may play *in vivo*, a similar hypothesis for the 'housecleaning activity' of NADH-cleaving Nudix hydrolases on toxic isomeric forms of β-NAD(P)H molecules was tested. Experiments set up to support this hypothesis will be discussed in Chapter 5.

Several techniques can be used to look at interactions between fluorescent molecules. Fluorescence Ratiometric assays (Lakowicz, 2010) are based one such method, involving changes in the spectrum of a substrate upon enzyme action. FR techniques may be used to be study Nudix cleavage of NADH, because the spectra of NADH and NMNH differ. This new assay will be discussed in Chapter 6.

The human genome encodes for 22 nudix proteins. Nudt20, more commonly referred to as Dcp2, was the first human mRNA decapping enzyme to be discovered (Wang et al., 2002). It removes the m^7G cap from the 5'-end of eukaryotic mRNA, orthologous to the yeast Dcp2. The diphosphoinositol polyphosphate phosphohydrolase Nudt3 has also been demonstrated as an mRNA decapping enzyme (McLennan et al., 2006; Song et al., 2013; Kiledjian et al., 2016). Another human nudix enzyme, Nudt16 has been reported to have 5'-end U8 snoRNA decapping activity (Grzela et al., 2018). Both Nudt16 and Nudt20 hydrolyzes the α-β-phosphate bond of the mRNA cap, whereas Nudt3 can hydrolyze either α-β- or β-γ-phosphates with similar activity (Grudzien-Nogalska et al., 2017). The cofactor nicotinamide adenine dinucleotide (NAD^+) was recently discovered as a transcriptional modification of prokaryotic mRNA (Chen et al., 2009) and

eukaryotic mRNA (Julius et al., 2018). It has since then been suggested that NudC is involved in prokaryotic RNA decapping, eventually triggering its decay (Cahová et al., 2014). Its functional homolog in mouse, Nudt12 has also been shown to decap both canonical capped mRNA, between the β- and γ- phosphate moieties and NAD^+-capped RNA *in vitro* (Grudzien-Nogalska et al., 2019). It could be reasoned that for the human Nudt3, Nudt12, Nudt16 and Nudt20 (Dcp2) and the bacterial NudC Nudix hydrolases to be active RNA decapping enzymes, there has to be direct interaction between these RNA decapping Nudix proteins and their oligonucleotide substrates. This hypothesis is tested in Chapter 7.

To further support the results observed in Chapter 7, it has been reported that Nudt20 (Dcp2) in budding yeast has an additional well conserved RNA binding channel that promotes decapping by the Dcp1/Dcp2 complex. The interactions between the protein and its ^{7}mG-capped RNA substrate have been shown using gel shift assays (Deshmukh et al., 2008). Although human Nudt3 and Nudt16 are functional RNA decapping enzymes, they do not have any domain additional to the Nudix catalytic site. *E. coli* RNA decapping enzyme, NudC has been shown to have a positively charged area adjacent to the NAD^+ binding domain, suggesting its role in nucleic acid interaction (Höfer et al., 2016). Its functional homolog in humans, Nudt12 also has an additional Ankyrin repeat domain, essential for NAD^+-capped RNA decapping activity (Grudzien-Nogalska et al., 2019). Additionally, both NudC and Nudt12 have Zinc-finger domains, suggesting yet another possible binding site for nucleic acids.

Another technique to look at interactions between fluorescent molecules is single molecule protein induced fluorescence enhancement (smPIFE/PIFE), which only needs a single fluorescent tag attached to nucleic acids to which an unlabeled protein is bound (Hwang et al., 2014). The local assay environment such as the interacting protein reduces the rate at which the fluorophore

isomerizes from the photo-active trans state to the photo-inactive cis state, resulting in an increase of quantum yield. This technique is well used to study the energetics of interactions between fluorescent tags and interacting protein molecules in Chapter 8.

Liquid chromatography–mass spectrometry (LC/MS) is an analytical technique, combining the physical separation of liquid chromatography with the mass analysis of mass spectrometry. Non-canonical caps on the terminal end of RNA molecules from *E. coli* and *S. venezuelae* were identified using LC/MS (Liu et al., 2009). The catalytic activity of proteins on their substrates may be studied using this technique as well. The decapping activity of NudC (Cahová H et al., 2014) and Nudt12 (Grudzien-Nogalska et al., 2017) on ncinRNA has been demonstrated using radiolabeling. It may be argued that more quantitative results may be achieved using a more analytical approach such as LC/MS, as discussed in Chapter 7.

The role of the cofactor NAD^+ on the terminal end of both prokaryotic and eukaryotic mRNA is yet to be explained. It has been suggested that this transcriptional modification might stabilize mRNA similar to the 7mG cap on the 5'-end of eukaryotic mRNA molecules. NAD existing in both the oxidized form, NAD^+ and its reduced form, NADH are cofactors that are essential to metabolism. Chapter 7 is the first study ever to demonstrate that the NAD^+/NADH on the terminal end of RNA may play an important role in cellular redox reactions. We tested this hypothesis using mammalian heart and muscle L-lactate dehydrogenase, a vital enzyme in anaerobic respiration. The results from this experiment can be further supported by the fact that several NAD^+/NADH using metabolic enzymes have been previously reported to be mRNA binding proteins as discussed. Chapter 9 is the first ever study to show a clear biochemical role of ncinRNAs participating in redox reactions. It may therefore be suggested that NAD^+-capped RNAs

might form a new class of key ribonucleoproteins or even ribozymes capable of catalyzing redox reactions, *in vivo*.

This thesis addresses the role that NADH-cleaving nudix protein may play in the cellular environment. For the first time, the housecleaning activity of this subclass of nudix enzymes are studied. With the discovery of ncinRNAs, its physiological role has never quite been understood. For the first time, this thesis shows a clear biochemical activity of this non-canonical transcriptional modification.

Chapter 2 Literature review

2.1 Bacterial Nudix hydrolases

Members of this super family of proteins hydrolyze a wide variety of unrelated substrates all having a common nucleoside diphosphate linked to some other moiety X, hence their name Nudix. The *Escherichia coli* genome encodes for 13 such Nudix hydrolase genes. Several of these enzymes initially discovered in *E. coli* have since then been identified in other prokaryotes, archaea and eukaryotes. Of the 13 *E. coli* Nudix hydrolases, most of them have the well conserved Nudix motif with the exception of NudK which has a conservative replacement of lysine for arginine and NudD (orf1.9) which has a slight reshuffle of amino acids as well.

2.1.1 NudA (MutT)

The *E. coli* genome encodes for a *mut*T mutator gene, expressing the MutT pyrophosphohydrolase (or NudA) protein. Initially, MutT was thought to be responsible for only a single, unidirectional AT → CG transversion unlike other defective mutator genes causing a variety of mutations in DNA such as transitions, frameshifts or transversions. However, with further studies, this enzyme was found to also catalyze the hydrolysis of canonical and mutagenic nucleoside triphosphates, most commonly the toxic form of dGTP: 8-oxo-dGTP. It does so by substituting at the seldom attacked β- phosphate, to yield nucleoside monophosphate and inorganic pyrophosphate. 8-oxo-dGTP is the product of oxidative damage to guanine containing nucleotides, which often mispairs with template adenine during DNA replication. NudA (MutT) was hence believed to be "sanitizing" (Bessman et al., 1998) the nucleotide pool at the site of DNA synthesis. Typical to members of this family, two divalent metal ions are essential for its catalytic activity, one coordinated to the β- and γ- phosphoryl groups of the substrate and the second coordinated to

the protein. The tertiary structure of NudA (MutT) is globular and the specific binding sites for divalent metal ions and nucleotides have since then been identified via NMR relaxation method (Abeygunawardana et al., 1995).

2.1.2 NudB (Orf17)

The *E. coli* genome encodes for orf17 encoding the highly conserved Nudix motif characteristic of members of the MutT family of proteins. The gene expresses the NudB protein, a nucleoside triphosphate pyrophosphohydrolase, with a marked preference for deoxyadenosine triphosphate (dATP) over other deoxynucleoside triphosphates. NudB catalyzes the hydrolysis of dATP via a nucleophilic attack at the β- phosphate to produce deoxyadenosine monophosphate (dAMP) and inorganic pyrophosphate (O'Handley et al., 1995). Similar to the other proteins in this family, NudB also has an alkaline pH optimum and a requirement for divalent cations (Bessman et al., 1996). Despite the sequence similarity, NudB does not share the same antimutator properties as NudA (MutT). Almost a decade after the enzyme's discovery, it was detected that the deletion of the *nud*B gene led to a lag in bacterial growth and increased sensitivity to drugs commonly used for bacterial infection, namely sulfamethoxazole (SMX) and trimethoprim (TMP) in both *E. coli* and *Salmonella enterica* (Deng et al., 2017). This is because the deletion of *nud*B causes dihydroneopterin triphosphate to flux more into the tetrahydromonapterin biosynthesis pathway, leading to an excess production of tetrahydromonapterin, which then leads to an increased sensitivity to the drugs, both SMX and TMP.

2.1.3 NudC (Orf257)

Several proteins cleaving NAD into NMN and AMP have been reported in a large variety of prokaryotes and eukaryotes, following the purification of NAD pyrophosphatases from potato extracts (Kornberg et al., 1950). One such protein is expressed from the *E. coli* open reading frame

orf257, homologous to the active site of the MutT enzyme (Frick & Bessman, 1995). Unlike the other members of the MutT family of proteins, NudC does not hydrolyze nucleoside triphosphates. Interestingly, this enzyme is selectively active only on ß-isomers of dinucleotides and not the α-isomers of NAD. NudC is can hydrolyze a wide array of substrates ranging from NAD^+, NADH, $NADP^+$, NADPH, FAD, ADP-ribose, to a family of bis(5'-nucleosidyl) polyphosphates such as diadenosine tetraphosphate (AppppA). Typical to this family of proteins, NudC enzymatic catalysis was observed to be the most active at alkaline pH conditions, peaking at pH 8.5, at 37 °C in the presence of divalent metal ions, with most activity in the presence of Mn^{2+} or Mg^{2+}, lower activity in the presence of Zn^{2+}, Co^{2+} or Fe^{2+} to no activity detected in the presence of Cu^{2+} or Ca^{2+}. Initially, it was thought that the remarkable preference for the reduced form of NAD^+, NADH may be related to its physiological function. It has been hypothesized that NudC acts as a 'housecleaning enzyme', which may regulate intracellular NADH/NAD^+ ratio (Bessman et al., 1996). Why the genome would express a protein that hydrolyzes and eventually inactivates an important redox cofactor in cellular metabolism is still a concern.

In recent years, the metabolic cofactor NAD was found to be covalently attached to the terminal end of small regulatory bacterial RNAs. Bacterial nudix hydrolase NudC has been detected to be an active NAD decapping enzyme both *in vitro* and *in vivo* (Höfer et al., 2016). The enzyme efficiently removes the NAD moiety from the terminal end by hydrolyzing the pyrophosphate bond to produce free nicotinamide mononucleotide (NMN) and 5'-monophosphorylated RNA. *E. coli* NudC protein prefers NAD-capped RNA over free NAD by 5-folds and NADH by 170-fold, indicating that the primary cellular substrate of NudC might be NAD-capped RNA and not NAD^+ or NADH, as previously thought. Although the NAD cap has been reasoned to stabilize the sRNAs against *in vitro* endonucleolytic decay, similar to the role of

m^7G caps on the terminal end of eukaryotic mRNA transcripts, it was essential to investigate for an RNA decapping enzyme.

The high-resolution crystal structures of *E. coli* NudC in complex with NAD and NMN uncovered the structural basis of decapping of NAD-capped RNA by the NudC protein (Hofer K et al., 2016). NudC binds a diverse set of cellular RNAs in an unspecific fashion with a surprisingly strong preference for a purine as first nucleotide (Höfer et al., 2016). The structure of each of the NudC monomeric units is constituted of two tandem Nudix-fold domains, namely the N-terminal domain (NTD) and the C-terminal domain (CTD). The Nudix fold comprises of a beta sheet with alpha helices on each side, while the Nudix motif comprises of the catalytic site. Between the two domains, four cysteine residues coordinate one Zn^{2+} ion to form an extended zinc-binding motif, which protrudes out from the NTD. The catalytic activity resides in the highly conserved 23-amino acid Nudix motif and has been found to be dependent on the conserved glutamate residues. In addition to the Nudix motif, residues engaged in substrate binding are also essential for its enzymatic function. Since the first report of the purification of the NudC protein, it has been found to co-purify with a highly diverse population of tightly interacting nucleic acids (Frick & Bessman, 1995), with very little enrichment or depletion of any specific sequences. It has been suggested that the positively charged surface neighboring the entrance to the catalytic center could be involved in electrostatic interactions for RNA binding, however never confirmed. NGS analysis revealed that adenosine was the first base in all RNA transcripts covalently modified with NAD (Cahova et al., 2015). When the adenosine of NAD is substituted by guanosine, cytidine or uridine, the rate of decapping by NudC was considerably reduced for the pyridine replacements, further suggesting a preference for a 5'- purine nucleotide (Höfer et al., 2016).

Although growing crystals of NudC in complex with NAD-capped RNA was unsuccessful, NudC in complex with free NAD was successfully solved by molecular replacement method at 2.6 Å resolution (Höfer et al., 2016, PDB: 5IW4). Each of these monomeric unites binds a NAD ligand, where the nicotinamide moiety of NAD is buried in a hydrophobic binding pocket through stacking and hydrogen-bonding interactions, while the adenine ring extends into another hydrophobic pocket at the dimer interface. The adenine moiety of NAD is stacked between the side chains from one NudC monomer to another, confirming that dimerization is crucial for substrate recognition and binding (Höfer et al., 2016). Interestingly, there are several positively charged residues huddled outside the entrance of the NAD binding pocket, suggesting that they may be involved in the recognition of the sugar-phosphate backbones of NAD modified RNA transcripts. Owing to the narrow dimensions of the cleft above the adenosine ribose in the NAD ligand bound form of NudC, it was confirmed that NudC is single-strand specific.

Additionally, the crystal structure of NudC in complex with its cleavage product, NMN was solved at 2.7 Å resolution (Höfer et al., 2016, PDB: 5IW4, 5IW5). Similar to the NudC-NAD complex, the NMN molecule too, is deeply buried in a hydrophobic binding pocket between the NTD and the CTD, with the pyridine ring facing towards the bottom of this pocket. Surprisingly, when the NTDs of one monomer of ligand-free, substrate NAD-bound and product NMN-bound NudC were superimposed, a significant change in the orientation of CTD was observed, suggesting a conformational change in free, substrate bound and product bound NudC protein. Also, the relative orientation between the two monomers gradually move a little closer upon binding the substrate, revealing that the catalytic activity is dependent not only on the conformation of each monomer, but also on the dimeric arrangement.

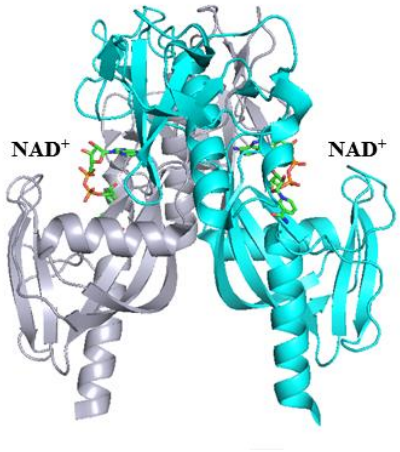

Figure 2-1| Crystal structure of *E. coli* NudC dimer
Crystal structure of the bacterial NudC (PDB: 5IW4) in complex with its substrate, NAD^+. Its two monomeric units, highlighted in grey and cyan, are in complex, each have a binding site for the substrate. This was solved at 2.7 Å resolution. (Höfer et al., 2016)

Thus, a study by the Jaschke Lab (Höfer et al., 2016) revealed a possible biological role for NudC in the cleavage of NAD-capped RNA over known small-molecule substrates such as NAD^+ and NADH. The *E. coli* genome encodes for 13 Nudix enzymes, most of which have no clear physiological function. It may be hypothesized that these hydrolases might process RNAs capped with other non-canonical caps such as nucleotide sugars, dinucleoside polyphosphates, or other dinucleotide coenzymes. Interestingly enough, NudC was not linked with McaS (IsrA) sRNA, one of the most highly NAD modified sRNAs in bacteria (van Nues et al., 2016). This indicates that the differential decapping activity by NudC might be much more precise.

Over the years, Nudix proteins from the plant pathogen *Pseudomonas syringae* and from the human pathogen *Pseudomonas aeruginosa* have also been well studied (Modzelan M et al., 2014). *P. syringae* pv. tomato str. DC3000 and *P. aeruginosa* encodes for 10 and 12 Nudix hydrolases respectively. Additionally, *Ps*NudC and *Pa*NudC contain SQPWPXPXS motif specific for NADH Nudix hydrolases (Dunn et al., 1999), and very similar to that of *E. coli* NudC. They have similar and preferential *in vitro* activity on the reduced NADH over oxidized NAD^+ under alkaline pH conditions, and in the presence of divalent metal ions. Similar to other NADH Nudix phosphohydrolases, the homologous proteins, *Ps*NudC and *Pa*NudC exists as dimers in solution. The conserved glutamic acid residue (E190) in the Nudix motif is responsible for cofactor binding. Site directed mutagenesis of this glutamate residue removes its catalytic activity, without affecting the protein's ability to form homodimers. It has been hypothesized that intracellular levels of

$NADH/NAD^+$ in bacteria are regulated by an alternative pathway, with NADH being accumulated when terminal oxygen acceptors become limited. This was confirmed when increased levels of $NADH/NAD^+$ was observed in the late exponential and stationary phases of growth of the *Ps*NudC mutant, indicating that the Nudix NADH hydrolase is involved in regulating the intercellular redox status under limiting oxygen stress. However, the same was not observed for its homologous counterpart in *P. aeruginosa.* Of course, further scrutiny is required to solve these discrepancies.

2.1.4 NudD (Orf1.9)

The *E. coli* genome encodes for yet another gene, the *nud*D (aka orf1.9 or yefc) gene that expresses NudD, a protein of the same Nudix hydrolase superfamily of enzymes (Frick et al., 1995). NudD forms a novel subclass of this family, by catalyzing the hydrolysis of GDP-mannose or GDP-glucose by nucleophilic substitution at carbon to yield GDP and mannose or glucose respectively (Bessman et al., 2000). Because of this difference in its nucleophilic mechanism, it has been questioned whether NudD is a member of the Nudix protein family or simply an example of convergent evolution (Bessman et al., 2006). Perhaps the hydrolysis of GDP-mannose is not the sole biological role of the enzyme.

Surprisingly, the enzyme has little to no activity on other common Nudix hydrolase substrates, such as nucleotides, dinucleotides, nucleotide sugars, or sugar phosphates. Because of its substrate specificity, NudD is often referred to as the *E. coli* GDP-mannose mannosyl hydrolase (GDPMH). This enzyme, comprising of 160 amino acids contains the well conserved 23-amino acid Nudix sequence responsible for novel nucleoside diphosphate binding site and catalytic activity. Similar to the members of this family, NudD too has an alkaline pH optimum between 9.0 and 9.5. However, unlike the other proteins in the Nudix family, NudD only requires one

divalent cation per active site for its catalytic activity by facilitating the removal of the GDP leaving group (Mildvan et al., 2002).

2.1.5 NudE (Orf186)

Another gene encoded by the *E. coli* genome, *nud*E (aka orf186) is also a member of the Nudix hydrolase family of genes. The gene expresses NudE, a protein that has been identified as an enzyme highly specific for compounds containing adenosine diphosphate (ADP). Typical to members of this family, NudE too has the well conserved 23-amino acid Nudix motif. The three major substrates for NudE are adenosine 5'-triphospho-5'-adenosine (AP_3A), ADP-ribose, and NADH, all of which are involved in a variety of essential regulatory processes *in vivo*. This substrate specificity supports the hypothesis that Nudix hydrolases may play an important role to monitor the concentrations of reactive nucleoside diphosphate derivatives and in the regulation of their accumulation during metabolism (Bessman MJ et al., 1998). NudE is not only specific for *E. coli* and has since then been identified in the bacterial virus, T4 bacteriophage. The T4 gene e.1 expresses for a protein of the Nudix hydrolases superfamily and most closely resembles the *E. coli* NudE, hence its name NudE.1. Expectedly, NudE.1 is also active on a similar range of substrates including FAD, AP_3A and ADP-ribose at an alkaline pH optimum requiring divalent metal ions (Bessman et al., 2002).

2.1.6 NudF (Orf135)

The *E. coli* genome encodes for yet another gene, *nud*F (aka orf135), expressing a protein NudF, which is a member of the Nudix hydrolase family of enzymes with substrate specificity for cytidine triphosphate (CTP), deoxycytidine triphosphate (dCTP), but mostly active on 5’-methyl-dCTP. Unlike other members of the Nudix hydrolase superfamily of proteins with similar catalytic activity, NudF is very specific for pyrimidine deoxy-nucleoside triphosphates. The protein cleaves

its substrates to produce a nucleoside monophosphate and inorganic pyrophosphate at alkaline pH conditions, requiring divalent metal cations for optimal catalysis. It has been hypothesized that NudF may be involved in pyrimidine biosynthesis, lipid biosynthesis, and in controlling levels of 5-methyl-dCTP *in vivo* (Bessman et al., 2001).

2.1.7 NudH (RppH, Orf176)

The *E. coli* genome encodes for the *nud*H (aka *orf*176 or *ygd*P) gene, connected to the invasion of brain microvascular endothelial cells. This gene expresses NudH (aka *O*rf176 or YgdP) or more recently termed as the RppH protein which has been identified as another member of the dinucleoside oligophosphate pyrophosphatase subfamily of the Nudix hydrolase super family of proteins. NudH catalyzes the hydrolysis of diadenosine tetra-, penta- and hexa- phosphate with a striking preference for diadenosine pentaphosphate, a precursor of ADP and ATP. Common to Nudix hydrolases, this protein too has a requirement for divalent metal cations and a pH optimum between 8.5 and 9. It should be noted that this is the second identification of a member of the Nudix hydrolase subfamily of dinucleoside oligophosphate pyrophosphatases associated with the invasiveness of a human pathogen (Bessman et al., 2001), after IalA. The first identified gene associated with the invasion of human red blood cells by *Bartonella bacilliformis*, ialA was identified by Bessman et al. (1999). The protein product of the gene, IalA contains the 23-amino acid sequence representative of Nudix hydrolases. The enzyme cleaves the pyrophosphate linkage of dinucleoside polyphosphates to yield nucleoside triphosphate and the remaining nucleotide moiety. It is most active on adenosine 5'-tetraphospho-5'-adenosine (Ap_4A), but also poorly hydrolyses Ap_5A, Ap_6A, Gp_4G and Gp_5G.

The hypothesis that degradation of messenger RNA (mRNA) in bacteria is initiated by endonucleolytic cleavage had been challenged by the discovery of a non-nucleolytic event that

triggers mRNA decay and its rapid turnover. This was better supported by endonuclease RNase E-mediated catalysis on the 5'- monophosphate of mRNA transcripts. However, an enzyme to remove the terminal pyrophosphate was yet to be identified in any bacterial species. Since then, Belasco JG et al. identified the *E. coli* protein RppH (*Ec*RppH, formerly NudH or YgdP) as the RNA pyrophosphohydrolase that initiates mRNA decay by this 5′- end dependent pathway. *Ec*RppH has been demonstrated to efficiently remove pyrophosphate from the terminal end of triphosphorylated RNA transcripts, irrespective of the terminal nucleotide, *in vitro*. *In vivo*, *Ec*RppH accelerates the degradation of mRNA transcripts by the conversion of triphosphorylated 5′ ends to their monophosphorylated forms which can undergo further ribonuclease cleavage (Belasco et al., 2008). This activity of *Ec*RppH to trigger bacterial mRNA decay by removing a protective structure at the 5′- terminal is in accordance to the removal of cap structures from the 5′-end of eukaryotic mRNA substrates by Dcp2 (Nudt20), also a member of the Nudix hydrolase superfamily. Despite the significant structural differences between bacterial and human mRNAs, the proteins involved in its decapping seem to have evolved from a shared ancestor.

Soon after, the crystal structure of Nudix hydrolase from *Bdellovibrio bacteriovorus* (BdRppH) was solved at 1.9Å resolution (Amzel et al., 2009). BdRppH showed significant similarities to eukaryotic proteins involved in decapping, by the presence of positively charged residues that may be the binding site for nucleic acids. The hypothesis was further supported by the structure of the complex of BdRppH with GTP, where GTP was bound in a position comparable to that observed in the m^7GpppA-X29 complex, a decapping enzyme from *Xenopus laevis* in complex with the eukaryotic mRNA cap structure (Scarsdale et al., 2006). In 2013, Piton J et al. solved the crystal structure of the RppH protein from *Bacillus subtilis* (BsRppH). This study elucidated the structural and functional differences between several RNA decapping enzymes in

distantly related bacteria. BsRppH has a binding pocket that specifically prefers guanosine residues in the second position of its RNA targets, unlike BdRppH which has a binding pocket only for the first residue of its RNA substrates. EcRppH requires at least two or more single stranded nucleotides at the terminal mRNA end and although it seems to tolerate variation in sequence on the terminal end, the protein has some preference for adenine over guanine at the first position and for a purine at the second position (Foley et al., 2015). Also, BdRppH releases inorganic pyrophosphate from the terminal ends of their primary transcripts, whereas BsRppH catalyzes the same reaction in two different steps, involving exonucleolytic degradation by a second enzyme, RNase J, releasing two phosphates (Richards et al., 2011). EcRppH too catalyzes a two-step 5'-end-dependent mRNA decay starting with the removal of γ-phosphate, by a yet to be identified bacterial enzyme, leading to a subsequent β-phosphate removal by EcRppH (Luciano et al., 2017). It was soon confirmed that this diphosphorylated intermediate form is the preferred biological substrates for the bacterial enzyme (Luciano et al., 2018).

ADP-ribosylation is a post-translational modification found extensively in diseased cellular environments. Surprisingly, the *E. coli* RppH protein was found to be catalytically active on another substrate, protein-conjugated ADP-ribose (protein-conjugated ADPr), hydrolyzing it to its phosphoribose attachment site, *in vitro*. It was confirmed that a short, novel 310-helix downstream from the well conserved Nudix signature motif was responsible for the degradation of protein-conjugated ADPr (Daniels et al., 2015).

2.1.8 NudI (Orf141)

The *E. coli* genome encodes for *nud*I (aka orf141 or yfaO) expressing the NudI (Orf141) protein, a member of the Nudix hydrolase superfamily of proteins. NudI is a nucleoside triphosphatase with preference for pyrimidine deoxynucleoside triphosphates, such as

deoxyuridine triphosphate (dUTP), deoxythymidine triphosphate (dTTP) and dCTP, with much less activity on their respective diphosphate substrates. Typical to this class of hydrolases, NudI has a divalent metal ion requirement for activity and an alkaline pH optimum (Bessman et al., 2006) as well.

2.1.9 NudJ (Orf153)

The *E. coli* genome encodes for *nud*J (orf153 or ymfB) expressing the NudJ protein, also a member of the Nudix hydrolase superfamily of enzymes. Unlike the other *E. coli* other Nudix nucleoside triphosphatases, NudJ is a nonspecific nucleoside tri- and diphosphatase and surprisingly, releases inorganic orthophosphate from triphosphates instead of the usual inorganic pyrophosphate. None of the other typical Nudix hydrolase substrates tested, including NADH, GDP-mannose and ADP-ribose, are hydrolyzed by NudJ. NudI seems to have similar if not better catalytic activity on their mutual substrates except GDP, thus questioning the physiological role of NudJ *in vivo*. The enzyme also has no difference preference between deoxyribose over ribose substrates. Typical to this class of hydrolases, NudJ also has a divalent cation requirement for its activity and a pH optimum between 8.5 to 9 (Bessman et al., 2006).

2.1.10 NudK (Orf191)

The *E. coli* genome encodes for *nud*K (aka orf191 or *yff*H) responsible for the expression of the NudK protein, another member of the Nudix hydrolase superfamily. Although NudK hydrolyzes ADP-ribose, it has a much higher catalytic activity on GDP-mannose (Bessman MJ et al., 2006) in addition to NudD. Further studies revealed that NudK has a marked preference for purine over pyrimidine nucleotide sugars and for the 6-keto over the 6-amino group amongst the tested purine substrates. The nudk gene contains the consensus Nudix motif, with a conservative replacement of the lysine residue for arginine (Bradford et al., 1976).

2.1.11 NudL (Orf192)

The *E. coli* genome encodes for *nud*L (aka orf192) gene expressing NudL, a CoA pyrophosphatase. It has also been designated as member of the Nudix hydrolase superfamily of proteins because nudL has the very well conserved Nudix box and an amino acid motif upstream of the Nudix sequence characteristic of coA pyrophosphatases (Bessman et al., 2006).

2.2 Human nudix hydrolases

The human genome encodes for a total of 22 Nudix hydrolases, six of which have been reported to possess mRNA decapping activity. Owing to their name, these enzymes have catalytic activity on a wide range of substrates including canonical (d)NTPs, oxidized (d)NTPs, non-nucleoside polyphosphates and capped mRNA transcripts.

Table 2-1| Substrate specificity of Nudix proteins

Nudix protein	SUBSTRATE
Nudt1 (MTH1)	8-oxo dGTP
Nudt3	Diphosphoinositol-polyphosphate
NudC **Nudt12**	NAD or NADP
Nudt16	m^7G-5′-pppN or m^7G-5′-ppp-mRNA
Nudt20 (Dcp2)	m^7G-5′-pppN or m^7G-5′-ppp-mRNA

The substrate specificity of the Nudix proteins of our interest amongst the 347 proteins of this superfamily that have been functionally characterized, structurally determined or have phylogenetically important Nudix homology proteins domains. From (Brenner et al., 2017).

Figure 2-2| Sequences of Nudix proteins
The sequences of the Nudix proteins of our interest has been shown here, with each protein having the characteristic Nudix motif (blue), while NAD-cleaving NudC and Nudt12 proteins both have a Zinc-finger domain (red), known to interact with nucleic acids. Nudt12 also has an additional ankyrin repeat (orange), unlike the other Nudix proteins.

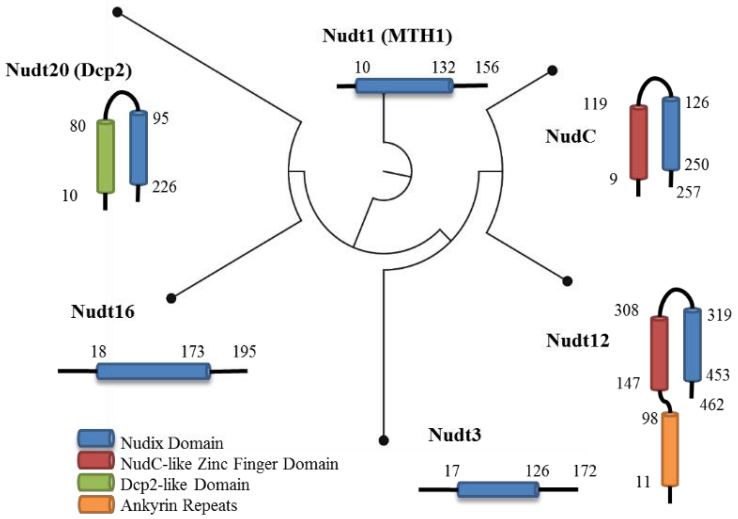

2.2.1 Nudt1 (MutH1)

8-oxo-7,8-dihydrodeoxyguanosine triphosphate (also known as 8-oxo-dGTP) is produced by active oxygen species in the nucleotide pool *in vivo* and can be misincorporated into DNA during replication. The human genome encodes for the MTH1 (aka NUDT1) gene, the mutT human homolog, expressing Nudt1 protein, an 8-OH-dGTPase. Nudt1 hydrolyzes 8-oxo-dGTP to yield 8-oxo-dGMP, thereby preventing DNA mutations (Furuichi M et al., 1994), localized *in vivo* both in the cytoplasm and the mitochondria (Kang D et al., 1995).

A subset of mammalian Nudix enzymes have been shown to lack decapping activity, including Nudt1 (Song et al. 2010), thus suggesting that decapping is not a characteristic feature of all 8-OH-dGTPases. However, the Nudt1 protein has been found to be required for the efficient survival of cancer cells (Carreras-Puigvert et al., 2017). The protein is overexpressed in most analyzed cancer cells with an increased activity in lung cancer tissues (Speina E. et al, 2005). Nudt1 prevents the misincorporation and damage after DNA replication caused either by increased levels of reactive oxygen species (ROS) or dysfunctional redox regulation, leading to oxidative damage to DNA, or to the free nucleotide bases in the cellular and mitochondrial deoxynucleoside triphosphate (dNTP) pool (Helleday et al., 2014). Thus initially, selectively inhibiting NUDT1 was

thought to be a novel anticancer therapeutic approach, however later disproved, considering selective small molecule inhibitors, siRNA knock-down and CRISPR-mediated knockout of NUDT1 did not support this previous hypothesis of the Nudt1 protein being essential for the survival of cancer cells (Kettle et al, 2016).

2.2.2 Nudt3

The human genome encodes for the NUDT3 gene expressing Nudt3, a protein characterized as a diphosphorylated inositol phosphate phosphohydrolase. This was the first identified mammalian Nudix hydrolase to share the common highly conserved Nudix motif with *Bartonella bacilliformis* Ap6A/Ap5A hydrolase, responsible for a preferential activity on Ap6A and Ap5A over other diadenosine polyphosphates (Safrany et al., 1999). Nudt3 has been identified as a cytoplasmic protein, suggesting its role in the decay of mRNAs in the cytoplasm (McLennan et al., 2006). Since then, Nudt3 has also been shown to be have *in vivo* mRNA decapping activity (Kiledjian et al., 2016). The protein can cleave its nucleic acid substrate either between the α- and β- phosphate, or between the β- and γ- phosphate with similar activity to yield either m^7GMP or m^7GDP from a monomethylated capped RNA substrate (Song et al., 2013). Surprisingly, Nudt3 can also decap unmethylated capped RNA to yield the expected GDP or GMP products. Similar to other members of the protein family, Nudt3 has decapping activity only on a small subset of mRNAs, preferentially mRNAs encoding proteins that are integral for cell motility (Nogalska et al., 2016). Nudt3 is the third mammalian Nudix hydrolase to be identified as an mRNA decapping enzyme, suggesting the existence of several other decapping enzymes targeting specific mRNA subsets instead of a single mammalian decapping enzyme that nonspecifically targets all cellular mRNAs. The *S. cerevisiae* orthologue of Nudt3, Ddp1 also shares similar robust decapping activity *in vitro* at least (Song et al., 2013), confirming that the presence of multiple RNA decapping

enzymes is not restricted to multicellular organisms alone. Whether Ddp1p functions as a decapping enzyme in yeast cells *in vivo* is yet to be seen.

2.2.3 Nudt4

The human genome encodes for NUDT4 gene expressing the Nudt4 protein, a diphosphoinositol polyphosphate phosphohydrolase (DIPP). A member of the Nudix hydrolase superfamily of proteins, Nudt4 does not seem to have mRNA decapping activity either. Interestingly, high expression of the NUDT4 gene has been detected throughout normal tissues, with a significant downregulation in all analyzed cancer cells (Carreras-Puigvert et al., 2017).

2.2.4 Nudt7

The human genome encodes for the NUDT7 gene expressing the Nudt7 protein, a member of the Nudix hydrolase superfamily of proteins. Nudt7 hydrolyses coenzyme A (CoA), CoA esters and oxidized CoA to yield 3',5'-ADP and the corresponding acyl-phosphopantetheine derivatives as products. The mouse ortholog of the human NUDT7 gene, NUDT7α expresses a similar CoA diphosphatase. *In vivo* studies revealed that Nudt7α is confined to the peroxisome and has a C-terminal peroxisomal targeting signal type 1 (PST1) that directs the enzyme to the organelle. In cells, CoA is found in three distinct pools in the cytosol, mitochondria and peroxisome. CoA synthesis is finished in the cytosol and only a minor portion of the cytosolic CoA is transported into mitochondria and peroxisomes in liver cells. It is hypothesized that the Nudt7α may either be involved in the removal of oxidized CoA from peroxisomes, although preliminary *in vitro* studies to confirm this idea have not been successful. Alternatively, Nudt7α may also regulate CoA and acyl-CoA levels in the peroxisome in response to metabolic demand (Gasmi et al., 2001). Expectedly, the removal of the C-terminal PTS1 alters Nudt7α cellular localization. It did not however affect the catalytic activity of Nudt7α. Neuron-specific expression of PTS1 deficient

Nudt7α confined it to the cytoplasm and resulted in reduced brain CoA levels which interestingly led to a significant decline in motor function (Shumar et al., 2015). It should also be noted that Nudt7 lacks mRNA decapping activity (Song et al., 2010).

Cellular localization experiments of the human NUDT7 protein showed cytoplasmic staining of hepatocytes and testicular Leydig cells, thus failing to corroborate with the above murine results (Carreras-Puigvert et al., 2017).

Upregulation of its orthologue in pigs, the expression of NUDT7 in muscle cells is thought to reduce succinyl-CoA content and hence reduce the level of heme biosynthesis (Taniguchi et al., 2010).

2.2.5 Nudt9

The human gene NUDT9 was first identified in bacteria and yeast encoding for a protein belonging to a subfamily of Nudix hydrolases active on ADP-ribose (Dunn et al., 1999), a product of NAD hydrolysis. Later discovered in humans as well, the Nudt9 protein hydrolyzes ADP-ribose and IDP-ribose to their corresponding nucleoside 5'-monophosphates and ribose 5-phosphate, with minimal to no activity on other nucleotide substrates (Lin et al., 2002). The NUDT9 gene has a proline residue downstream of the characteristic Nudix box, common to the ADP-ribose pyrophosphatase subfamily. Also characteristic to the Nudix family of proteins, Nudt9 hydrolyzes its substrates in a divalent metal ion dependent manner at near neutral pH optimum with a nucleophilic attack on the adenosyl phosphate moiety (Gabelli et al., 2002). The analysis of the human NUDT9 gene indicated two isoforms named, NUDT9α, the dominant form and NUDT9β, a product of unusual mRNA splicing. The protein expressed by NUDT9α has been identified as an N-terminal signal peptide, localized specifically to the mitochondria. Similar specific cellular localization has not been identified for the protein of the NUDTβ transcript (Perraud et al., 2003).

Interestingly enough in humans, the protein was differentially expressed in endometrial glandular cells at different phases of the menstrual cycle and more prominently in the epithelial glandular component than in the stromal component of endometrial carcinomas (Chen et al., 2009). Human Nudt9 showed cytoplasmic staining of glandular cells in the fallopian tube and of neurons and neuropil in the cortex (Carreras-Puigvert et al., 2017).

Two enzymatically indistinguishable human proteins, the highly specific ADP-ribose purified from placenta and a considerably less active recombinant Nudt9, both having submicromolar K_m for their respective substrates confirms that ADP-ribose pyrophosphatase present in human tissues is indeed a product of the NUDT9 gene (Ribeiro et al., 2001; Carloto et al., 2006). Thus, making Nudt9 a major candidate to control the accumulation of free ADP-ribose in humans, a potentially toxic compound due to its non-enzymic reactivity towards protein side chains. ADP-ribose can regulate calcium entry in vertebrate (Perraud et al., 2001), where the proteolytically resistant C-terminal domain of the Nudt9 protein serves as a binding site for ADP-ribose (Yu et al., 2017), enhanced by the proteolytically labile N-terminal portion. This eventually led to the detection of Nudt9 as a modulator of the hypoxia inducible factor-1α (HIF-1α) accumulation in cancer cells preceded by the activation of Ca^{2+}/calmodulin-dependent protein kinase kinase β (CaMKKβ) (Yoon et al., 2018). Similar to only a few members of the Nudix hydrolase superfamily, Nudt9 is deficient of mRNA decapping activity as well (Song et al. 2010).

2.2.6 Nudt10

Although phylogenetic analysis of the Nudix hydrolase Nudt10 identified the protein as a diphosphoinositol polyphosphate phosphohydrolase, no activity on its major substrate, 5-diphosphoinositol pentakisphosphate (5-PP-InsP5) could be detected (Carreras-Puigvert et al., 2017). Interestingly, given the very similar sequences, the human Nudt10 and Nudt11 mRNAs

encode identical proteins (Song et al., 2013) and the expression of both proteins was found to be essential for cancer cell survival. Nudt10 lacks efficient mRNA decapping activity (Song et al. 2010).

2.2.7 Nudt12

The human genome contains 24 genes encoding proteins belonging to the Nudix superfamily. NUDT12 is a member of a subset of this superfamily encoding for NADH diphosphatases and the closest homolog of the bacterial NudC protein. The successful recombination of NUDT12 from pET vectors in *E. coli* BL21 (DE3) cells has not been reported yet. Characterization of the human Nudt12 protein was thus done using a baculovirus expression system (Abdelraheim et al., 2003). Not only does the human NUDT12 gene have a very well conserved Nudix motif close to the C terminus, it also has a downstream sequence CQPWPMPSS characteristic of other known NADH diphosphatases. The large N-terminal domain also contains the Nudix fold and a single ankyrin repeat sequence which is required for RNA deNADding activity but unnecessary for the hydrolysis of NAD alone (Grudzien-Nogalska et al., 2019). This class of enzymes have a clear preference for reduced nicotinamide nucleotides.

Table 2-2| Substrate specificity of Nudt12

SUBSTRATE	RELATIVE ACTIVITY (%)
ADP	2
ADP-ribose	57
AMP	0.2
dATP	4.9
FAD	63
NAD^+	59
NADH	100
$NADP^+$	63
NADPH	136

Each activity has been calculated at substrate concentration= 250 µM and normalized, where 100% activity is assumed to be 11.5 µmol NADH hydrolyzed• min^{-1}• $(mg\ protein)^{-1}$ under similar conditions. Values are averages of duplicate experiments. Data from (Abdelraheim et al., 2003).

As expected, Nudt12 has also been found to be enzymatically active on a wide range of substrates, most active on NADH and NADPH and least active on deoxynucleoside 5'-triphosphates, nucleoside 5'-diphosphates and 5'monophosphates. Assays to determine substrate specificity and kinetic parameters were measured colorimetrically under physiological conditions at alkaline pH and 0.4 mM Mg^{2+} ion concentration.

In 2003, Nudt12 was expressed as a C-terminal fusion to enhanced green fluorescent protein and found to be localized to the peroxisomes and larger, unidentified structures in the cytoplasm by the C-terminal tripeptide PNL acting as a novel peroxisomal targeting signal type 1 (PTS1). They were later confirmed in the cytoplasm in kidney cells (Carreras-Puigvert et al., 2017). Deletion of this PTS1 obliterated the peroxisomal localization. HeLa cells were also co-transfected with the recombinant C-terminal fluorescent construct of Nudt12 and another C-terminal fusion to red fluorescent protein of a known peroxisomal protein- mouse Nudt7 CoA diphosphatase. The two signals were found to co-localize, leading to the belief that the role of Nudt12 may be to regulate peroxisomal nucleotide cofactor coenzyme concentrations or to remove unknown and probably toxic oxidized nucleotide metabolites generated within the cell organelle.

Mammalian cells contain more than 20 genes encoding proteins belonging to the Nudix superfamily. Mouse Nudt12 and Nudt13 are members of this superfamily encoding for NADH diphosphatases. His-tagged recombinant proteins were expressed from cDNAs encoding the for these diphosphatases and their activity on mRNA decapping has been studied extensively. The tested recombinant proteins have a well conserved Nudix motif.

Nudt12 among other Nudix hydrolases also effective decapping activity on unmethylated capped RNA (Song et al., 2013). Nudt12 can cleave either between the α- or β- phosphate to yield

GMP. For monomethylated capped RNA substrates, Nudt12 can hydrolyze between the α-β- and β-γ- phosphates.

Figure 2-3| Possible cleavage site(s) within the cap structure

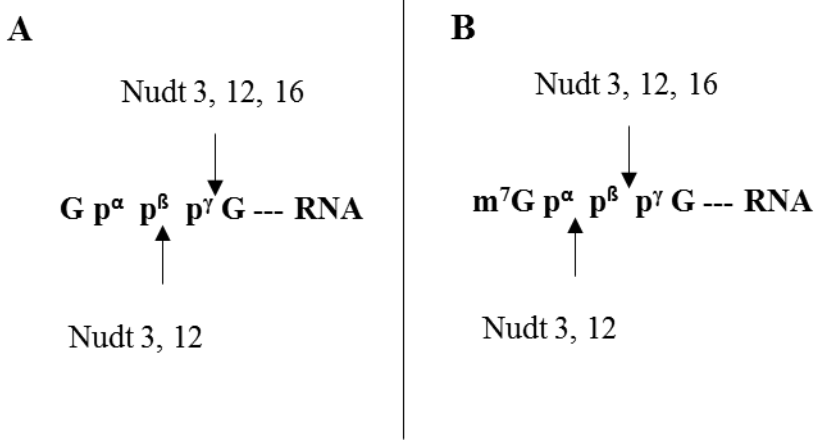

Nudt3, Nudt12 and Nudt16 have effective decapping activity on both (A) unmethylated and (B) monomethylated capped RNA, cleaving either between the α- or β- phosphate to yield GMP, or between the α-β- and β-γ- phosphates, respectively. Based on information from (Song MG et al., 2013)

When compared to DcpS, a scavenger mRNA decapping pyrophosphatase, the scavenger decapping of Nudt12 on m^7GpppG cap structure, although existent is not comparable *in vitro*. Similar to the bacterial and human Nudix NADH diphosphatase, mouse Nudt12 can also hydrolyze free NAD into nicotinamide riboside monophosphate (NMN) and adenosine monophosphate (AMP). As predicted, Nudt12 cleaves the NAD-capped RNA substrate between the diphosphate linkage, mimicking the activity of NudC releasing NMN from NAD-capped RNA yet different from that of the Decapping and eXOribonuclease (DXO) protein, which removes the entire NAD moiety from the RNA substrate (Grudzien-Nogalska et al., 2019). Nudt12 uses the same active site to both deNAD and decap m^7G-capped RNA and has an impressive preference for deNADding over decapping. DeNADding enzymes have thus been classified into three broad categories. The

first class is the DXO family proteins that remove the entire NAD moiety from the 5' end of the RNA substrate. The second one comprises of NudC and Nudt12 which cleaves the pyrophosphate linkage within the NAD alone or on the 5'end of the RNA substrate. The third class comprises of RppH which is minimally active on free NAD but does cleave NAD off the 5'end of RNA. These classes of deNADding enzymes also function differently under environmental stress.

Table 2-3| Classes of deNADding enzymes

CLASS	ENZYME	SUBSTRATE	PRODUCT
1	DXO	NRppA--- RNA	NRppA + p--- RNA
2	NudC Nudt12	NRppA or NRppA --- RNA	NRp + pA or NRp + pA--- RNA
3	RppH	NRppA --- RNA	NRp + pA--- RNA

The first class of DXO family of proteins remove the entire NAD modification from the terminal end of RNA, while the second class of NAD-cleaving Nudix hydrolases cleaves the phosphodiester linkage within the NAD alone, or when attached to RNA. The third class, the bacterial RppH cleaves NAD off the terminal end of RNA transcripts. Table based on information from (Kiledjian, 2019).

Not only does Nudt12 function as a deNADding enzyme *in vivo* as it does *in vitro,* it also modulates the stability of NAD-capped RNAs. Cells lacking either Nudt12 or DXO or both contained an increase in total NAD-capped RNA levels, indicating that Nudt12 and DXO target specific and distinct groups of cellular mRNAs. mRNAs involved in oxidative phosphorylation are specifically targets for Nudt12, unlike the snoRNAs and the related small Cajal body RNAs that are deNADded by DXO. Cellular stress, either heat shock or glucose deprivation led to an impressive increase in NAD-capped RNA transcripts. The specific Nudt12 targeted NAD-capped mRNAs favorably increased after glucose deprivation, but not heat shock confirming that Nudt12 indeed modulates mRNAs involved in cellular metabolism. This suggests that there may be a physiological connection between the metabolic cellular environment and its mRNA composition. However, how these deNADding enzymes target specific RNA substrates is still a mystery.

Certain Nudix hydrolases, including Nudt12 is overexpressed in a variety of cancer cells. The human protein is involved in the regulation of endogenous HIF-1α protein under hypoxic conditions in HeLa cells. Highly oxidative environment in these cells lead to the accumulation of ADP-ribose, which initiates homeostasis by overexpression of ADP-ribose cleaving Nudix hydrolases. Even though Nudt12 does not completely remove the substrate, the cells survive by enhancing HIF-1α protein expression (Yoon et al., 2018).

The catalytic domain of mouse Nudt12 consists of a N-terminal subdomain, a zinc-binding motif and a C-terminal subdomain. It forms a dimer of similar conformational monomers. This has been solved in complex with AMP and three Mg^{2+} ions. Although the structure of mouse Nudt12 and *E. coli* NudC are very similar, there are noticeable structural differences in the N-terminal domain. The interactions between the phosphate group of AMP and Nudt12 are mediated by the three Mg^{2+} ions, unlike the AMP portion of NAD in complex with NudC.

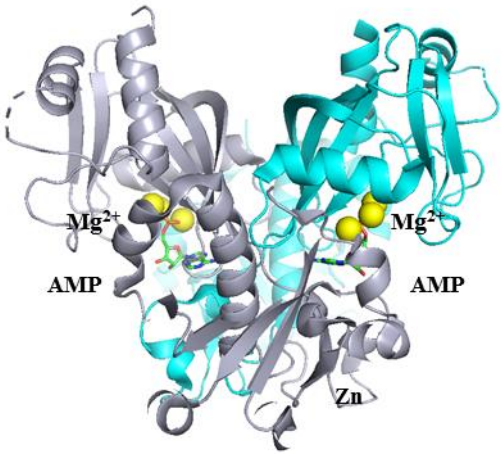

Figure 2-4| Crystal structure of the mouse Nudt12 dimer
Crystal structure of the mouse Nudt12 (PDB: 6O3P) protein (Kiledjian, 2019). Its two monomers, highlighted in grey and cyan, are in complex with AMP and three Mg^{2+} ions (yellow). This was solved by at 1.6Å resolution.

2.2.8 Nudt13

The human genome encodes for NUDT13, containing a sequence typical of the NADH pyrophosphohydrolase subfamily of the Nudix hydrolases. The gene expresses the Nudt13 protein, with *in vitro* hydrolytic activity on NADH/NADPH to yield NMNH and AMP/2',5'-ADP. Characteristic to this class of Nudix hydrolases, Nudt13 too had a striking preference for the reduced pyridine nucleotides over nucleotide substrates. Expression of Nudt13 as an N-terminal

fusion to green fluorescent protein confirmed that it is explicitly a mitochondrial protein, directed to the organelle by the N-terminal targeting peptide. Its subcellular localization suggests that the physiological role of Nudt13 may be to regulate the concentration of reduced pyridine nucleotide cofactors and in the maintenance of $NAD(P)^+$/NAD(P)H ratio in the mitochondria (Abdelraheim SR, et al., 2017). Interestingly enough, compared with all other analyzed Nudix enzymes, Nudt13 was essential for the survival of human epithelial CCD841 cells (Carreras-Puigvert J et al., 2017).

2.2.9 Nudt16

The mammalian genome encodes for NUDT16 gene expressing Nudt16, a Nudix inosine triphosphate (ITP)/xanthosine triphosphate (XTP)/GTP-binding protein (Iyama et al., 2010). Initially, the protein was identified in Xenopus as X29, a nucleolar decapping enzyme that specifically binds the U8 snoRNA (Tomasevic et al., 1999). Typical to this class of enzymes, the Nudt16 protein utilizes divalent metal ions, with a very efficient yet unspecific hydrolysis and decapping activity in the presence of Mn^{2+} or Co^{2+} for all RNA transcripts, and with very specific activity for only U8 snoRNAs in the presence of Mg^{2+} (Peculis et al., 2007).

In vivo, Nudt16 was found to be predominantly localized in the nucleus, especially in the nucleolus and to be involved in mRNA decapping (Song et al. 2010; Iyama et al., 2010). Interestingly, Nudt16 also has *in vitro* hydrolytic activity on protein-conjugated ADP ribose. As discussed previously, this activity is owed to the 3_{10} helix sequence found downstream from the Nudix box (Daniels et al., 2015). Initially, Iyama et al. (2010), proposed that Nudt16 is a (deoxy)inosine diphosphatase, protecting the cells from deleterious effects of (d)ITP, accumulation of single-strand breaks in nuclear DNA and/or increased levels of inosine in RNA.

However, subsequently the protein was found to have mRNA decapping activity *in vitro*. Nudt16 predominantly cleaves capped mRNA transcripts between the α- and β- phosphate, while

substrates with an unmethylated cap is cleaved both between the α- and β-, and β- and γ-phosphates with comparable activity (Song et al., 2013). Other cap analog structures containing additional modifications such as $m^7Gpppm^{2'-O}G$, $m^{2,2,7}GpppG$, GpppG and ApppG were also hydrolyzed by Nudt16, with an efficiency comparable or higher to that for canonical cap hydrolysis (Grzela et al., 2018). Under similar conditions, the protein also has minimal activity on isolated cap structures and short capped oligonucleotides. Together, confirming that the enzyme recognizes the first transcribed nucleotide alone.

2.2.10 Nudt20 (Dcp2)

The Nudt20 (Dcp2) protein was first identified in yeast by Parker et al. (1999) to be associated with the major pathway of mRNA degradation and for long believed to be the only mRNA decapping enzyme. The protein, containing a MutT/Nudix motif in its N-terminal domain, both necessary and sufficient for mRNA decapping, was recruited for the decapping of both nascent and aberrant mRNA transcripts. Later, the protein was confirmed as pyrophosphatase and renamed Nudt20 as a member of the Nudix hydrolase superfamily of proteins. The core decapping enzyme, encoded by the DCP1 gene comprises of the regulatory Dcp1 and the catalytic Dcp2 subunit, which interacts with further accessory enhancer proteins such as the Lsm1-7 complex, Pat1, Edc1-Edc2 and/or Edc3 to reach its catalytic optimum (Charenton et al., 2016). Human Dcp2 protein cleaves the canonical capped RNA transcripts to yield m^7GDP and 5'-phosphorylated mRNAs, that are subsequent substrates for 5'-3' exonuclease decay. Consistent to members of the Nudix family, Dcp2 has an alkaline pH optimum. However, unlike typical members of the family, human Dcp2 requires the presence of a long RNA substrate, preferably longer than ~25 nucleotides, attached to the cap structure. This substrate specificity alone confirms that capped mRNA transcripts are natural substrates for the enzyme. *In vivo*, human Dcp2 co-localizes mostly

in specific sub-structures in the cytoplasm with very minimal traces in the nucleus suggesting that mRNA decay may occur in a dedicated cellular compartment (van Dijk et al., 2002; Wang et al., 2002), subsequently better confirmed by the identification of P-bodies (Sheth et al., 2003).

Substrate specificity for Dcp2 is achieved in multiple possible ways. RNA cap recognition occurs during the catalytic step of the enzyme, with an ATP molecule bound in the catalytic pocket in the closed complex formation. The transcript, within 10 nucleotides of the cap structure, itself may promote decapping by binding to the dorsal surface of the Nudix motif or the secondary structure of the stem-loop commonly termed as the "Dcp2 binding and decapping element", thereby increasing the local concentration of the cap for formation of weak, but specific interactions (Deshmukh et al., 2008; She et al., 2008). Alternatively, decapping can also be stimulated by a cis-element in the mRNA target (such as an AU-rich element in the 3'- UTR or oligouridylation at the 3'- end of an already deadenylated RNA), which is recognized by Dcp2, which in turn employs the Dcp1:Dcp2 complex (Li et al., 2010).

2.3 Pyridine Dinucleotides in Biology

Initially, the pyridine dinucleotides, $NADP^+$ and NADPH, were believed to be functional as essential coenzymes in reductive-oxidative glycolysis alone. Soon, its role in human nutrition and cofactor biosynthesis was confirmed. More recently, the role of NAD^+ in protein deacetylation shed new light. In 2006, Belenky et al. classified NAD^+ consumers into three broad classes; first, ADP-ribose transferases or poly (ADP-ribose) polymerases, second are the cADP-ribose synthases and third are type III protein lysine/histone deacetylases.

2.3.1 Metabolism

Nicotinamide adenine dinucleotide (NAD), its oxidized form, NAD^+, its reduced form, NADH, and their phosphorylated forms, $NADP^+$ and NADPH, are electron carriers and cofactors

of various metabolic redox reactions thereby essential for the maintenance of *in vivo* cellular redox homeostasis. In mammalian cells, NAD^+ is synthesized by three different pathways: the *de novo* pathway, the *Preiss–Handler* pathway and the salvage pathway using tryptophan, nicotinic acid, nicotinamide and nicotinamide riboside as precursors. Upon metabolic pathway analysis, the concentration of the NAD moiety is usually assumed to be constant, even though its redox state may change. Although recently, several NAD-consuming reactions have been identified, challenging this exact assumption. NAD-consuming reactions are typical of NAD^+-dependent signaling and gene regulation pathways such as DNA-repair or regulation of enzymes fundamental to metabolism, including poly-ADP-ribosylation of proteins, NAD^+-dependent deacetylation by sirtuins and the formation of messenger molecules such as cyclic ADP-ribose (cADPR). Imbalance in NAD homoeostasis has been associated with various diseases, thus the complete understanding of the dynamics of NAD metabolism is essential for efficient pharmacological development in this area (Opitz et al., 2015; Xiao et al., 2018).

Intracellular concentrations of these cofactors usually range in the micromolar range, in human cells. The inner mitochondrial membrane is impermeable to NADH and NADPH, hence have to be regulated by multiple shuttle systems, thus maintaining *in vivo* subcellular localization (Houtkooper et al., 2010). These shuttle mechanisms aid the cells to maintain redox homeostasis in both normal and stressed conditions, arising from excess levels of cellular NADH and/or NADPH.

2.3.2 Sirtuins (Histone Deacetylases)

Histone deacetylases (HDACs) are enzymes that deacetylate lysine side chains in histones and some non-histone proteins, leading to altered states of conformation and activity of these proteins. The catalytic activity of one subclass of these enzymes depends on NAD^+. Nicotinamide

(Nam) and O-acetyl ADP ribose are formed as a result of this acetyl transfer. These NAD^+-dependent deacetylases are more commonly termed sirtuins because of the homologous yeast histone deacetylase silent information regulator 2 (Sir2). Sirtuins contain a Nam binding that site that may be occupied in the presence of substrate or enzyme intermediate, leading to product inhibition. Thus, the salvage of Nam is essential for NAD^+ metabolism (Sauve et al., 2005). Sirtuins are very well conserved from prokaryotes to eukaryotes and have since then been implicated in the regulation of molecular mechanisms of aging. Sirtuins also function as sensors for glucose uptake in response to NAD^+ levels (Trapp et al., 2006).

2.3.3 Poly (ADP-ribose) Polymerase

Poly (ADP-ribose) polymerases (PARPs) catabolizes NAD^+ to yield an ADP-ribosyl protein modification and/or form an ADP-ribose polymer (PAR). In response to DNA damages, PARP-1 utilizes NAD^+ as a substrate to catalyze the covalent attachment of negatively charged PAR moieties on PARP-1 itself (automodification) or on acceptor proteins which are usually involved in DNA transactions (heteromodification), as a unique post-translational modification. It has been hypothesized that the inhibition of PARP may be linked with the protection of *in vivo* levels of NAD^+, which leads to the regulation of cell survival, transcriptional regulation and telomere cohesion during cell division and energy metabolism (Belenky et al., 2006; de Murcia et al., 2006).

2.3.4 DNA Ligase

DNA ligases catalyzes the closure of nicks in the phosphodiester backbone of double-stranded DNA, hence is crucial for DNA replication and repair. They are classified as NAD^+ or ATP-dependent enzymes based on their preference for the respective co-factors. The NAD^+-dependent ligases (LigA) are found exclusively in eubacteria and some viruses (Sriskanda et al.,

2001). The ATP-dependent ligases are found in all other kingdoms, including both prokaryotes to eukaryotes. Either cofactor is recognized as an AMP-donor triggering the transfer of bound AMP to a free 5′- phosphate on DNA, which in turn catalyzes the joining of the nick and finally releases free AMP (Khorana et al., 1970; Sgaramella et al., 1970).

2.3.5 NAD Binding Pocket composed of RNA

A complex secondary structure of the RNA aptamer, containing two interacting stem-loops was identified as nicotinamide-binding site. Site-directed mutation within the binding site confirmed the comparative specificity between the two redox states of the nicotinamide-containing cofactor (Lauhon et al., 1995).

2.3.6 NAD Ribozymes

Ribozymes are RNA molecules, capable of catalyzing chemical reactions. Compared to a protein enzyme, the catalytic unit of an RNA molecule is only a small portion, yet its activity is considerably higher. Two essential cellular processes are known to be catalyzed by ribozymes: the peptidyl transferase by the large subunit of the ribosome and eukaryotic mRNA splicing by the U2-U6 snRNA.

RNA can specifically bind cofactors, namely riboflavin and beta-nicotinamide mononucleotide (NMN) with low micromolar affinity (Lauhon et al., 1995). These RNA molecules are able to discriminate between the two redox states of the nicotinamide-containing cofactors, as well. This discovery led to a framework for generating novel ribozymes that might catalyze metabolic redox reactions.

An RNA molecule (ribox02), coupled with a Zn^{2+}-dependent redox relay between NADH and FAD to give a NAD^{+}-regeneration system, was identified to have catalytic activity similar to protein alcohol dehydrogenase (Tsukiji et al., 2003). Ribox02 oxidizes benzyl alcohol derivatives

to its corresponding aldehyde, covalently attached to the 5′-end of RNA in the presence of NAD+ and Zn^{2+}. Interestingly enough, the conjugate of the same ribozyme is able to catalyze the reverse reduction reaction in a NADH and Zn^{2+} dependent mechanism (Tsukiji et al., 2004).

2.3.7 RNA binding metabolic enzymes

Initially, proteins that bind RNA were considered functionally distinct from proteins that bind DNA which was eventually debunked with the discovery of long non-coding RNAs (lncRNAs). Nucleic acid binding proteins regulates several cellular processes like transcription, translation, gene silencing, microRNA biogenesis and telomere maintenance (Hudson et al., 2014).

Several NAD^+-dependent glycolytic enzymes, such as lactate dehydrogenase (LDH), glyceraldehyde-3-phosphate dehydrogenase (GAPDH) (Pekala et al., 1996) and phosphoglycerate kinase (PGK) (Shetty et al., 2004), have been demonstrated to bind RNA. LDH catalyzes the reversible hydride transfer from lactate to pyruvate and back, in a NAD^+/NADH dependent manner. The direct interaction of LDH with an AU-rich element RNA-binding protein 1 (AUF1) has been confirmed to exist as a complex *in vivo* (Pioli et al., 2002). These glycolytic enzymes also possess a coenzyme binding domain and it has been revealed that NAD^+ or NADH binding can compete with RNA binding.

GAPDH is a noncanonical RNA-binding protein (RBP) that binds to a variety of RNA transcripts, including tRNA, ribozymes and viral RNAs, to regulate the stability and translation of cellular mRNAs (Garcin et al., 2015; Garcin, 2018). GAPDH was classified as an AU-rich sequence binding protein (AUBP) because the enzyme showed a strong preference for RNAs containing AU-rich sequences in the NAD^+-binding site (Nagy et al., 1995; White et al., 2016).

2.4 Damaged NADH

Human renalase (*Hs*Ren) was first discovered as a flavoprotein secreted into the blood by the kidney as a hormone to decrease concentrations of catecholamine neurotransmitters, hence lowering blood pressure and cardiac rate (Xu et al., 2005). Initially, it was suggested that the catalytic role of the enzyme is to oxidize epinephrine to adrenochrome (Desor et al., 2012). However, this conversion is effortless under a variety of other conditions and has led to question the direct role of renalase with the breakdown of catecholamines. More recently, it has been established that renalase is not the third monoamine oxidase (Beaupre et al., 2015) and is in fact responsible for the catalytic oxidation of isomeric forms of NAD(P)H molecules that are reduced at the 2 or 6 position of the nicotinamide ring instead of the metabolically active 4-position. This is the first instance that a flavoprotein has been shown to catalyze an anomerization reaction and redefines the metabolic function of renalase as a house-keeping enzyme than a regulator of blood pressure (Beaupre et al., 2013).

Although the renalase sequence is not very well conserved among species and makes it difficult to recognize the protein across various species, three renalases from Human, *Pseudomonas phaseolicola* and *Pseudomonas aeruginosa* have common catalytic activity (Moran et al., 2017). Regardless of the poor sequence conservation, these proteins have similar tertiary structure. Like most other redox active flavoproteins, renalase has a flavin adenine dinucleotide (FAD) cofactor hidden deep within the protein.

The discovery of isomeric forms of NAD(P)H as a substrate for renalase was almost serendipitous. The 2-dihyhdroNAD (2DHNAD(P)) and 6-dihydroNAD (6DHNAD(P)) differs from NAD(P)H in the position of the hydride which resides on either the 2 or the 6 position of the nicotinamide instead of the native 4 position. In-vitro, these molecules can be synthesized from nonspecific borohydride reduction of $NAD(P)^+$ or tautomerization of NAD(P)H.

Figure 2-5| Reduction of β-NAD(P)$^+$

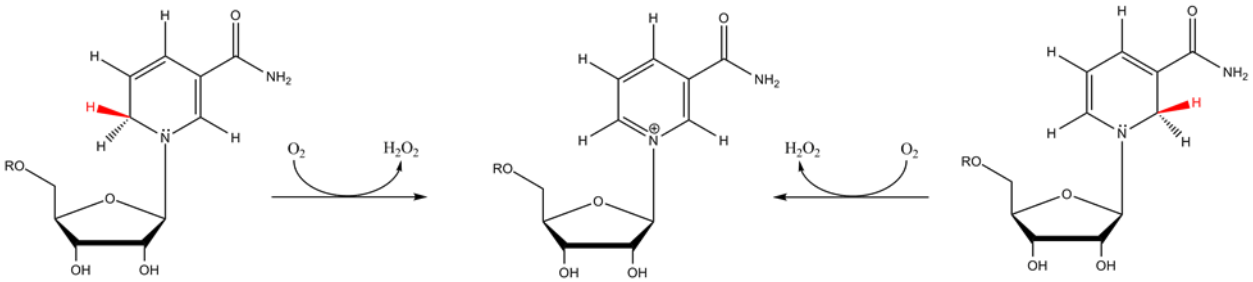

In vitro borohydride reduction places the hydride on either the 2 or 6 position of the nicotinamide instead of the canonical 4 position, highlighted in red to yield wither 2-dihyhdroNAD (2DHNAD(P)) or 6- dihydroNAD (6DHNAD(P)) respectively. Figure based on information from (Moran, 2016).

The quick and complete reduction of the renalase Flavin cofactor was initiated with saturating amounts of an aged NAD(P)H solution stored at -20°C. When the 6- and 2-DHNAD species formed by nonenzymatic reduction of NAD^+ was reacted with renalase, two out of the three products formed were oxidized to NAD^+ by the enzyme, indicating that the enzyme can oxidize two separate isomeric forms of the substrate. The bacterial renalase (PpRen) reduces 2-DHNAD(P) more rapidly than 6-DHNAD(P). However, the human form (HsRen) reduces 6-DHNAD relatively slower than 2-DHNAD. For both renalases, NADH seems to bind tighter than NAD(P)H which is probably because of the solvent exposed 2'-phospho group having no favorable interactions with the enzyme. Although HsRen seems to bind 2-DHNAD and 6-DHNAD slightly better than 4-DHNAD (NADH), PpRen does not share the same isomeric selectivity. This incompetence of renalase to distinguish between NAD(P)H isomers suggested that other cofactor dependent enzymes may experience similar inhibition by 2- and 6-DHNAD(P). This proves that the isomeric forms of β-NAD(P)H are possibly toxic to the cell, hindering the activity of several primary metabolic enzymes (Beaupre et al., 2015).

Table 2-4| Inhibitory effect of 6DHNAD

ENZYME	6DHNAD K_i (µM)
P. phaseolicola *GAPDH*	1.63 ± 0.195
P. phaseolicola *IDH*	1.39 ± 0.130
P. phaseolicola *ME*	4.51 ± 0.185
P. phaseolicola *DLD*	ND
E. coli *MDH*	0.585 ± 0.037
Pig *DLD*	3.1 ± 0.3
Rabbit *LDH*	ND

Inhibition constants, K_i were calculated by IC_{50} analysis at a ß-NADH substrate concentration equivalent to the Km value. No inhibition was observed for either *P. phaseolicola* DLD or rabbit LDH. Table based on information from (Moran et al., 2017).

It may be hypothesized that in the cellular environment, the metabolic role of renalase is to oxidize the inhibitory isomers of NADH to form NAD^+ and deliver the electrons gathered to dioxygen using the flavin cofactor forming H_2O_2 and $NAD(P)^+$. Although the isomers are inhibitory towards an array of enzymes, the obvious concern is whether these toxic isomers of β-NAD(P)H exist in-vivo. Renalase oxidizes these toxic isomers more rapidly than catecholamines with or without NAD(P)H. To support this concern, it may be argued that renalase has been identified in species, where they do not require catecholamines or experience hypertension such as *Pseudomonas*.

2.5 Canonical caps

Initially, the presence and absence of a molecular cap structure on the 5'- end of messenger RNAs was considered to be the distinction between eukaryotes and prokaryotes. In eukaryotic cells, the m^7G 5'- cap structure is added co-transcriptionally to the 5'- end of nascent pre-mRNA transcripts. The cap is attached in parallel with RNA transcription, due to the combined effect of three enzymatic steps. The function of this cap feature and cellular cap binding proteins in gene expression regulation has been studied extensively. This modification stabilizes mRNAs by protecting them against exonucleases and leads to polyadenylation, splicing and nuclear export of mRNAs. Thus, the cap structure plays a significant role in the life cycle of mRNA and is crucial for efficient gene expression and cell viability. The cap structure is needed for optimal translation of a vast majority of cellular mRNAs (Topisirovic et al., 2011). It is extensively found on eukaryotic viral and parasitic mRNA transcripts. In the eukaryotic cellular environment, two cap-binding proteins have been studied extensively: eukaryotic translation initiation factor 4E (eIF4E) in the cytoplasm and the nuclear cap binding complex (nCBC), a nuclear complex consisting of cap binding protein 20 (CBP 20) and cap binding protein 80 (CBP 80).

2.6 Non-canonical caps

More recently, chemical modifications have been discovered in bacterial RNAs that structurally resembles the eukaryotic mRNA cap, although the capping mechanism is fundamentally different than that of eukaryotes (Bird et al., 2016). Using MS-based technique, two essential coenzymes in bacterial physiology, nicotinamide adenine dinucletide (NAD^+) and 3'-dephospho-coenzyme A (dpCoA) have been identified on the 5'- end of RNA transcripts from *E. coli* and *Streptomyces venezuelae*. This explains how coenzyme-modified RNA is synthesized in bacteria. It has been confirmed that the coenzymes and metabolites, such as NAD^+, its reduced

equivalent NADH, Flavin adenine dinucleotide (FAD), uridine containing precursors of oligosaccharide and cell wall biosynthesis and dpCoA compete with the regular NTP, adenosine triphosphate, in the initiation step of transcription, and is incorporated by bacterial RNA polymerase (RNAP) into a full-length RNA at the +1 position. Although whether NADH, FAD, UDP-glucose and UDP-N-acetylglucosamine modified RNA exist in cellular environments is yet to be proven. The k_m for NAD^+ in transcription initiation is considerably lower than the *in vivo* concentration of NAD^+. RNAP successfully incorporates an array of known nucleotide-containing molecules and identified yet uncharacterized moieties at the terminal end of RNA substrate, suggesting a wide range of RNA caps *in vivo*. Upon crystallization of RNAP in complex with a short NAD capped RNA, the NMN part of the molecule does not contact DNA but faces the protein instead. Also, two domains of the RNAP enzyme, the rifampicin-binding pocket and the RNAP active center determine NAD^+ capping efficiency. It is interesting to note that rifampicin resistant RNAPs are deficient in capping (Julius et al., 2017).

Human mitochondrial RNAP, too, can cap RNA with NAD^+ and other ADP-containing cofactors, on one of the two human mitochondrial promoters, light strand promoter (LSP) *in vitro* (Julius et al., 2018). Although the efficiency of NAD^+ initiation is markedly lower than that of ATP, the mitochondrial RNAP is probably responsible for mitochondrial NAD^+ modified RNA transcripts.

Unfortunately, the technique to identify these chemical modifications required the complete hydrolysis of the RNA substrates and failed to identify the sequences. A novel capture protocol, the NAD captureSeq was designed, combining enzymatic transglycolation with “click” chemistry (Cahová et al., 2015). The technique involved the isolation of NAD-modified RNA by reacting with ADP-ribosyl cyclase (ADPRC) followed by a “click” reaction by copper-catalyzed

azide alkyne cycloaddition (CuAAC) and specific enrichment, cDNA preparation and the validation of NGS results. In *E. coli*, sRNAs regulating plasmid replication (RNAI and CopA), mRNAs encoding for proteins involved in cellular metabolism (gatY, pgk, hdeD) or leader peptides with known regulatory functions (*ilv*L, *his*L) were identified with this approach. It is worth mentioning that tRNAs and rRNAs were not enriched with this protocol. In yeast and human cells, a subset of eukaryotic RNAs (mRNA, snoRNA and small Cajal body RNAs [scaRNAs]) were enriched with the NAD captureSeq technique.

The main concern that remains is the biological role of these NAD modifications on RNA transcripts. The role of bacterial NAD^+ cap on translation is not known yet, although it is believed that the NAD^+ cap structure enhances RNA stability. However, whether selective stabilization and degradation are the only functions of these unconventional RNA headgears still remains to be seen. It may be argued that the deletion of the decapping enzyme, NudC did not affect the overall *in vivo* stability of the RNA transcripts most abundantly modified by heavily NAD+ namely RNAI and GcvB. In *E. coli*, proportion of NAD-capped RNA found in the stationary phase was much higher than the exponential phase, suggesting that non-canonical capping may be responsive to alterations in cellular metabolism. The coenzymes and metabolites attached to RNA may provide a layer of 'epitranscriptomic' information that modifies the activity of RNA without altering its sequence, has recently been proposed as a possible role as well. However, in eukaryotic cells, NAD-capped mRNA failed to translate.

Terminal modifications of RNAs are reversible to allow RNA turnover. Thus, removal of the 5'-cap is essential to controlling mRNA stability and efficient gene expression. Its regulation is dependent on the availability of the decapping enzyme and the recognition of the mRNA transcript containing the 5'-end modification. Eukaryotic mRNA decay is initiated with the

removal of the 3'-poly(A) tail. It is followed by either 3'→5' decay where the RNA transcript is exonucleolytically degraded by the cytoplasmic exosome and the potentially toxic cap structure is hydrolyzed by scavenger decapping enzymes or 5'→3' degradation where the cap pyrophosphate bond is first cleaved by decapping enzymes proceeded by exoribonucleolytic degradation of the monophosphorylated RNA. Mammalian cells express multiple mRNA decapping enzymes, all Nudix proteins such as Dcp2 (Nudt20), Nudt2, Nudt3, Nudt12, Nudt15, Nudt16, Nudt17, and Nudt19 (Grudzien-Nogalska E et al., 2017). Decapping is not only restricted to eukaryotic proteins, the bacterial Nudix protein RppH is involved in the hydrolysis of the 5' triphosphorylated ends to their monophosphorylated forms in a '5'- dependent pathway'. Similar to the eukaryotic Nudix hydrolases, bacterial Nudix NADH diphosphatase NudC efficiently removes the NAD+ caps from RNA to produce 5'- monophosphorylated RNA. Additional bacterial Nudix hydrolases have been characterized with potential but poor decapping activity, suggesting redundancy. In yeast, decapping is carried out by the Nudix hydrolase NPY1 and by Nudt19 in *Oryza sativa* (Zhang et al., 2016).

Eukaryotic and prokaryotic RNA decapping enzymes have been classified into four categories based on their different catalytic mechanisms and structures. First are the nudix hydrolases, which account for most eukaryotic decapping enzymes hydrolyzing the cap phosphate bond. Second are the DXO family of proteins, which are involved in mRNA cap quality control, selectively degrade mRNAs with a mutated cap or non-canonical caps. Third are the Histidine triad (HIT) family of proteins, which are involved in the cleavage of a pyrophosphate bond of capped di- or oligonucleotides. Fourth are the ApaH-like phosphatases, which are involved in the 5'→ 3' decay of capped mRNA transcripts.

2.7 Assays

2.7.1 Colorimetric assay

As early as in 1966, a simple and quantitative protocol was demonstrated for the easy colorimetric determination of inorganic phosphate. This assay was based on the principle that a alkaline triphenylmethane dye, such as malachite green (MG) at lower pH forms a complex with phosphomolybdate, causing a shift in its absorption maximum (Itaya & Ui, 1966). Release of inorganic phosphate as low as 50 ng can be detected by this method. Since the initial discovery of the quantitation assay, it has been modified by Penney (1976) by eliminating the use of detergents altogether while Rosenfeld et al. (1978) replicated the same principle to quantify organic phosphorus in phospholipids, and Karl et al. (1982) investigated the effects of interfering proteins and detergents in this assay.

Catalytic activity may also be monitored upon the incubation of Nudix hydrolase, coupling enzyme (phosphatase) and an inorganic phosphate (Pi) sensor (Brune M et al., 1998) with an already identified Nudix substrate. The Nudix hydrolase cleaves between the diphosphate bond, yielding a molecule with a terminal phosphate group. A coupling phosphatase then releases an inorganic pyrophosphate, which is captured by the Pi sensor, generating an increase in fluorescence (Xu A et al., 2013).

2.7.2 High Performance Liquid Chromatography (HPLC)

The identity of substrates and enzyme-treated products can be confirmed from high-pressure liquid chromatography (HPLC) analysis. After incubation, the sample is filtered to remove the protein and subjected to identical HPLC analysis. The samples injected onto a Waters Xterra C18 cartridge column (4.6 × 150 mm^2) are run isocratically at 0.5 mL/min with 10 mM

NaPi, pH 7.5, coupled to a Waters 600E pump and a Waters 2487 detector. The elution of the components can then be observed at their absorption maxima (Beaupre et al., 2013).

2.7.3 In vitro transcription of ncinRNA

Adenosine-containing coenzymes CoA, NAD, NADH and FAD can initiate *in vitro* transcription under the T7 class II promoter by T7 RNA polymerase to yield these coenzymes covalently attached to the terminal end of the RNA transcripts. *In vitro* transcription of non-canonical capped RNA was confirmed, either by polyacrylamide gel electrophoresis, excision and recovery by ethanol precipitation and recorded to have a fluorescence (FAD emission wavelength at 530 nm when excited at 370 nm) spectrum (Huang, 2003) or identified by mass spectrometry after exonucleolytic treatment (Höfer et al., 2016) or by acryloylaminophenyl boronic acid (APB) affinity gel electrophoresis (Nübel et al., 2017).

2.7.4 Fluorescence Enhancement Assay

Unlike fluorescence resonance energy transfer (FRET) which requires two fluorescent dyes, protein induced fluorescence enhancement (PIFE/PIFE) only needs a single dye attached to nucleic acids to which an unlabeled protein is bound (Hwang et al., 2014). A method similar to the PIFE protocol to study T7 DNA polymerase binding to DNA was the first every report of protein binding to fluorescently labeled DNA, by monitoring a change in the intensity with single molecule resolution (Luo et al., 2007).

Hwang et al., explained that PIFE is a photophysical phenomenon, where the intensity of a fluorophore increases upon proximal binding to a protein (Hwang et al., 2011). This is commonly demonstrated by fluorophores such as Cy3 attached to nucleic acid substrates, undergoing a cis-trans photoisomerization reaction. The local molecular environment with the addition of proteins reduces the rate at which the fluorophore can isomerize from the photo-active trans state to the

photo-inactive cis state, resulting in an increase of quantum yield. The lifetime of the fluorescent dye and an increase in viscosity of the *in vitro* experimental environment are factors affecting fluorescence enhancement.

2.7.5 Lactate dehydrogenase assay

Vanderlinde (1985) studied the bidirectional redox reaction catalyzed by lactate dehydrogenase between pyruvate and lactate. The production of NADH at 340 nm in the lactate to pyruvate oxidation and the decay of NADH at 340 nm produced in the pyruvate to lactate reduction reaction has been monitored spectrophotometrically (Vanderlinde, 1985).

2.7.6 Liquid chromatography–mass spectrometry (LC/MS)

David Liu's lab (Chen et al., 2009) demonstrated a general protocol for the easy identification of small molecule-RNA conjugates in both *E. coli* and *S. venezuelae.* NAD-modified RNAs were identified amongst whole cellular RNAs isolated form whole cellular extracts. Nuclease P1 treated samples were injected into high-resolution LC/MS. The stationary phase used was a C18 column (1.7 µm, 2.1 mm x 100 mm), while the mobile phase was a combination of 0.1% aqueous ammonium formate, and 100% methanol. Electrospray ionization (ESI) was used, keeping the flow rate at 0.300 $mLmin^{-1}$ (Chen et al., 2009). These conditions will be mimicked in our LC/MS experiments as well.

Chapter 3 Materials & Methods

3.1 Materials

3.1.1 Plasmid Vectors

pET24d-NudC and pET33-Nudt12 were constructed, as described in sections 3.1.2.1 and 3.1.2.2. Plasmids expressing NUDT1 (MutH1), NUDT3A, NUDT16A and NUDT20 (Dcp2) were purchased from Addgene. The purchased construct was transformed into BL21(DE3) cells for protein expression.

3.1.1.1 pET24d-NudC

*E. coli nud*C gene was amplified using PCR from DH5α colonies, with primers (Integrated DNA Technologies, Coralville, IA) containing NcoI and BamHI restriction sites. The PCR product was then cut with NcoI and BamHI and ligated into a similarly digested pET24d plasmid (Novagen).

3.1.1.2 pET33-Nudt12

NUDT12 gene was amplified using PCR from pCMV-Nudt12, with primers (OriGene Technologies Inc, Rockville, MD) containing BamHI and NdeI restriction sites. The PCR product was then cut with NotI and ligated into a similarly digested pET33 plasmid (Novagen).

3.1.1.3 Nudt1

The vector expressing NUDT1 was designed and purchased through Addgene (Addgene plasmid # 74660). The purchased construct was transformed into BL21(DE3) cells for protein expression.

3.1.1.4 Nudt3A

The vector expressing NUDT3A was designed and purchased through Addgene (Addgene plasmid # 42348). The purchased construct was transformed into BL21(DE3) cells for protein expression.

3.1.1.5 Nudt16A

The vector expressing NUDT16A was designed and purchased through Addgene (Addgene plasmid # 42404). The purchased construct was transformed into BL21(DE3) cells for protein expression.

3.1.1.6 pET28a-hDcp2

The vector expressing pET28a-hDcp2 was designed and purchased through Addgene (Addgene plasmid # 72214) (Wang et al., 2002). The purchased construct was transformed into BL21(DE3) cells for protein expression.

3.1.2 Proteins

The Nudix proteins of interest in this thesis have been listed below (Table 3-1). Subsequent experiments discussing purification, concentration calculations and SDS-PAGE analysis of these proteins are based on this table.

Table 3-1| Nudix hydrolases (properties)

Protein	Amino Acids	Fusion Tag	Mass (kDa)	Extinction Coefficient
NudC	257	None	27	61880 $M^{-1}cm^{-1}$
Nudt1	158	N-His	22.5	33,460 $M^{-1}cm^{-1}$
Nudt3A	194	N-His	19.7	28,420 $M^{-1}cm^{-1}$
Nudt12	339	N-His	52	66,640 $M^{-1}cm^{-1}$
Nudt16A	200	N- His	22	12,950 $M^{-1}cm^{-1}$
Nudt20 (hDcp2)	167	N-His	49	49,390 $M^{-1}cm^{-1}$

3.1.2.1 NudC purification

NudC was purified from BL21(DE3) *Escherichia coli* cells. The protein was purified from soluble cell extracts by first precipitating the protein with nucleic acids using streptomycin sulfate. The pellet was then dissolved and fractionated using a DEAE Sepharose column eluted over a 0-500 mM NaCl gradient.

3.1.2.2 Nudt12 purification

Nudt12 was purified from BL21(DE3) *Escherichia coli* cells. One-liter cultures were harvested, lysed by sonication, and purified by using Ni-NTA column chromatography, gel filtration column chromatography, and ultrafiltration. Final protein concentrations were determined from absorbance at 280 nm using the extinction coefficients (Table 3-1).

3.1.2.3 Nudt1, Nudt3A, Nudt16A, hDcp2 purification

Nudt1, Nudt3A, Nudt16A, hDcp2 were purified from BL21(DE3) *Escherichia coli* cells. One-liter cultures were harvested, lysed by sonication, and purified using Ni-NTA column chromatography, gel filtration column chromatography, and ultrafiltration. Final protein concentrations were determined from absorbance at 280 nm using appropriate extinction coefficients (Table 3-1).

3.1.3 Oligonucleotides

Oligonucleotides were purchased from Integrated DNA Technologies and used for cloning (Table 3-2), DNA Binding (Tables 3-3, 3-5) and RNA binding (Table 3-4).

Table 3-2|Oligonucleotides used for cloning

Name	Sequence
NudC (NcoI)	5′-GCG CGCCAT GGA TCG TAT AAT TGA AAA ATT AGA TC- 3′
NudC (BamHI)	5′-CGC GCG CGG ATC CTC ACT CAT ACT CTG CCC GAC- 3′
Nudt12 (NdeI)	5′-GCG GCG CAT ATG ATG TCT TCT GTA AAA AGA AGT CTG AAG CAA G-3′
Nudt12 (BamHI)	5′-GCG GCG GGA TCC TTA GAG ATT AGG ATT TAT TCT AAT CCA GTG- 3′

Table 3-3|DNA oligonucleotides used by binding assays

Name	Sequence
3' Cy3	5′-GGTTCTGCGGGTGGCGGTACTA[Cy3] -3′
[HF]DNA45 (TYE45)	5′-[TYE563]TGGCGACGGCAGCGAGGCACCGATCACATGTTTTTTTTTTTTTTT-3′
[HF]DNA45 (HF45)	5′-[HEX]TGGCGACGGCAGCGAGGCACCGATCACATGTTTTTTTTTTTTTTT- 3′
[FAM]DNA18 (F18)	3′-[FAM]ACCGCTGCCGTCGCTCCG- 5′
[FAM]DNA38 (F38)	3′-[FAM]ACCGCTGCCGTCGCTCCGTTTTTTTTTTTTTTTTTT-5′
[Cy5]dT15	5′-[Cy5]TTTTTTTTTTTTTT-3′

GA9	5′-GAGAGAGAGAGAGAGAGA-3′
C18	5′-CCCCCCCCCCCCCCCCCC-3′
DNA29	5'-GCTCCCCGTTCATCGATTGGGGAGCTTTT-3′

Table 3-4|RNA oligonucleotides used by binding assays

Name	Sequence
[FAM]RNA36	5′-[FAM]UAGUACCGCCACCCUCAGAACCUUUUUUUUUUUUUU-3
RNA18	5′-GCCUCGCUGCCGUCGCGA-3′
RNA36	5′-UAGUACCGCCACCCUCAGAACCUUUUUUUUUUUUUU- 3′
[Cy5]U15	5′-[Cy5]UUUUUUUUUUUUUU-3′
RNA29	5'-GCUCCCCGUUCAUCGAUUGGGGAGCUUUU-3'

3.1.4 Duplex Nucleic Acids

Duplex DNA strands were made by DNA annealing from two complementary single-stranded DNA (ssDNA) strands to yield a heteroduplex formation (Table 3-5).

Table 3-5|Partially Duplex DNAs used for Binding Assays

Name	Sequence
HF45:comp15	3′-ACCGCTGCCGTCGCT [HEX]TGGCGACGGCAGCGAGGCACCGATCACATGTTTTTTTTTTTTTTT-3′
HF45:comp20	3′-ACCGCTGCCGTCGCTCCGTG [HEX]TGGCGACGGCAGCGAGGCACCGATCACATGTTTTTTTTTTTTTTT-3′
HF45:comp25	3′-ACCGCTGCCGTCGCTCCGTGGCTAG [HEX]TGGCGACGGCAGCGAGGCACCGATCACATGTTTTTTTTTTTTTTT-3′
HF45:comp30	3′-ACCGCTGCCGTCGCTCCGTGGCTAGTGTAC [HEX]TGGCGACGGCAGCGAGGCACCGATCACATGTTTTTTTTTTTTTTT-3′
HF45:comp35	3′-ACCGCTGCCGTCGCTCCGTGGCTAGTGTACAAAAA [HEX]TGGCGACGGCAGCGAGGCACCGATCACATGTTTTTTTTTTTTTTT-3′

Experiments described in Chapter 8 make use of fluorescently labelled nucleic acids, properties of which have been listed below (Table 3.6).

Table 3-6|Fluorophores

Name	Excitation peak (nm)	Emission peak (nm)
[FAM]	495	520
[Cy5]	649	670
[HEX]	535	556

3.1.5 Longer RNA transcripts

Reaction mixture containing final concentrations of 1 mM GTP, 1.25 mM CTP, 1.25 mM UTP, 1.25 mM ATP, 2.5 mM NAD^+ (or NADH, NADPH, $NADP^+$),4 mM ARCA mix, 1 µg DNA template, 2 µl T7 RNA Polymerase Mix was made to a total volume of 20 µl. Initial reactions used the provided CluC vector DNA template. Subsequently, gel extracted *Hind*III digested pET24d-NudC was used as DNA template for *in vitro* ncinRNA transcription. The mixture was incubated at 37 °C for 30 minutes followed by DNase I treatment, after which it was incubated 37 °C for another 15 minutes. Newly synthesized RNA was precipitated using LiCl solution after incubation at -20 °C for 30 minutes and centrifuged at 4 °C for 15 minutes. The RNA was rinsed with cold ethanol and finally stored in a final volume of 50 µl 0.1 mM EDTA. This entire protocol was followed from HiScribe T7 ARCA mRNA Kit (New England Biolabs).

3.2 Enzyme Assays

3.2.1 NAD Hydrolysis: Colorimetric

To test the enzymatic activity of Nudix hydrolases on NAD^+, NADH, $NADP^+$ and NADPH, a colorimetric assay was used. Standard phosphate concentrations were made using dilutions of 0.5 mM KPO_4 made up to a total volume of 25 µl. Reactions containing 50 mM Tris pH 8.5, 2 mM $MgCl_2$, 1 mM DTT, NAD^+ or NADH and Nudix hydrolase and made up to a total volume of 40 µl. The reactions were incubated at 37 °C for 30 minutes, 1 unit of calf intestinal

alkaline phosphatase (CIAP) was added and incubated at 37 °C for another 30 minutes. Samples were terminated by adding 200 µl of the malachite green reagent (3 volumes 0.045% (w/v) malachite green: 1 volume 4.2% ammonium molybdate in 4N HCl: 0.01 volume 10% Tween 20), followed immediately by 25 µl of 35% sodium citrate. Absorbance at 630 nm was recorded on Varian Cary 50 UV-Vis Spectrophotometer and net phosphate produced from a reaction was calculated from the phosphate standard curve. Colorimetric assays could not be used to measure the enzymatic activity of Nudix hydrolases on 6DNAD, as it was purified in phosphate containing buffer.

3.2.2 NAD Hydrolysis: HPLC

Following the limitations on the colorimetric assay, an HPLC assay was designed to analyze the enzymatic activity of Nudix hydrolases on NADH and its isomeric form, 6DNAD. Standard solutions containing 100 µM AMP, ADP, ATP, NADH and 6DHNAD were made up to a total volume of 50. Each sample was then injected onto a Waters Xterra C18 cartridge column (4.6×150 mm^2) run isocratically at 1 ml/min with 10 mM Phosphate buffer pH 7.5, coupled to a waters 600E pump and Waters 2487 detector. The elution of the components was observed at both 260 and 340 nm. Samples containing 500 mM Tris pH 8.5, 2 mM $MgCl_2$, varying concentrations of substrate (NAD^+, NADH or 6DNAD) and made up to a total volume of 500 µl. Reaction mixtures containing additional Nudix hydrolases were incubated at 37 °C for 30 minutes, for optimal activity or varying time points for time course experiments. To terminate any further reaction, the samples were incubated 4 °C for 2 minutes and then filtered using a centrifugal filter device. 50 µl of each sample was run on the instrument under identical conditions. Substrate and products were identified and quantified by comparison of retention time and UV absorbance from the initial standard curve, respectively.

3.2.3 NAD Hydrolysis: Ratiometric Florescence

To test the enzymatic activity of NudC on the toxic isomer of NADPH, a novel assay was designed with reaction mixtures containing 50 mM Tris pH 8.5, 2 mM $MgCl_2$, 50 µM NADH and 0.74 nM NudC were incubated at 37°C. Following a brief incubation period, varying concentrations of 6DHNADP was added to one cuvette. As a negative control for inner filter effect, equal volumes of water were added to another cuvette. Emission was simultaneously observed at 460 nm (Ex. 260 nm, 340 nm) on a Varian Cary Eclipse Fluorescence Spectrophotometer. This innovative assay may be used extensively in the future to study either the kinetics of NADH cleaving Nudix hydrolases on ncinRNA or to identify possible inhibitors of the same class of enzymes.

3.2.4 NAD Hydrolysis: LC/MS

No enzyme mixtures containing 500 mM Tris pH 8.5, 2 mM $MgCl_2$, either NAD^+ or NADH or ncinRNA were made to a total volume of 200 µl. Reaction mixtures containing additional Nudix hydrolases were incubated at 37 °C for 30 minutes. Before injecting the sample into LCMS-2020 Single Quadrupole Liquid Chromatograph Mass Spectrometer, the protein was filtered using a centrifugal device. Samples containing ncinRNA were also analyzed on the LCMS-2020. *In vitro* transcribed ncinRNAs were run on an agarose gel and gel extracted following EZNA Gel Extraction Kit - Omega Bio-tek protocol. The activity of nudix hydrolases on agarose gel extracted ncinRNA was also analyzed on the LCMS-2020. Proteins were precipitated out of the samples before injection into the LCMS using 50:50 phenol:chloroform solution. Stationary phase used was a 1.7 µm EVO C18 column, while the mobile phase was ammonium formate pH6 and Methanol. Injection volumes were varied between 5-20 µl for optimal results. Total Ion Count (TIC) was collected for m/z ranging from 100 to 1000. Photodiode Array (PDA) was collected

between 190-700 nm. Selected Ion Monitoring (SIM) for NAD^+ (m/z: 662, 664), NADH (m/z: 664, 666), AMP (m/z: 346, 348), NMN (m/z: 332, 334) and NMNH (m/z: 334, 336) were selected both in negative and positive ionization mode respectively.

3.2.5 Nucleic Acid Binding: EMSA

To test the binding between DNA or RNA and NudC, a more traditional approach using gel shift assays was taken. Mixtures containing single and double stranded fluorescently labelled oligonucleotides and NudC were made to a final volume of 10 µl with 50 mM Tris pH 8.5 were incubated on ice for 20 minutes. A 12 % native gel was pre run at 4°C at 120 V for 30 minutes. Samples were mixed 6:1 with a 6X Loading Dye (0.75 % Bromophenol Blue, 0.25 % Xylene Cyanole FF and 10 ml 40% w/v Dextrose) and run on the pre-run native gel at 4°C at 100 V for 60 minutes. Gel shifts were a UV illuminator.

3.2.6 Nucleic Acid Binding: Fluorescence Intensity

To test the binding between DNA or RNA and Nudix hydrolases, a fluorescence-based assay was designed. Assays were plated in 384 well black plates (ThermoFisher Scientific). Assay conditions were kept at 50 mM Tris pH7.5, 5 mM $MgCl_2$. Additionally, negative controls contained 1 mM DTT, 0.1 mg/ml BSA, 0.01% Tween and fluorescently labelled RNA substrate, whereas experimental conditions contained fluorescently labelled RNA substrate and Nudix hydrolase. Fluorescence (Ex. wavelength= 485 nm, Em. wavelength= 520 nm for FAM labelled oligonucleotides and Ex. wavelength= 640 nm, Em. wavelength= 670 nm for Cy5 labelled oligonucleotides) was measured on FLUOstar Omega (BMG LABTECH) at 25°C. The observed fluorescence (F_{obs}) was fit to Eq. 1.

$$F_{obs} = F_D * (D_T - ED) + F_c * ED; \quad \text{(Eq. 1)}$$

$$\text{where } ED = (K_d + E_T * n + D_t) - \sqrt{\frac{(K_d + E_T * n + D_t)^2 - (4 * E_T * n * E_t)}{2}})$$

and E_T is the concentration of Nudix hydrolase with D_T being the total oligonucleotide= 20 nM or 40 nM or 80 nM; K_d is the dissociation constant, F_s is a coefficient relating probe concentration to F_{obs} (i.e. oligo alone), F_c is a similar coefficient relating F_{obs} to the concentration of an Enzyme-DNA complex (ED).

3.2.7 Nucleic Acid Binding: Fluorescence Polarization

To test the binding between DNA or RNA and Nudix hydrolases, a fluorescence-based assay was designed. Assays were plated in 384 well black plates (ThermoFisher Scientific). Assay conditions were kept at 50 mM Tris pH7.5, 5 mM $MgCl_2$. Additionally, negative controls contained 1 mM DTT, 0.1 mg/ml BSA, 0.01% Tween and fluorescently labelled RNA substrate, whereas experimental conditions contained fluorescently labelled RNA substrate and Nudix hydrolase. G-factor reference well was set with 1 nM Fluorescein in 0.01 M NaOH, while blank well was set with 50 mM Tris pH7.5. Polarization (Ex. wavelength= 470 nm, Em. wavelength= 520 nm for FAM labelled oligonucleotides and Ex. wavelength= 640 nm, Em. wavelength= 670 nm for Cy5 labelled oligonucleotides) was measured on TECAN infinite M1000 at 25°C, with ex/em slit widths 5 nm/10 nm. The raw data was fit to Eq. 1 (Section 3.2.6).

3.2.8 Nucleic Acid Binding: Probe Displacement Assays

Probe displacement assay was designed to estimate binding of unlabeled RNA or DNA ligands, to test preferential binding between Nudix hydrolases and DNA or RNA. Unlabeled oligonucleotides were added to the above described reaction mixtures to displace existing binding between fluorescently labelled oligonucleotide and Nudix hydrolases. A decrease in the fluorescence emission with an increase of unlabeled oligonucleotides was interpreted to mean that Nudix hydrolase bound to the unlabeled oligonucleotides instead of the existing fluorescently

labelled oligonucleotides. The raw data was fit to an inhibition dose response curve. IC_{50} values were calculated using Eq. 2.

$$F_{obs} = F_0 + \frac{(F_c - F_s)}{(1+10^{((Dt-LogIC50))})} \quad \text{(Eq. 2)}$$

where D_t is the concentration of unlabeled oligonucleotide titrated, both the maximum fluorescence F_s and F_c were as defined in Eq. 1.

Dissociation constants for RNA's were determined by assuming they act as competitive inhibitor and fitting datasets to Eq. 3:

$$F_{obs} = F_D * (D_T - ED) + F_c * ED; \quad \text{(Eq. 3)}$$

$$\text{where } ED = (K_d (1 + I/Ki) + E_T * n + D_t) - \sqrt{\frac{(K_d (1+X/Ki) + E_T*n + D_t)^2 - (4*E_T*n*E_t)}{2}})$$

In Eq. 3, "I" is the concentration of unlabeled DNA/RNA, E_T is the concentration of Nudix hydrolase with D_T is the total labeled oligonucleotide probe concentration, K_d is the dissociation constant for enzyme:probe complex (calculated for Eq. 1), F_s is a coefficient relating probe concentration to F_{obs} (*i.e.* oligo alone), F_c is a similar coefficient relating F_{obs} to the concentration of the Enzyme-probe complex (ED).

3.2.9 LDH Redox

Lactate dehydrogenase (LDH) catalyzes the conversion of lactate to pyruvate and back, by transferring a hydride. Simultaneously, the cofactor NAD^+ is converted to NADH and back with the conversion of lactate to pyruvate. The hypothesis that ncinRNA may be a substrate of both bacterial and mammalian lactate dehydrogenase was tested. *E. coli* LDH was purchased from Sigma-Aldrich (59747), bovine heart LDH was purchased from Sigma-Aldrich (L2625), while rabbit muscle LDH was purchased from Sigma-Aldrich (L2500). Reactions containing 220 mM Tris pH7.3, 0.2 mg *E. coli* or 0.368 mg bovine heart or 0.68 mg rabbit muscle LDH was initiated with varying concentrations of lactic acid, purchased from Dot Scientific Inc. (DSL17500-500),

containing either NAD^+ or NAD^+-capped RNA. The increase in the absorbance at 340 nm was recorded in kinetic mode on Varian Cary 50 UV-Vis Spectrophotometer every 0.1 seconds for 3-5 minutes. The reverse reaction containing 220 mM Tris pH 9, LDH was initiated with varying concentrations of sodium pyruvate containing either NADH or NADH-capped RNA. The decay in the absorbance at 340 nm was recorded in kinetic mode on Varian Cary 50 UV-Vis Spectrophotometer, under similar conditions.

Chapter 4 Cloning & Purification of Nudix Enzymes

4.1 Summary

The cloning of bacterial *nud*C from DH5α cells using colony PCR and the human NUDT12 gene from pCMV-Nudt12 will be discussed in this chapter. This chapter also focusses on the purification of mammalian Nudt1, Nudt3, Nudt12, Nudt16, Nudt20 and bacterial NudC protein. At the time this work was done, the human Nudt12 gene had not yet been cloned in a bacterial expression system, for consequent protein purification.

4.2 Background

The *nudC* gene was amplified from DH5α cells using insert-specific primers in colony PCR. The method used for the purification of the prokaryotic NudC protein was exactly as previously described (Frick et al., 1995). As for most nucleic acid-binding protein purifications, NudC was precipitated with streptomycin sulfate to isolate the nucleic acids binding to the protein. Then, the bacterial protein was purified using ion-exchange chromatography. The resin, comprising of positively charged diethylaminoethyl cellulose (DEAE-C), interacts with negatively charged proteins. The protein is then eluted from the resin by increasing the salt concentration of the solvent, to compete for binding to the tertiary amine. Subsequently, the solubility of the NudC protein was altered with the addition of ammonium sulfate. The precipitate from this fractionation containing the NudC protein was then further extracted using gel filtration (GF) chromatography. GF chromatography is a size-exclusion based chromatography technique, that separates the desired protein from other contaminating proteins and nucleic acids.

The mammalian Nudix proteins, Nudt1, Nudt3, Nudt16, Nudt20 and Nudt12 however had a polyhistidine tag on either their N- or the C- terminal domain. The His-tagged proteins were

purified following protocols described in earlier studies (Frick et al., 2010). Each protein was purified using IMAC (Immobilized metal affinity chromatography), where the Histidine residues chelates the Nickel ion, which is immobilized on an IMAC ligand, nitrilotriacetic acid (NTA). It is assumed that other proteins lacking the His-tag do not bind with the ligand and may be removed by washing the NTA column with an imidazole containing buffer. Following the NiNTA step, each Nudix protein was further enriched by GF chromatography. These proteins were then concentrated using ultrafiltration and used for all future assays discussed in Chapter 5 though Chapter 9.

4.3 Results

4.3.1 Cloning nudC from DH5α

*E. coli nud*C gene was amplified using PCR from DH5α colonies, with primers (Integrated DNA Technologies, Coralville, IA) containing *Nco*I and *Bam*HI restriction sites (underlined).

BamHI primer: 5′-CGC GCG CG▼G ATC CTC ACT CAT ACT CTG CCC GAC-3′

NcoI primer: 5′-GCG CGC▲CAT GGA TCG TAT AAT TGA AAA ATT AGA TC-3′

The PCR product was then cut with NcoI and BamHI and ligated into a similarly digested pET24d plasmid (Novagen). The plasmid map of the desired construct was made using the program ApE- A plasmid Editor (http://jorgensen.biology.utah.edu/wayned/ape/) (Fig. 4-1).

Figure 4-1| Plasmid map of pET24d-nudC construct
The *nud*C insert (PCR product) was digested with *Nco*I and *Bam*HI and ligated into a similarly treated pET24d vector. The resulting construct was then transformed in DH5α cells for increased insert stability and subsequently into BL21 (DE3) cells for protein expression.

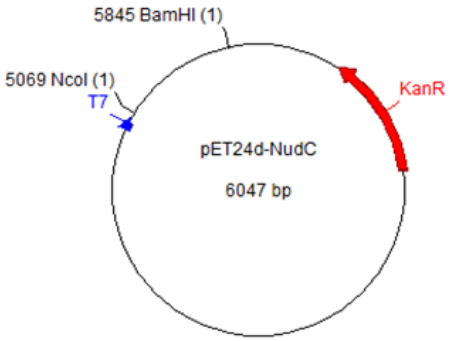

The *nudC* gene studied by Frick et al., in 1995 was amplified from *E. coli* K-12 MG1655 strain, while the *nudC* gene studied in this thesis has been amplified from DH5α cells. Surprisingly, when the sequences of the two genes were aligned, the 33rd residue was found to be different (Fig. 4-2).

Figure 4-2| Sequence similarity between NudC from *E. coli* DH5α and MG1655

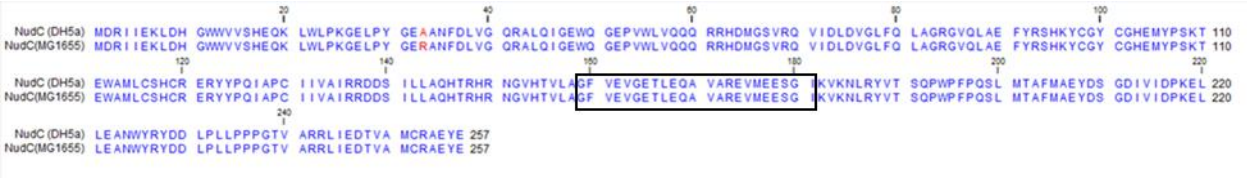

The *nud*C insert amplified from DH5α colonies has a hydrophobic alanine at the 33rd position, as opposed to the nudC gene encoded by the MG1655 strain of E. coli K-12, which has an arginine, as shown in red. The highlighted sequence is the highly conserved Nudix motif, GXXXXXEXXXXXUAXREXXEEXGU

4.3.2 Purification of NudC

Single colonies of BL21 (DE3) cells harboring pET24-nudC plasmid were inoculated into 3 ml of LB medium containing 100 µg/ml kanamycin. After the cells grew to an OD_{600} of 0.6, they were transferred to 1 liter of fresh medium containing kanamycin. After the cells reached an OD_{600} of 0.6 again, they were induced with 1 mM isopropyl-β-D-thiogalactoside (IPTG). The induced cells were harvested by centrifugation and the cell pellet was suspended in buffer A (50 mM Tris, pH 7.5, 1 mM EDTA and 1 mM dithiothreitol), sonicated for 5 minutes and the crude extract was clarified using centrifugation (15,000 g).

4.3.2.1 Streptomycin Sulfate

The protein was first precipitated with nucleic acids using a 10% streptomycin sulfate solution added slowly to a final concentration of 1%.

4.3.2.2 DEAE Chromatography

The pellet containing the protein was collected by centrifugation (15,000 g, 30 min) and resuspended in buffer A. This solution was then loaded onto a DEAE Sepharose column and the

NudC protein was eluted over a 0-500 mM NaCl gradient (Fig. 4-3). Successful NudC protein purification was confirmed by the well-separated bands of the protein ladder loaded in lane 1, aligning with the estimated size (27 kDa) of the NudC protein in lanes 7-13.

Figure 4-3| Purification of NudC DEAE Chromatography

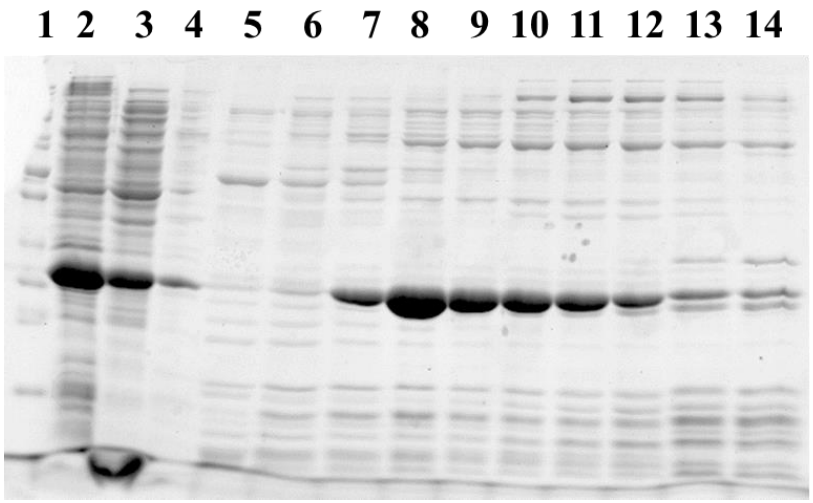

SDS gel electrophoresis of the fractions eluted over DEAE column. Lane 1: Pre-stained protein Marker, Lane 2: Crude Extract, Lane 3: Streptomycin sulfate supernatant, Lane 4: Streptomycin sulfate pellet, Lanes 5-14: DEAE fractions eluted with a 0-200 mM NaCl gradient.

4.3.2.3 Gel Filtration Chromatography

6.69 g of solid ammonium sulfate (50%) was added to 23 ml of the DEAE fraction containing the NudC protein, and the precipitate was collected by centrifugation and discarded. Next, 7.18 g of solid ammonium sulfate (90% saturation) was added to the supernatant and the precipitate containing the protein was dissolved in 7.5 ml of buffer A and loaded onto a Gel Filtration (GF) column. NudC was eluted with 50 mM Tris, 1 mM EDTA, 0.1 mM dithiothreitol, and 50 mM NaCl. The fractions containing the NudC protein (lanes 10-13) were combined, concentrated by ultrafiltration and stored at a final concentration of 74 μM (Fig. 4-4)..

Figure 4-4| Purification of NudC GF Chromatography

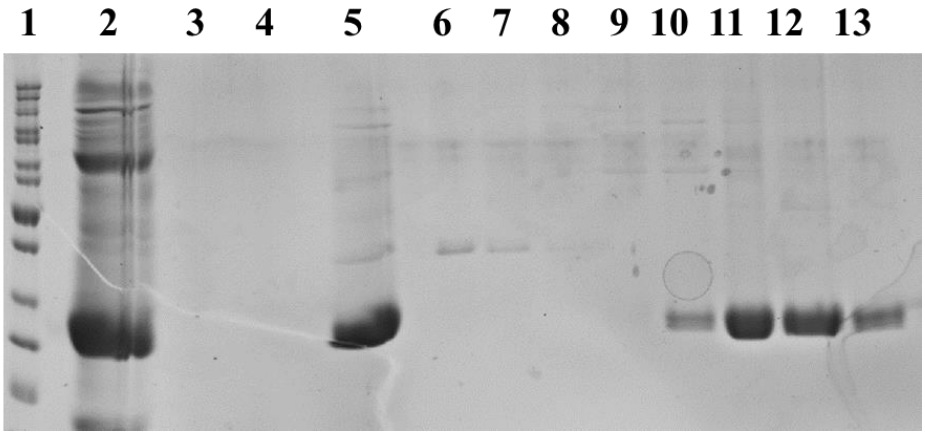

SDS gel electrophoresis of the fractions eluted over GF column. Lane 1: Pre-stained protein Marker, Lane 2: 50% ammonium sulfate pellet, Lane 5: 90% ammonium sulfate pellet, Lanes 6-13: GF fractions eluted with 50 mM NaCl.

4.3.3 Cloning NUDT12

NUDT12 gene was amplified using PCR from pCMV-NUDT12, with primers (OriGene Technologies Inc, Rockville, MD) containing *Bam*HI and *Nde*I restriction sites (underlined).

BamHI primer: 5′-GCG GCG G▾GA TCC TTA GAG ATT AGG ATT TAT TCT AAT CCA GTG-3′

NdeI primer: 5′-GCG GCG CA▴T ATG ATG TCT TCT GTA AAA AGA AGT CTG AAG CAA G-3′

The PCR product was then cut with NotI and ligated into a similarly digested pET33 plasmid (Novagen) (Fig. 4-5).

Figure 4-5| Plasmid map of pET33-NUDT12 construct
The NUDT12 insert (PCR product) was digested with *Nde*I and *Bam*HI and ligated into a similarly treated pET33 vector. The resulting construct was then transformed in DH5α cells for increased insert stability and subsequently into BL21 (DE3) cells for protein expression.

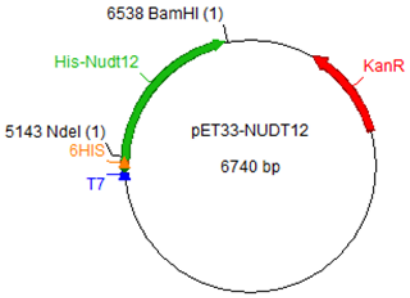

This is the first report to successfully express the human NUDT12 gene in a bacterial expression system, for successful protein purification.

4.3.4 Purification of Nudt12

Single colonies of strain BL21(DE3) cells harboring pET33-NUDT12 plasmid were inoculated into 3 ml of LB medium containing 100 µg/ml kanamycin. After the cells grew to an OD_{600} of 0.6, they were transferred to 1 liter of fresh medium containing kanamycin. After the cells reached an OD_{600} of 0.6 again, they were induced with 1 mM isopropyl-β-D-thiogalactoside (IPTG). The induced cells were harvested by centrifugation and the cell pellet was suspended in buffer A (20 mM Tris pH 8, 0.5 M NaCl, 5 mM imidazole), sonicated for 5 minutes and the crude extract was collected by centrifugation.

4.3.4.1 NiNTA Chromatography

The crude extract was loaded onto a 1 ml Ni-NTA column and the fractions were eluted over a 5-500 mM imidazole gradient (Fig. 4-6). Successful Nudt12 protein purification was confirmed by the well-separated bands of the protein ladder loaded in lane 1, aligning with the estimated size (52 kDa) of the Nudt12 protein in lanes 10-12.

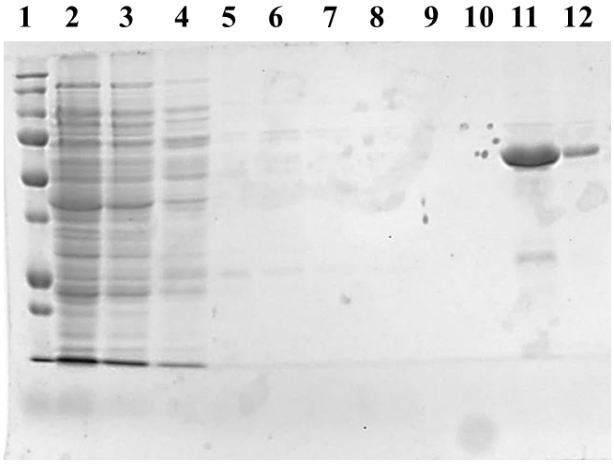

Figure 4-6| Purification of Nudt12 Ni-NTA Chromatography
SDS gel electrophoresis of the fractions eluted over Ni-NTA column, Lane 1: Pre-stained protein Marker, Lane 2: Flow Through, Lane 3: 5 mM Imidazole wash, Lane 4: 40 mM Imidazole wash, Lanes 5-8: Elutions with 40 mM Imidazole, Lanes 9-12: Elutions with 500 mM Imidazole.

4.3.4.2 Gel Filtration Chromatography

Nudt12 elutions collected over the Ni-NTA column with 500 mM Imidazole was loaded into a GF column and fractions were eluted with 50 mM Tris, 1 mM EDTA, 0.1 mM dithiothreitol,

and 50 mM NaCl. The fractions containing the Nudt12 protein were combined, concentrated by ultrafiltration and stored at a final concentration of 39 µM (Fig. 4-7).

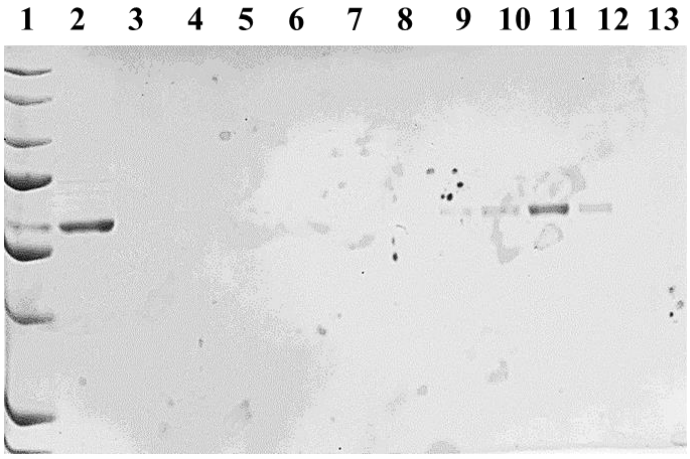

Figure 4-7| Purification of Nudt12 GF Chromatography
SDS gel electrophoresis of the fractions eluted over GF column, Lane 1: Pre-stained protein Marker, Lane 2: Load, Lanes 3-13: GF elutions with 50 mM NaCl.

4.3.5 Purification of Nudt1

Purchased plasmid containing NUDT1 were transformed into BL21 (DE3) cells for protein expression. Single colonies of these transformed cells were inoculated into 3 ml of LB medium containing 100 µg/ml Kanamycin. After the cells grew to an OD_{600} of 0.6, they were transferred to 1 liter of fresh medium containing Kanamycin. After the cells reached an OD_{600} of 0.6 again, they were induced with 1 mM isopropyl-β-D-thiogalactoside (IPTG). The induced cells were harvested by centrifugation and the cell pellet was suspended in buffer A (20 mM Tris pH 8, 0.5 M NaCl, 5 mM imidazole), sonicated for 5 minutes and the crude extract was collected by centrifugation.

4.3.5.1 NiNTA Chromatography

The crude extract was loaded onto a 1 ml Ni-NTA column and the fractions were eluted over a 5-500 mM imidazole gradient (Fig. 4-8). Successful Nudt1 protein purification was confirmed by the well-separated bands of the protein ladder loaded in lane 1, aligning with the estimated size (22 kDa) of the Nudt1 protein in lanes 7-12.

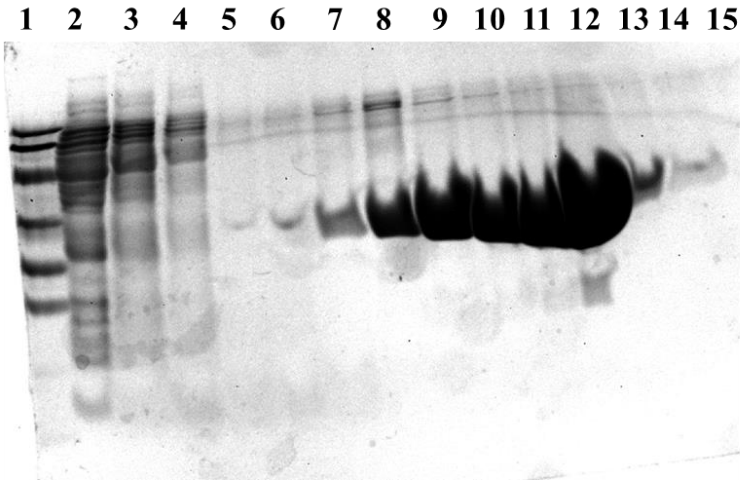

Figure 4-8| Purification of Nudt1 Ni-NTA Chromatography
SDS gel electrophoresis of the fractions eluted over Ni-NTA column, Lane 1: Pre-stained protein Marker, Lane 2: Flow Through, Lane 3: 5 mM Imidazole wash, Lane 4-5: Elutions with 5 mM Imidazole, Lanes 6-9: Elutions with 40 mM imidazole, Lanes 10-15: Elutions with 500 mM Imidazole.

4.3.5.2 Gel Filtration Chromatography

Elutions of Nudt1 (6 ml) collected over the Ni-NTA column with 40-500 mM Imidazole was loaded into a GF column and fractions were eluted with 50 mM Tris, 1 mM EDTA, 0.1 mM dithiothreitol, and 50 mM NaCl. The fractions containing the Nudt1 protein were combined and concentrated by ultrafiltration (Fig. 4-9).

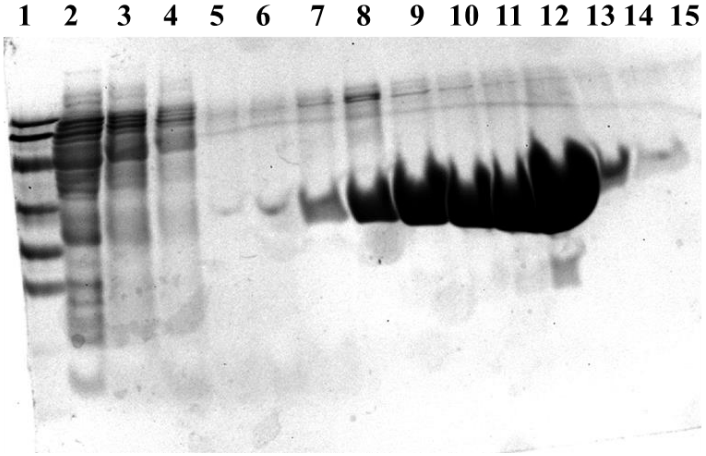

Figure 4-9| Purification of Nudt1 GF Chromatography
SDS gel electrophoresis of the fractions eluted over GF column, Lane 1: Pre-stained protein Marker, Lane 2-15: GF elutions with 50 mM NaCl.

4.3.6 Purification of NUDT3

Purchased plasmid containing NUDT3A were transformed into BL21 (DE3) cells for protein expression. Single colonies of these transformed cells were inoculated into 3 ml of LB medium containing 100 µg/ml Kanamycin. After the cells grew to an OD_{600} of 0.6, they were transferred to 1 liter of fresh medium containing kanamycin. After the cells reached an OD_{600} of 0.6 again, they were induced with 1 mM isopropyl-β-D-thiogalactoside (IPTG). The induced cells were harvested by centrifugation and the cell pellet was suspended in buffer A (20 mM Tris pH 8,

0.5 M NaCl, 5 mM imidazole), sonicated for 5 minutes and the crude extract was collected by centrifugation.

4.3.6.1 NiNTA Chromatography

The crude extract was loaded onto a 1 ml Ni-NTA column and the fractions were eluted over a 5-500 mM imidazole gradient (Fig. 4-10). Successful Nudt3 protein purification was confirmed by the well-separated bands of the protein ladder loaded in lane 1, aligning with the estimated size (20 kDa) of the Nudt3 protein in lanes 11-14.

Figure 4-10| Purification of Nudt3 Ni-NTA Chromatography
SDS gel electrophoresis of the fractions eluted over Ni-NTA column, Lane 1: Pre-stained protein Marker, Lane 2: Sonicated cells, Lane 3: Crude extract, Lane 4: Flow through, Lane 5: 5 mM Imidazole wash, Lane 6: 40 mM Imidazole wash, Lane 7-12: Elutions with 40 mM Imidazole, Lanes 13-15: Elutions with 500 mM Imidazole.

4.3.6.2 Gel Filtration Chromatography

Elutions containing the Nudt3A protein (5 ml) collected over the Ni-NTA column with 500 mM Imidazole was loaded into a GF column and fractions were eluted with 50 mM Tris, 1 mM EDTA, 0.1 mM dithiothreitol, and 50 mM NaCl. The fractions containing the Nudt1 protein were combined and concentrated by ultrafiltration (Fig. 4-11).

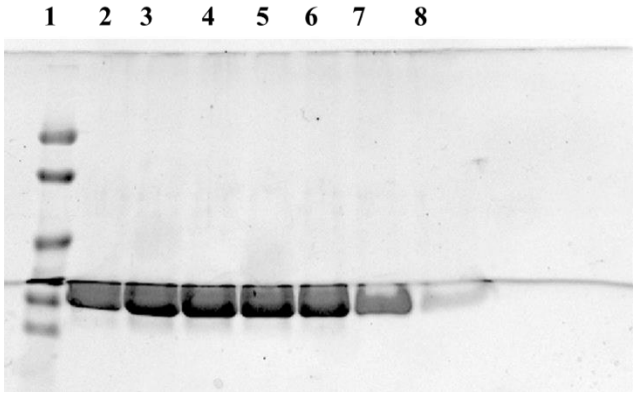

Figure 4-11 |Purification of Nudt3A GF Chromatography
SDS gel electrophoresis of the fractions eluted over GF column, Lane 1: Pre-stained protein Marker, Lane 2-8: GF elutions with 50 mM NaCl.

4.3.7 Purification of NUDT16

Purchased plasmid containing NUDT16 were transformed into BL21 (DE3) cells for protein expression. Single colonies of these transformed cells were inoculated into 3 ml of LB medium containing 100 µg/ml kanamycin. After the cells grew to an OD_{600} of 0.6, they were transferred to 1 liter of fresh medium containing kanamycin. After the cells reached an OD_{600} of 0.6 again, they were induced with 1 mM isopropyl-β-D-thiogalactoside (IPTG). The induced cells were harvested by centrifugation and the cell pellet was suspended in buffer A (20 mM Tris pH 8, 0.5 M NaCl, 5 mM Imidazole), sonicated for 5 minutes and the crude extract was collected by centrifugation.

4.3.7.1 NiNTA Chromatography

The crude extract was loaded onto a 1 ml Ni-NTA column and the fractions were eluted over a 5-500 mM Imidazole gradient (Fig. 4-12). Successful Nudt16 protein purification was confirmed by the well-separated bands of the protein ladder loaded in lane 1, aligning with the estimated size (21 kDa) of the Nudt16 protein in lanes 11-14.

Figure 4-12| Purification of Nudt16 Ni-NTA Chromatography

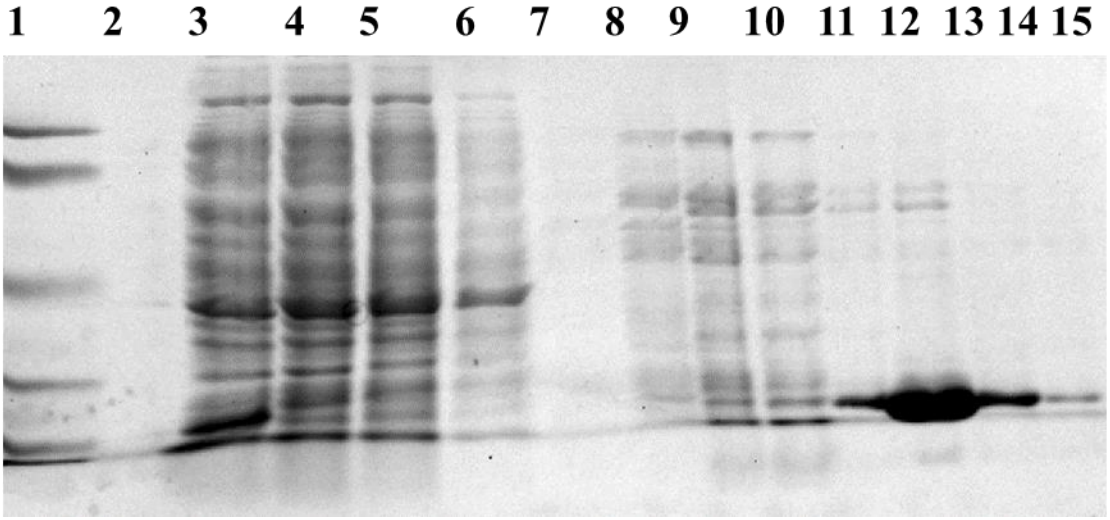

SDS gel electrophoresis of the fractions eluted over Ni-NTA column, Lane 1: Pre-stained protein Marker, Lane 3: Crude extract, Lane 4: Flow through, Lane 5: 5 mM Imidazole wash, Lane 6-7:

Elutions with 5 mM Imidazole, Lane 8-10: Elutions with 40 mM Imidazole, Lanes 11-15: Elutions with 500 mM Imidazole.

4.3.7.2 Gel Filtration Chromatography

Elutions containing the Nudt16 protein (3 ml) collected over the Ni-NTA column with 500 mM Imidazole was loaded into a GF column and fractions were eluted with 50 mM Tris, 1 mM EDTA, 0.1 mM dithiothreitol, and 50 mM NaCl. The fractions containing the Nudt16 protein were combined and concentrated by ultrafiltration (Fig. 4-13).

Figure 4-13| Purification of Nudt16 GF Chromatography

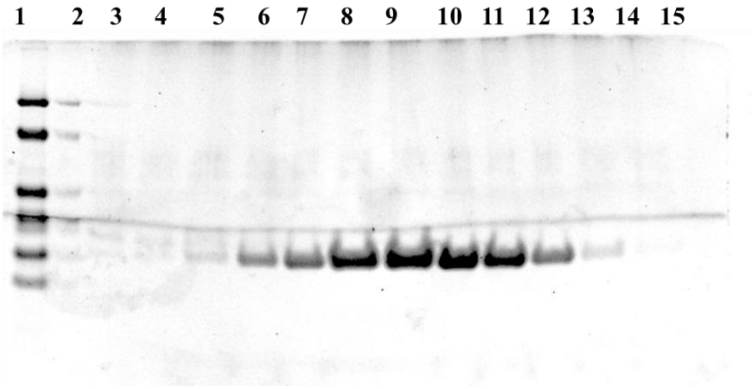

SDS gel electrophoresis of the fractions eluted over GF column, Lane 1: Pre-stained protein Marker, Lane 2-15: GF elutions with 50 mM NaCl.

4.3.8 Purification of NUDT20

Purchased plasmid containing NUDT20 was transformed into BL21 (DE3) cells for protein expression. Single colonies of these transformed cells were inoculated into 3 ml of LB medium containing 100 µg/ml Kanamycin. After the cells grew to an OD_{600} of 0.6, they were transferred to 1 liter of fresh medium containing Kanamycin. After the cells reached an OD_{600} of 0.6 again, they were induced with 1 mM Isopropyl-β-D-thiogalactoside (IPTG). The induced cells were harvested by centrifugation and the cell pellet was suspended in buffer A (20 mM Tris pH 8, 0.5

M NaCl, 5 mM Imidazole), sonicated for 5 minutes and the crude extract was collected by centrifugation.

4.3.8.1 NiNTA Chromatography

The crude extract was loaded onto a 1 ml Ni-NTA column and the fractions were eluted over a 5-500 mM Imidazole gradient (Fig. 4-14). Successful Nudt20 protein purification was confirmed by the well-separated bands of the protein ladder loaded in lane 1, aligning with the estimated size (49 kDa) of the Nudt20 protein in lanes 10-11.

Figure 4-14| Purification of Nudt20 Ni-NTA Chromatography

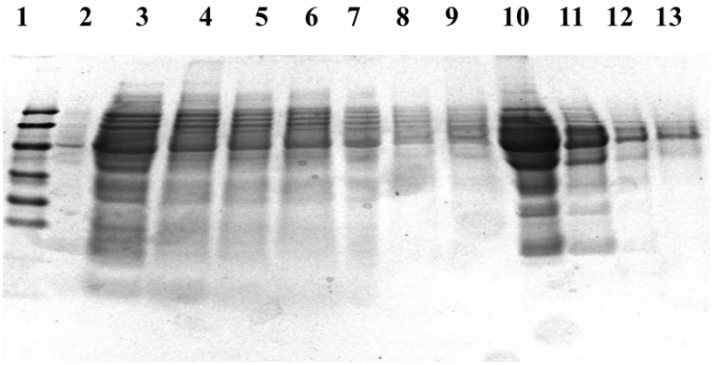

SDS gel electrophoresis of the fractions eluted over Ni-NTA column, Lane 1: Pre-stained protein Pre-stained protein Marker, Lane 2: crude extract, Lane 3: Flow through, Lane 4: 5 mM Imidazole wash Lanes 5-7: Elutions with 40 mM Imidazole, Lanes 8-13: Elutions with 500 mM Imidazole.

4.3.8.2 Gel Filtration Chromatography

Elutions containing the Nudt20 protein (2 ml) collected over the Ni-NTA column with 500 mM Imidazole was loaded into a GF column and fractions were eluted with 50 mM Tris, 1 mM EDTA, 0.1 mM dithiothreitol, and 50 mM NaCl. The fractions containing the Nudt20 protein were combined and concentrated by ultrafiltration (Fig. 4-15).

Figure 4-15| Purification of Nudt20 GF Chromatography

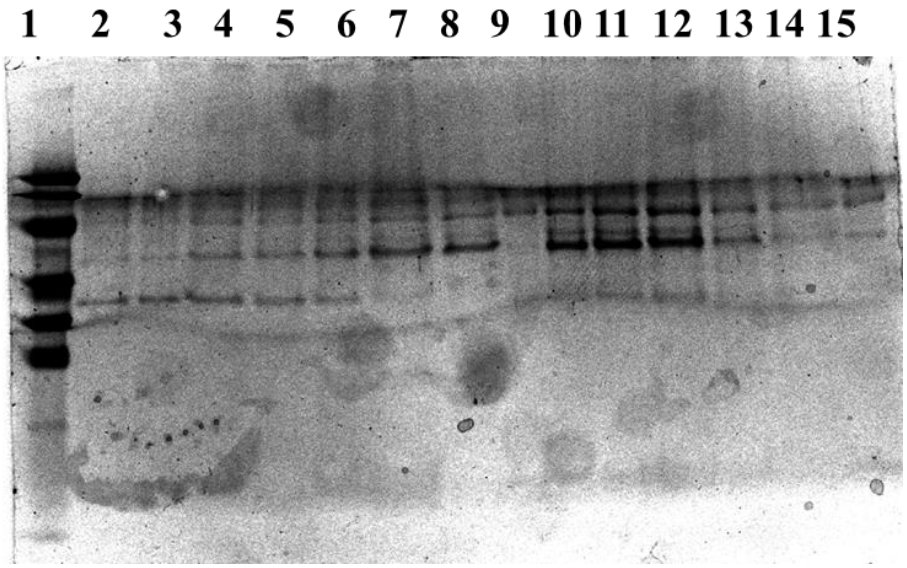

SDS gel electrophoresis of the fractions eluted over GF column, Lane 1: Pre-stained protein Pre-stained protein Marker, Lane 2-15: GF elutions with 50 mM NaCl.

Finally, all the purified and concentrated proteins were run on a denaturing SDS polyacrylamide gel (Fig. 4-16). I assume that the two bands for NudC, at ~ 25 kDa and ~ 50 kDa are because NudC exists as a homodimer.

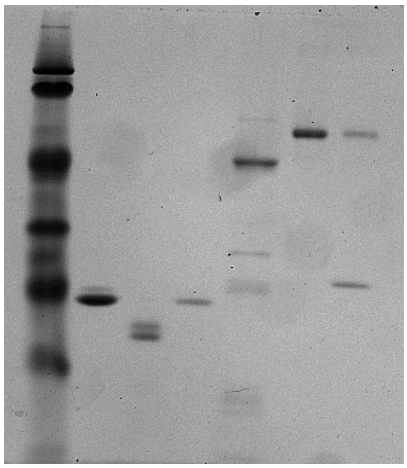

Figure 4-16| SDS PAGE of Nudix Proteins
Lane 1: Pre-stained protein Pre-stained protein Marker (120, 85, 50, 35, 25, 15 kDa), Lane 2: Nudt1 (0.1 µg), Lane 3: Nudt3A (0.1 µg), Lane 4: Nudt16 (0.1 µg), Lane 5 (0.1 µg): Nudt20 (Dcp2) (0.1 µg), Lane 6: Nudt12 (0.1 µg), Lane 7: NudC (0.1 µg).

4.4 Discussion

Clones expressing the human decapping Nudix proteins Nudt3, Nudt16 and Nudt20 were purchased and retransformed into BL21 (DE3) cells for protein expression. Nudt1, a Nudix proteins that does not bind nucleic acids, was also purchased from and

retransformed for successful protein expression. This is the first report of successfully cloning the human NAD-cleaving Nudt12 protein into a bacterial expression system. These mammalian Nudix proteins were purified using NiNTA chromatography, then gel filtration chromatography. The bacterial *nudC* gene was cloned from DH5α cells using colony PCR and the NudC protein was purified using DEAE chromatography, then gel filtration chromatography. All Nudix proteins were then concentrated using ultrafiltration and used for all future assays discussed in chapter 5 though chapter 9.

Chapter 5 NudC and Nudt12 cleave Toxic Dinucleotides

5.1 Summary

In this chapter, our data supports for the first time that NAD-cleaving Nudix hydrolases, bacterial NudC and its functional homolog in humans, Nudt12 may be 'housecleaning' enzymes, cleansing the cell of toxic isomeric forms of NADH. Our results suggest that both the bacterial and human NADH-cleaving nudix proteins can hydrolyze 6DHNAD, with the human Nudt12 protein preferring 6DHNAD considerably over NADH.

The HPLC-based assay described in this chapter is an alternative to the colorimetric assay usually used to test the activity of NAD-cleaving Nudix hydrolases. The colorimetric assay quantifies the activity of this class of proteins in a two-step protocol, first the Nudix hydrolase catalyzed cleavage of NAD to NMN and AMP and second, the release of inorganic phosphates from AMP by phosphatase. As suspected, this discontinuous colorimetric assay has its drawbacks. Also, the 6DHNAD, sourced from the Moran Lab, was purified in a phosphate rich buffer, making this assay even more challenging. Thus, we designed a more efficient protocol to study the activity of NADH-cleaving Nudix proteins on such toxic isomeric substrates.

Experiments were set up as described in Section 3.2.2.

5.2 Background

The Moran Lab (Beaupre et al., 2015) first discovered that isomeric forms of NAD(P)H molecules that are reduced at either the 2 or 6 position of the nicotinamide ring instead of the metabolically active 4-position arises from catalytic oxidation. Subsequently it was shown that this isomer of NADH, 6DHNAD is an inhibitor of several essential metabolic enzymes (Moran GR et al., 2017) and hence deemed as toxic NADH isomeric forms. *In vivo,* these isomers of β-NADH

were discovered unexpectedly as a substrate for the enzyme, renalase. *In vitro*, these isomeric forms of ß-NADH arise from its non-specific borohydride reduction, resulting in different positions of the hydride on either the 2 (2D(H)NAD) or the 6 (6DHNAD) position of the nicotinamide ring instead of the usual 4 position.

The *E. coli* genome encodes for the MutT pyrophosphohydrolase (or NudA) protein, the progenitor of the Nudix family (Treffers et al., 1954; Bhatnagar et al., 1988). This enzyme hydrolyzes both canonical and mutagenic nucleoside triphosphates, most commonly the toxic form of dGTP: 8-oxo-dGTP, preventing its misincorporation during DNA replication (Maki et al., 1992). Soon after, the *E. coli* genome was discovered to also encode for NudC (Frick et al., 1995) and its functional homolog Nudt12 in humans (Abdelraheim et al., 2003). They are members of a subclass of the Nudix protein family, that cleave dinucleotides, such as NADH, NAD(P)H, $NAD(P)^+$, ADP-ribose and AppA to yield two nucleoside monophosphates. This subclass of Nudix proteins are found to have a marked preference for the reduced form of NAD, NADH. It should be noted that for the regeneration of each molecule of NADH, the cell spends energy. Why the cell would express a protein that hydrolyzes not only an important cofactor in cellular metabolism but also an energy rich molecule has remained a mystery.

Similar to MutT (NudA), ever since the discovery of NADH-cleaving Nudix proteins, it has been suggested they may be involved in 'housecleaning activities' cleansing the cellular environment of potentially deleterious metabolites (Bessman et al., 1996). However, this hypothesis has never been tested.

5.3 Results

5.3.1 Both NADH and 6DHNAD are substrate for NudC and Nudt12

NADH-cleaving Nudix hydrolases cleave the phosphodiester bond in its substrate, NADH to yield two products, AMP and NMNH. Typical to this subclass of enzymes, this reaction is catalyzed in an alkaline environment and in the presence of divalent cations. To test the catalytic activity of this class of Nudix proteins on its substrates, colorimetric assays were set up to quantify the amount of phosphate hydrolyzed. Each reaction contained 1 mM DTT, 2 mM $MgCl_2$ and 1 mM NAD substrate incubated with ~ 40 μM Nudix protein NudC or Nudt12 at 37°C for 30 minutes. The volume was made up to 50 μl with 50 mM Tris pH8.5. Hydrolysis reactions were then terminated by boiling the sample at 100 °C for 2 minutes. 1 unit of Calf Intestinal Alkaline Phosphates (CIAP) sourced from ThermoFisher Scientific (Catalog no. 18009019) was added to the reaction mixture and incubated at 37°C for an additional 30 minutes. Fresh Malachite Green (MG) reagent was prepared, consisting of three parts of 0.045% solution of MG, 1 part of 4.2% solution of Ammonium Molybdate in 4.0 N HCl and 0.01 part ~ 10% Tween-20 solution. To quantify the amount of phosphate released, colorimetric assays were set up in 96-well plates containing MG reagent. 35% sodium citrate solution was added into each sample, almost immediately to raise the pH. A standard curve with various amounts of inorganic phosphate was measured with the freshly prepared MG reagent as well. OD at 625 nm was recorded for each well, on a Varian Cary 50 UV-Vis Spectrophotometer. Net phosphate released for each reaction was calculated using the standard curve. To calculate the amount of phosphate hydrolyzed, released phosphate concentrations was subtracted from the initial 2 mM phosphate concentration and normalized using GraphPad Prism (v.6). Each normalized response was plotted against substrate concentration and fit to the Michealis-Menten equation.

Figure 5-1| Effect of NAD-cleaving Nudix proteins on NAD substrates

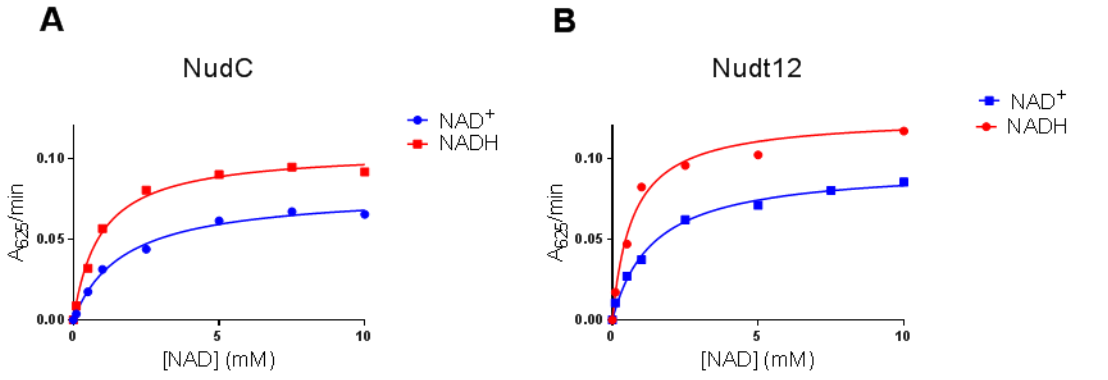

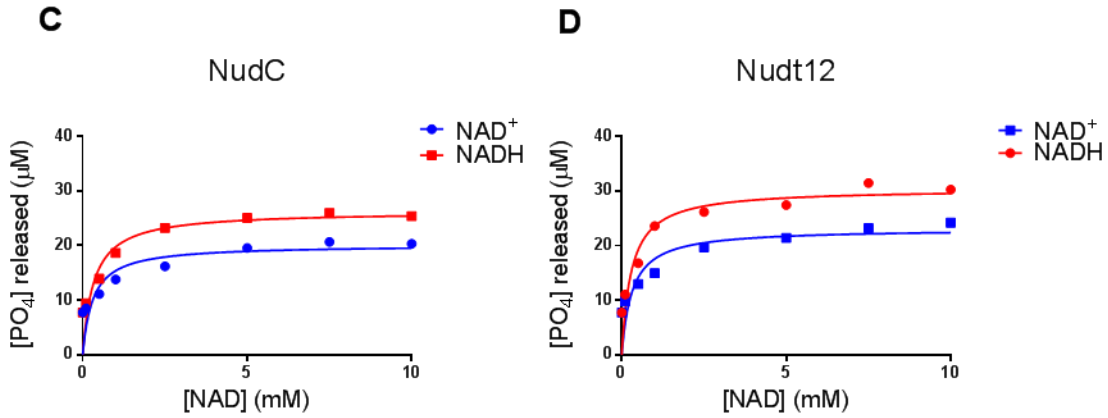

	NAD+	NADH
V_{max}	20	26
K_m	1.7	0.9

	NAD+	NADH
V_{max}	23	30
K_m	1.4	0.7

Various concentrations of either NAD^+ (blue) or NADH (red) ranging between 0.1 – 10 mM was incubated with 38 μM Nudix hydrolases, (A) NudC and (B) Nudt12 at 37 °C for 30 minutes, followed by another similar incubation with phosphatase. Absorbances of the complex formed was observed at 625 nm, divided by incubation time and plotted against NAD substrate concentration. The amount of phosphate released was then plotted for (C) NudC and (D) Nudt12 against substrate concentration and fir to a Michealis-Menten curve using GraphPad Prism v.6.

The amount of phosphate released from each reaction was calculated using the phosphate standard curve. Typical of NAD-cleaving Nudix proteins, both the bacterial NudC and the human Nudt12 preferred the reduced NAD substrate over its oxidized form. Similar experiments were set up with 6DHNAD. Since the 6DHNAD had been isolated under phosphate-rich conditions, the

initial OD at 625 nm, even without the addition of Nudix hydrolases was beyond the scope of this colorimetric assay. Since this assay failed to yield any definitive results for the NAD-cleaving hydrolytic activity of Nudix proteins on 6DHNAD, we proceeded to design a new assay using HPLC.

To correctly identify the samples on a HPLC chromatogram, standard solutions of 100 µM AMP, ADP, ATP, NADH and 6DHNAD were made up to a total volume of 50 µl and injected into a Waters Xterra C18 cartridge column (4.6 × 150 mm^2) run isocratically at 1 ml/min with 10 mM Phosphate buffer pH7.5, coupled to a waters 600E pump and Waters 2487 detector. The elution of each sample was observed at both 260 and 340 nm (Fig. 5-2A).

Figure 5-2| HPLC Standards

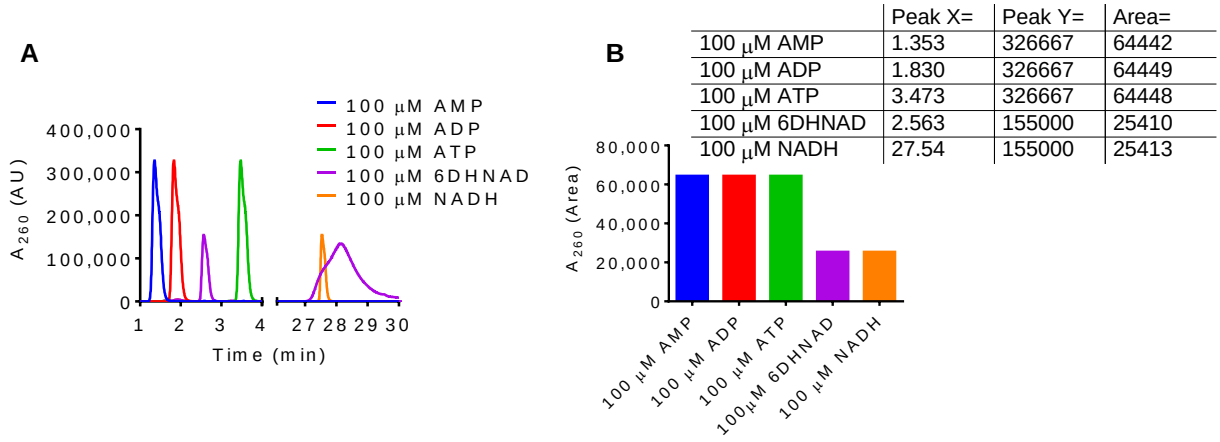

	Peak X=	Peak Y=	Area=
100 µM AMP	1.353	326667	64442
100 µM ADP	1.830	326667	64449
100 µM ATP	3.473	326667	64448
100 µM 6DHNAD	2.563	155000	25410
100 µM NADH	27.54	155000	25413

(A) Retention and absorbance of 100 µM solutions of AMP (blue), ADP (red), ATP (green), 6DHNAD (purple) and NADH (orange) at 260 nm (B) Area under the curves of each peak from (A) were plotted against their sample name and will be used to quantify the rate of substrate depletion using GraphPad Prism (v.6).

It should be noted that the chromatogram of 100 µM 6DHNAD (purple) is identical to that observed for 100 µM 6NMNH, with a peak absorbance at 2.56 mins and 28.1 mins elution time (Fig. 5-2A). The initial peak at 2.56 min is not characteristic of 6DHNAD. Areas under each peak

on the chromatogram was quantified using GraphPad Prism (v.6) and plotted against sample name (Fig. 5-2B). The retention time of each sample has been recorded under peak X.

To quantify the rate of product formation, serially diluted concentrations of the product, AMP was run under identical conditions for standardization. The elution of each sample elution was observed at 260 nm (Fig. 5-3A).

Figure 5-3| AMP Standard on HPLC

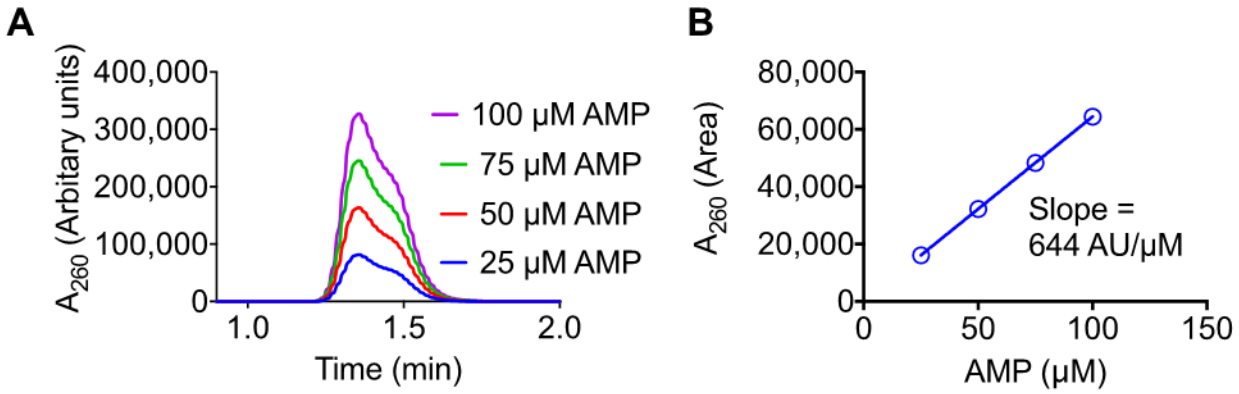

(A) 25 µM (blue) , 50 µM (red), 75 µM (green) and 100 µM (purple) of AMP were run on the HPLC under identical conditions and elution of the components was monitored at 260 nm (B) Areas under the curve for each sample from (A) eluting at 1.36 minutes was plotted against concentration to obtain a standard curve using GraphPad Prism (v.6).

It is assumed that the perfect linear response observed in the standard curve for AMP may be replicated for standardizing NADH (Fig. 5-3B).

1 µM NADH was incubated with 74 nM NudC at 37 °C, in the presence of 2 mM $MgCl_2$ and 1 mM DTT made up to a final volume of 500 µl with 50 mM Tris pH8.5. 50 µl was removed from the reaction mixture at varying time points, ranging from 5-30 minutes and run on the HPLC under identical conditions (Fig. 5-4A). The elution of components was observed at 260 nm for quantification of NADH depletion, eluting at 28.1 minutes and AMP formation, eluting at 1.3 minutes, both consistent with the sample standardization (Fig. 5-4B).

Figure 5-4| Time course HPLC assay of NudC hydrolysis of NADH

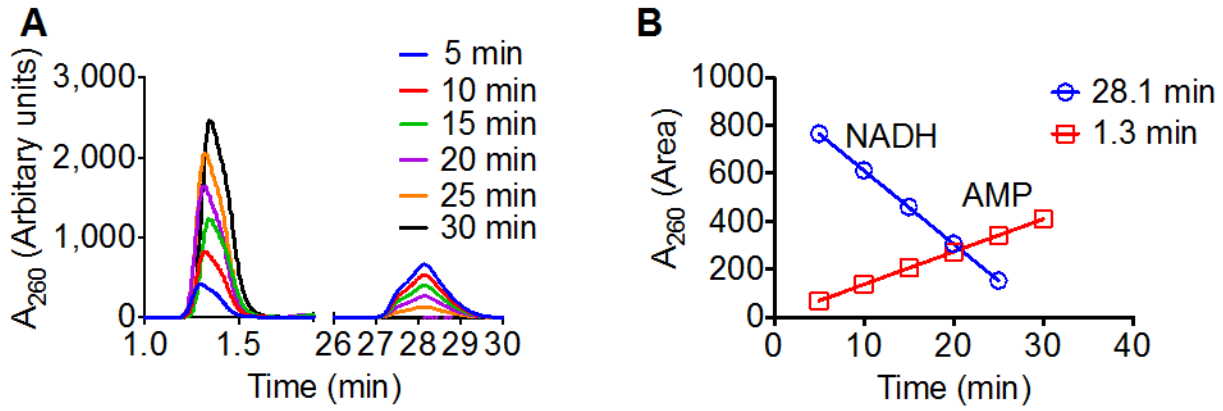

(A) 1 µM ß-NADH incubated with 74 nM NudC at 37°C. 50 µl of the reaction mixture was taken out at varying time points and run on the HPLC. The elution of products was observed at 260 nm (B) The area under the curves for the substrate, ß-NADH at 28.1 min elution time (blue) and product, AMP at 1.3 min elution time (red) were plotted using GraphPad Prism (v.6).

Similarly, 1 µM 6DHNAD was incubated with 74 nM NudC under otherwise identical conditions as described above (Fig. 5-5A). The elution of components was observed at 260 nm for quantification of 6DHNAD depletion (Fig. 5-5B), eluting at 28.1 minutes and AMP formation, eluting at 1.3 minutes. The second product from NudC hydrolytic cleavage, 6NMNH also absorbs at 260 nm and elutes at 2.6 minutes (Fig. 5-5A).

Figure 5-5| Time course HPLC assay of NudC hydrolysis of 6DHNAD

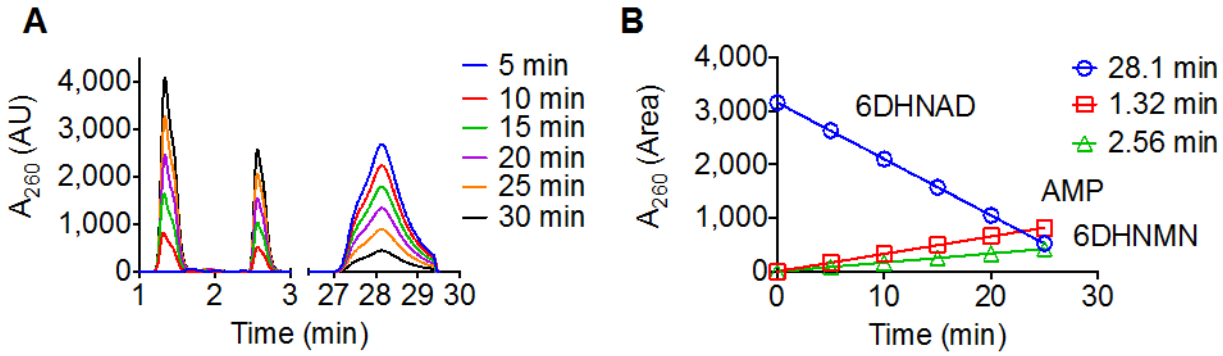

(A) 1 µM 6DHNAD was incubated with 74 nM NudC at 37°C. 50 µl of the reaction mixture was taken out at varying time points and run on the HPLC. The elution of products was observed at 260 nm (B) The area under the curves for the substrate, 6DHNAD at 28.1 min elution time (blue)

and product, AMP at 1.3 min elution time (red) and 6DHNMN at 2.56 min elution time (green)were plotted using GraphPad Prism (v.6).

This experiment was the first evidence of enzymatic activity of NADH-cleaving Nudix hydrolases on toxic isomeric forms of NADH.

Confirming that the NAD-cleaving NudC has hydrolytic activity on 6DHNAD, we quantified the disappearance of the substrates, NADH and 6DHNAD (Fig. 5-6A) and the rate if appearance of product, AMP (Fig. 5-6B) with incubation time. Quantification for each was done using areas under the curve. Surprisingly, it was demonstrated that the rates for both substrate disappearance and product appearance was almost three folds higher for the isomeric form, 6DHNAD compared to the canonical substrate of the enzyme, NADH.

Figure 5-6| Analysis of HPLC analysis of NudC hydrolysis

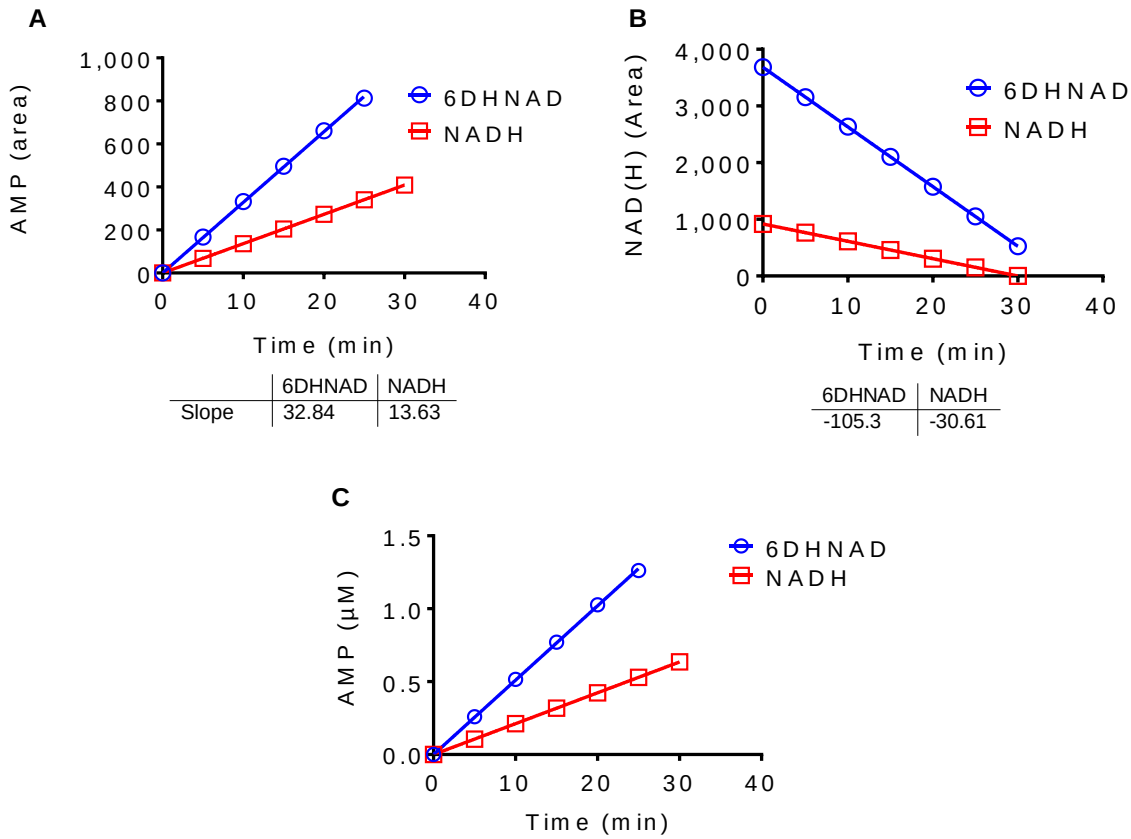

	6DHNAD	NADH
Slope	32.84	13.63

6DHNAD	NADH
-105.3	-30.61

(A) Areas under the curve for the substrate disappearance were plotted against incubation time and the slopes were calculated using GraphPad Prism (v.6). It was observed to be almost three folds higher for 6DHNAD (105 A_{260}units min^{-1}) over NADH (31 A_{260}units min^{-1}) (B) Areas under the curve for product, AMP, formation transformed to (C) concentration (µM) were plotted against incubation time and the slopes were calculated using GraphPad Prism (v.6). Each slope is an indication of the rate at which product is formed, calculated using GraphPad Prism (v.6). AMP formation was observed to be more than two folds higher for 6DHNAD (33 A_{260}units min^{-1}) over NADH (14 A_{260}units min^{-1}).

Confirming the activity of NudC on 6DHNAD, varying concentrations of the substrate was incubated with 74 nM NudC at 37 °C, in the presence of 2 mM $MgCl_2$ and 1 mM DTT made up to a final volume of 500 µl with 50 mM Tris pH8.5. Each reaction was terminated at 10 mins of incubation and the samples were treated as described above to filter out the protein and injected into the instrument under identical conditions. Varying concentrations of NADH (Fig. 5-7A) and

6DHNAD (Fig. 5-7B) ranging from 0.78 to 100 µM was incubated with NudC and the elutions of samples were observed at 260 nm. Surprisingly, both substrates NADH and 6DHNAD eluted at a similar time point, ~ 28 minutes. Products from each reaction was quantified using area under curve and plotted against substrate concentration for both NADH (blue) and 6DHNAD (red) (Fig. 5-5C). Fitting the data to a Michealis-Menten equation yielded similar V_{max} values, but an almost two-times lower K_m for 6DHNAD compared to NADH.

Figure 5-7| HPLC assay of NudC hydrolysis of NADH and 6DHNAD

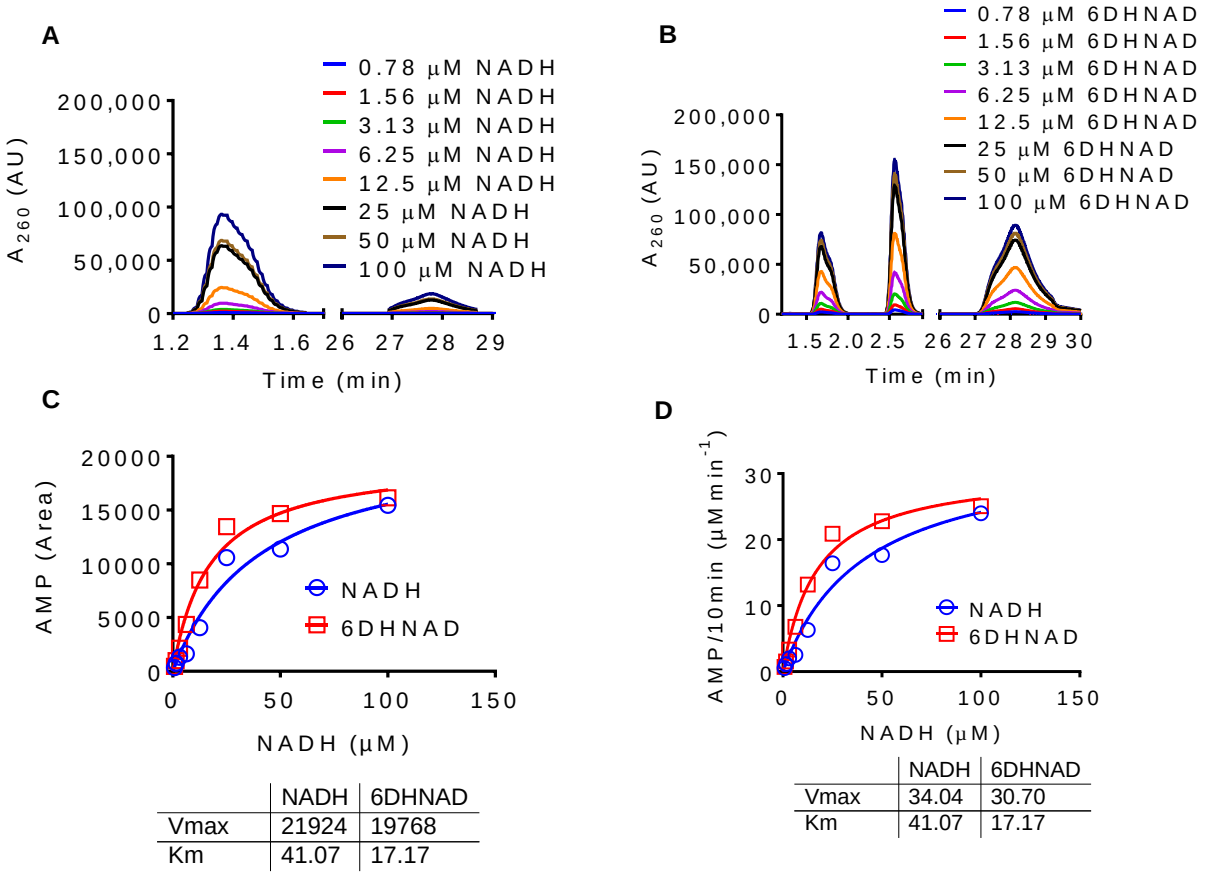

	NADH	6DHNAD
Vmax	21924	19768
Km	41.07	17.17

	NADH	6DHNAD
Vmax	34.04	30.70
Km	41.07	17.17

Serially diluted concentrations of 100 µM (A) NADH and (B) 6DHNAD was incubated with 74 nM NudC at 37°C for 10 minutes. The elution of components was observed at 260 nm, the substrate NADH and at 28.1 min elution time and product, AMP at 1.3 min elution time and 6NMNH at 2.56 min elution time (C) The areas under the curve for the product (D) transformed

to AMP concentration were plotted against substrate concentration and fit to the Michaelis-Menten equation using GraphPad Prism (v.6) to obtain a V_{max} and K_m.

HPLC analysis of both substrates, NADH and 6DHNAD hydrolyzed by NudC revealed comparable V_{max} values (2.1 vs 2.0 (x 10^4) units), while a two-fold higher K_m for NADH (41 µM) was observed compared to 6DHNAD (17 µM) (Fig. 5-5C). Whether either isomer of NADH is a more preferable substrate for NudC cannot be concluded from this experiment. The reproducibility of this assay along with the precise quantitation of substrates and products is still to be determined.

Next, we tested the hydrolytic activity of Nudt12, the human NADH-cleaving Nudix hydrolase on NADH and its toxic isomer, 6DHNAD. Varying concentrations of the substrate was incubated with 38.5 nM Nudt12 at 37 °C, in the presence of 2 mM $MgCl_2$ and 1 mM DTT made up to a final volume of 500 µl with 50 mM Tris pH8.5. Each reaction was terminated at 10 mins of incubation and the samples were treated as described above to filter out the enzyme and injected into the instrument under identical conditions.

Varying concentrations of NADH (Fig. 5-8A) and 6DHNAD (Fig. 5-8B) ranging from 0.78 to 100 µM was incubated with the human Nudt12 protein and the elutions of samples were observed at 260 nm. Products from each reaction was quantified using area under curve and plotted against substrate concentration for both NADH (blue) and 6DHNAD (red) (Fig. 5-5C). Fitting the data to a Michealis-Menten curve yielded similar v_{max} values, but a surprising five-folds lower km for 6DHNAD compared to NADH.

Figure 5-8| HPLC assay of Nudt12 hydrolysis of NADH and 6DHNAD

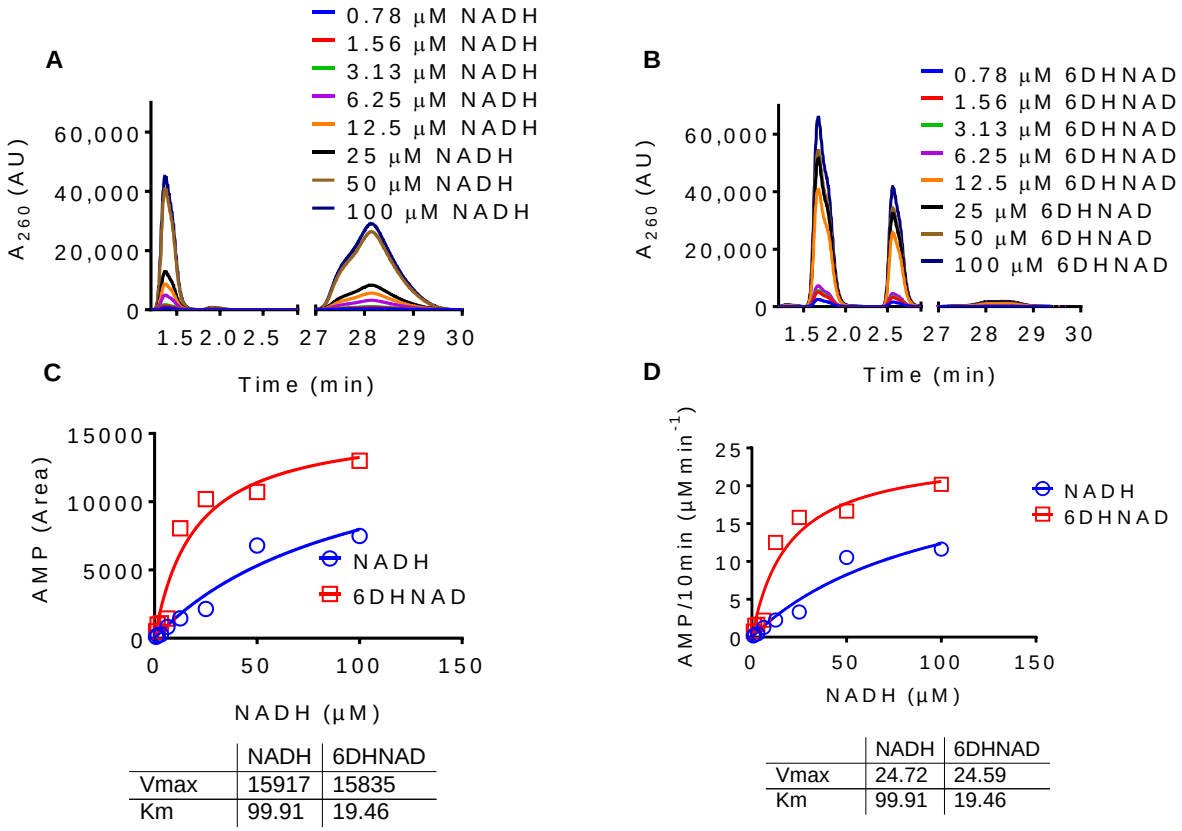

	NADH	6DHNAD
Vmax	15917	15835
Km	99.91	19.46

	NADH	6DHNAD
Vmax	24.72	24.59
Km	99.91	19.46

Serially diluted concentrations of 100 µM (A) NADH and (B) 6DHNAD was incubated with 38.5 nM Nudt12 at 37°C for 10 minutes. The elution of components was observed at 260 nm, the substrate NADH and at 28.1 min elution time and product, AMP at 1.3 min elution time and 6NMNH at 2.56 min elution time (C) The areas under the curve for the product were (D) transformed to concentration (µM) and plotted against substrate concentration and fit to a Michaelis-Menten plot using GraphPad Prism (v.6) to obtain a V_{max} and K_m.

In case of the human NADH-cleaving Nudix hydrolase, Nudt12 similar V_{max} values (15,000 A_{260} Units min^{-1}) were observed, with an impressive five-fold difference in K_m for NADH (100 µM) over 6DHNAD (19 µM) (Fig. 5-8C). The difference in the kinetic parameters may not be enough to conclude that 6DHNAD is a more preferred substrate for Nudt12 over NADH *in vivo* just yet. Reproducibility and precision of this HPLC-based assay is still to be determined.

5.4 Discussion

The purpose of NAD-cleaving activity of an energy-rich molecule of Nudix hydrolases has always been a concern. This chapter is the first report of experimental evidence of the hydrolytic 'housecleaning' activity of bacterial NudC and human Nudt12 on the toxic isomer of NADH. Moran et al., demonstrated the renalase catalyzed reduction of NADH to both 2DHNAD and 6DHNAD. However, it was only hypothesized that renalase may oxidize these inhibitory isomers of NADH to form NAD^+. Whether these isomers exist *in vivo* is still to be determined. This study shows that NAD-cleaving Nudix proteins have a strong preference to hydrolyze the toxic isomers, over NADH, displaying a clear biochemical role for this class of Nudix enzymes.

Chapter 6 A Continuous Assay to Monitor NADH Hydrolysis

6.1 Summary

Since the foundation of this project, we wanted to design a more continuous approach to study the activity of NAD-cleaving Nudix proteins on its substrates. NADH is a fluorescent molecule, with a fluorescence emission at 460 nm, when excited at both 260 nm and 340 nm. Bacterial NAD-cleaving Nudix hydrolase, NudC cleaves the phosphodiester bond in its substrate to yield AMP, which has an absorbance maximum at 260 nm and NMNH, with an absorbance maximum at 340 nm. In this chapter, we designed a continuous assay to observe the hydrolytic cleavage of NADH, using its fluorescent properties.

In this chapter, we also designed a novel Fluorescence Ratiometric (FR)-based assay to test the hydrolytic activity of NADH-cleaving Nudix hydrolases on the toxic isomeric form of NADPH, 6DHNADP. 6DHNADP too, like 6DHNAD, was purified under phosphate rich conditions making the previously discussed colorimetric assay challenging. 6DHNADP too has a fluorescence emission at 460 nm, albeit relatively low compared to canonical NADH, when excited at 260 nm and 345 nm. The low fluorescence of the toxic isomer made the continuous fluorescence-based assay difficult as well. Hence, we designed a novel FR-based assay to study the interaction between the donor fluorescent molecule, in this case NADH and its acceptor fluorescent competitor, 6DHNADP.

Although this chapter may not quantify the kinetics of the reaction between 6DHNADP and NudC, this new assay could be used to study the energetics of protein: ligand interactions.

All experiments were set up as described in Section 3.2.3.

6.2 Background

Isomeric forms, the 2-dihyhdroNAD (2DNADP) and 6- dihydroNAD (6DHNADP) differs from β-NADPH in the position of the hydride on the nicotinamide moiety. These non-canonical substrates have been identified as a substrate for the renalase protein, *in vivo.* It has been demonstrated that these molecules can arise from non-specific borohydride reduction of β-NADP+ or tautomerization of β-NADPH, *in vitro*.

6.3 Results

6.3.1 A continuous fluorescence assay to monitor NADH hydrolysis

50 µM NADH was incubated either 37 nM and 74 nM NudC at 37°C for 30 minutes, in the presence of 2 mM $MgCl_2$ and 1 mM DTT made up to a final volume of 500 µl with 50 mM Tris pH 8.5. A change in the fluorescence excitation spectrum (230-450 nm) was observed (Fig. 6-1), when fluorescence emission wavelength was set to 460 nm. With the formation of products and depletion of substrate as NudC cleaved NADH, a considerable decrease in fluorescence excitation at 260 nm was observed. The change in fluorescence excitation at 340 nm was assumed to be insignificant, compared to the decay in the excitation spectra at 260 nm.

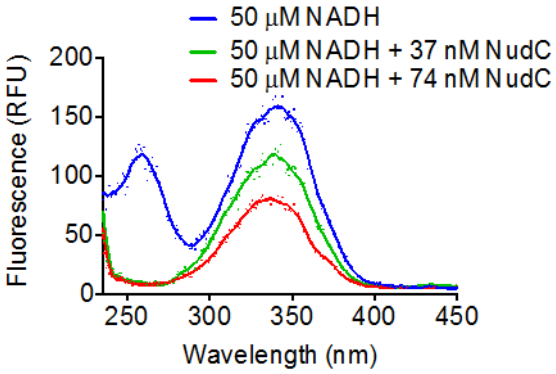

Figure 6-1| Excitation spectra of NADH ± NudC
Excitation spectra of 50 µM NADH (blue), or NADH incubated with 37 nM (green) and 74 nM (red) NudC, when emission wavelength is 460 nm. The data was collected on a Cary Eclipse fluorescence spectrophotometer with Ex/Em slit widths of 5 nm/5 nm.

Next, we examined the kinetics of this fluorescence change to monitor the enzymatic activity of NudC on NADH. 50 µM NADH was incubated with 37 nM NudC at 37 °C for 30 minutes, in the presence of 2 mM $MgCl_2$ and 1 mM DTT made up to a final volume of 500 µl with 50 mM Tris pH 8.5. Fluorescence excitation of the

reaction mixture was observed when emission wavelength was 460 nm, on Varian Cary Eclipse Fluorescence Spectrophotometer with Em/Ex Slit widths 5/10 nm. A decrease in fluorescence excitation at 260 nm was observed as the substrate depleted and led to product formation, when fluorescence emission was set at 460 nm. The fluorescence excitation at 340 nm did not change significantly (Fig. 6-2). This was a novel assay that observed the continuous depletion of NADH by Nudix hydrolysis.

Figure 6-2| Time dependent effect of NudC on NADH fluorescence

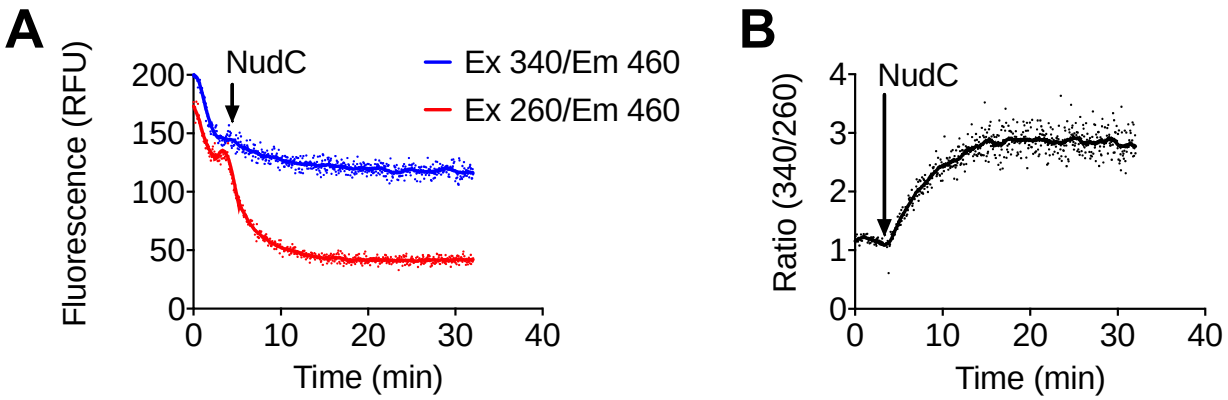

(A) The emission spectra at 460 nm, when 50 µM NADH is incubated with 37 nM NudC. The sample is excited at two wavelengths, 260 nm (red) and 340 nm (blue). The data was collected on a Cary Eclipse fluorescence spectrophotometer with Ex/Em slit widths of 5 nm/5 nm. Lines are smooth curves generated by GraphPad Prism (v.6) (B) The ratio of the fluorescence emissions at 340 nm and 260 nm is plotted against incubation time to observe an increase in the ratio (340/260)

Since a decay in the fluorescence intensities when excited at both wavelengths is observed, a ratio of the two fluorescence intensities with incubation gives a better measure of product formation. The intensity when excited at 340 nm is assumed to be comparatively stable compared to when the sample is excited at 260 nm, with product formation. Hence, with progressing incubation time, the ratio (340/260) continues to increase.

6DHNADP was obtained from Dr. Graham Moran's lab. *In vitro*, it was synthesized in a phosphate rich buffer, making Nudix hydrolase cleavage analysis using colorimetric assays

challenging. We proceeded to use this newly designed fluorescence assay to quantify the enzymatic activity of NADH-cleaving Nudix hydrolases on 6DHNADP. To initiate these experiments, a UV absorbance, excitation (Em. wavelength= 460 nm) and emission (Ex. Wavelength= 345 nm) spectra of 50 µM 6DHNADP was recorded on Varian Cary Eclipse Fluorescence Spectrophotometer with Em/Ex Slit widths set to 5/10 nm. In comparison, the same was done for 50 µM NADH, with excitation wavelength= 340 nm and emission wavelength= 460 nm (Fig. 6-3).

Figure 6-3| Optical properties of 6DHNADP

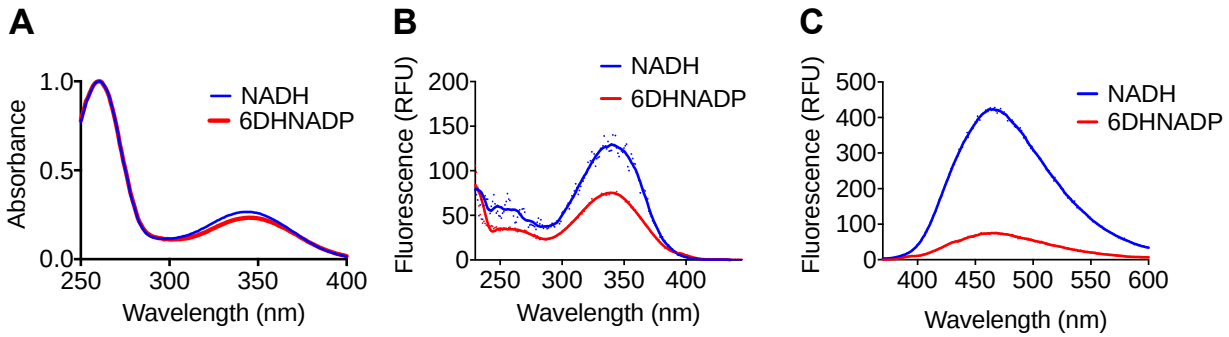

(A) Absorbance spectra (B) Excitation spectra when em. wavelength= 460 nm and (C) Emission spectra when ex. Wavelength of 340 nm for NADH and 345 nm for 6DHNADP of 50 µM ß-NADH (red) and 6DHNADP (blue). Lines are smooth curves generated by GraphPad Prism (v.6).

Even though the UV absorbances of the two substrates are comparable, the fluorescence excitation and emission of 6DHNADP were considerably lower compared to the canonical substrate, NADH. To further test the hydrolytic activity of NudC on 6DHNADP, reaction mixtures containing 250 µM 6DNAD was incubated with 37 nM and 74 nM NudC at 37°C for 30 minutes, in the presence of 2 mM $MgCl_2$ and 1mM DTT, made up to a total volume of 500 µl with 50 mM TrisCl pH8.5. Fluorescence emission spectra was collected on Varian Cary Eclipse Fluorescence Spectrophotometer with Em/Ex Slit widths set to 5/10 nm, when excitation wavelength= 345 nm (Fig. 6-4A).

Figure 6-4| Emission spectra of 6DHNADP ± NudC

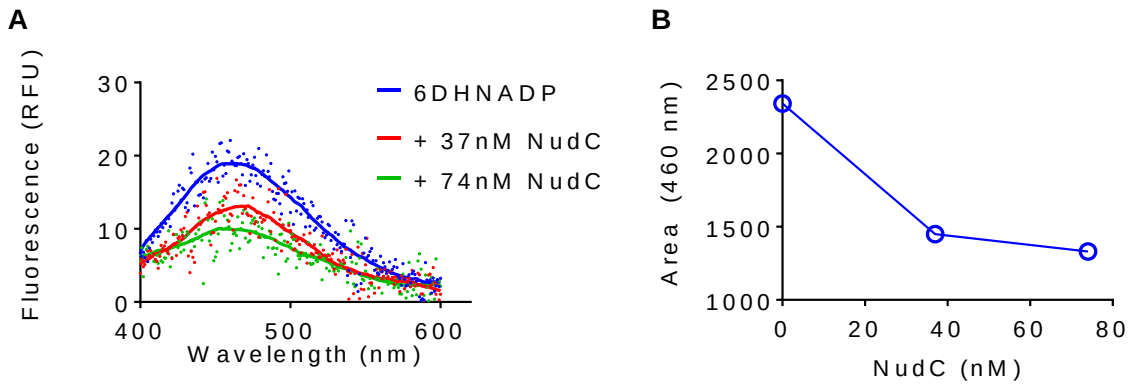

(A) Emission spectra of 50 µM 6DHNADP (blue), incubated with 37 nM (red) and 74 nM (green) NudC, when excitation wavelength= 345 nm. Since the fluorescence emission decay of the raw data did not look impressive, (B) Area under curves were plotted against concentration of enzyme using GraphPad Prism (v.6) to show the hydrolytic activity of NudC on 6DHNADP.

The fluorescence emission at 460 nm decayed with substrate depletion and product formation (Fig. 6-4B), however not significantly as the fluorescence emission of the substrate was considerably low to begin with.

Having confirmed that NudC has enzymatic activity on 6DHNADP, we repeated the continuous fluorescence assay as described above, to monitor its hydrolysis. 50 µM 6DHNADP was incubated with 37 nM NudC at 37°C for 30 minutes, in the presence of 2 mM $MgCl_2$ and 1 mM DTT made up to a final volume of 500 µl with 50 mM Tris pH 8.5. Fluorescence excitation of the reaction mixture was observed when emission wavelength= 460 nm, on Varian Cary Eclipse Fluorescence Spectrophotometer with Em/Ex Slit widths set to 10/10 nm. Even with product formation, we failed to observe any significant change in the fluorescence excitation at 260 nm and 345 nm, when fluorescence emission was set at 460 nm (Fig. 6-5), for initial time points. However, when the substrate was incubated with NudC for 30 minutes, a decay in the emission spectrum was observed.

Figure 6-5| Effect of NudC on 6DHNADP fluorescence
The excitation spectra of 50 µM 6DHNADP incubated with 37 nM NudC. Excitation at 260 nm (red) and 345 nm (blue) was observed when emission wavelength= 460 nm. Lines are smooth curves generated by GraphPad Prism (v.6). 12 nM NudC was added at each time point, although no visible change was observed in the emission spectrum.

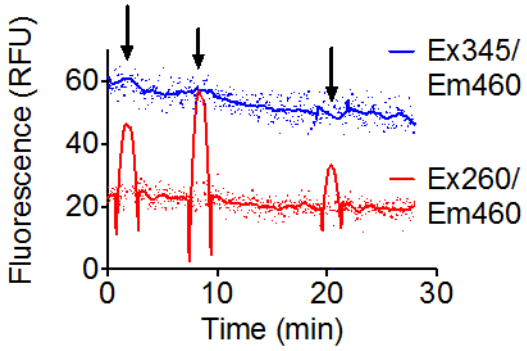

Since 6DHNADPH did not have an impressive fluorescence emission and the assay could not be used for kinetic analysis of NudC activity on 6DHNADP, we designed another assay exploiting fluorescence to check for Nudix hydrolytic activity on 6DHNADP.

6.3.2 Competitive inhibition by 6DHNADP

As the Nudix hydrolases acted on the substrate, a decrease in fluorescence emission (Ex. Wavelength= 260 nm) was observed with the production of NMNH. Two identical cuvettes were set up for this assay, each containing 50 µM NADH and 74 nM NudC at 37°C, in the presence of 2 mM $MgCl_2$ made to a final volume 500 µl with 50 mM Tris pH8.5. Following a very brief incubation period, varying concentrations of 6DHNADP was added to one cuvette, while equal volumes of water was added to rule out Inner Filter Effect. The emission spectrum at 460 nm was collected on Varian Cary Eclipse Fluorescence Spectrophotometer with Em/Ex Slit widths set to 5/10 nm, when excited at both 260 nm and 340 nm. The hypothesis was confirmed as the fluorescence emission continued to decay for the first cuvette compared to that of the negative control, which remained constant (Fig. 6-6A).

Inner Filter Effect was accounted for and the raw fluorescence data was corrected using equation 3:

$$F_{corr} = F_{obs}\, 10^{\frac{Aex+Aem}{2}} \qquad \text{(Eq. 3)}$$

Where F_{obs} and F_{corr} is the fluorescence emission before and after it has been corrected for inner filter effect respectively, A_{ex} and A_{em} are absorbance at 260 nm and 460 nm respectively (Fig. 6-6B).

Figure 6-6| Effect of 6DHNADP on NudC-induced NADH fluorescence changes

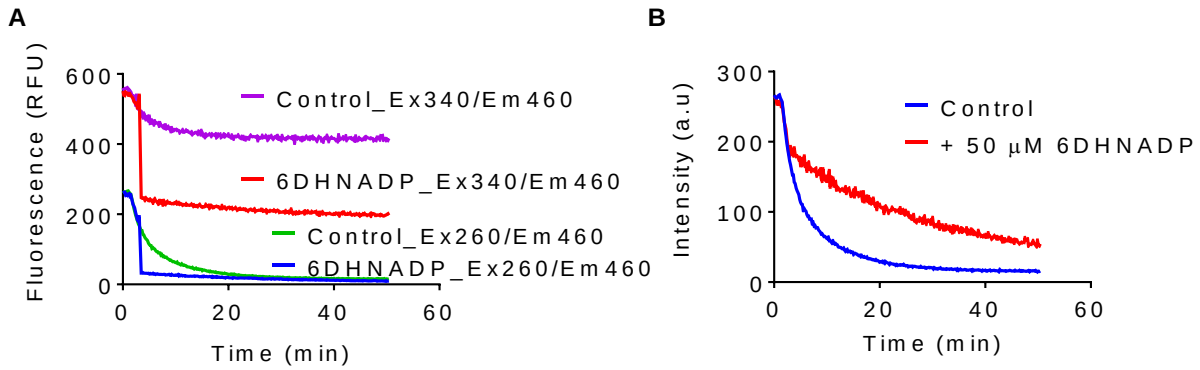

(A) Continuous fluorescence assay, monitoring the excitation spectra of 50 µM NADH incubated with 37 nM NudC at 37°C. After ~2 mins of incubation time, 12.5 µM 6DHNADP was added to one cuvette and its fluorescence excitation at 260 nm (blue) and 340 nm (red) was observed. Equal volume of water was added to the other (control) cuvette, and excitation at 260 nm (green) and 340 nm (purple) was observed when emission wavelength= 460 nm (B) The raw fluorescence excitation data at 260 nm was corrected for inner filter effect as described above.

Next, the change in fluorescence (ΔF) was calculated between the two excitation wavelengths, 260 nm and 340 nm for the above experiment, by taking the difference between the two values, using GraphPad Prism (v.6). Change in fluorescence, ΔF was then plotted against incubation time (Fig. 6-7A) and corrected for inner filter effect using Eq. 3 (Fig. 6-7B), also plotted against incubation time.

Figure 6-7| Normalized Effect of 6DHNADP on NudC-induced NADH fluorescence

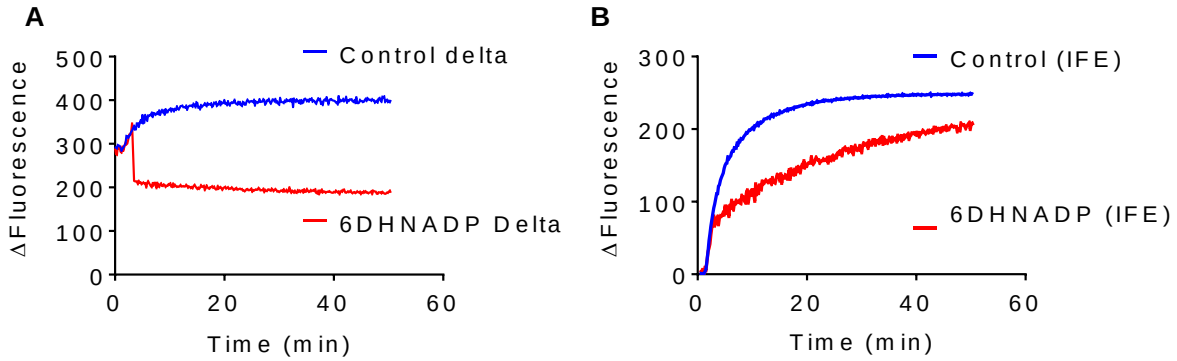

(A) ΔF was plotted against incubation time for both the reaction inhibited with 6DHNADP (red) and the control reaction with water (blue) (B) The ΔFluorescence excitation data was then corrected for inner filter effect as described above and plotted against incubation time (min).

Since the slope of Nudix hydrolase cleavage is significantly inhibited by the addition of 12.5 µM 6DHNADP, the above experiment was repeated under identical conditions, with varying concentrations of 6DHNADP ranging between 0.98-16.7 µM 6DHNADP (Fig. 6-8). The velocities for each reaction (v) were calculated using the Varian Cary Eclipse Fluorescence software. Next, the velocities were transformed by dividing each with the velocity of NADH cleavage by NudC in the absence of any 6DHNADP (v_O), yielding v/v_O. These resulting fractions were plotted against concentration of 6DHNADP and fit to a equation 4 using GraphPad Prism (v.6).

$$\frac{V_i}{V_o} = \frac{(K_m+S)}{K_m(1+\frac{I}{Ki})+S} \qquad \text{(Eq. 4)}$$

In Eq. 4, V_i is observed rate in the presence of inhibitor, V_o is observed rate in the absence of inhibitor, K_m is the Michaelis-Menten constant (100 µM), K_i is the inhibition constant, S is the substrate (NADH) concentration (50 µM) and "I" is the concentration of 6DHNADP titrated into each assay.

Figure 6-8| Effects of various concentration of 6DHNADP on NudC-induced NADH fluorescence decrease
v/v_O were plotted against the concentration of 6DHNADP, fit to competitive inhibition (relative activity) model and the K_i of 2.5 µM, 50 µM NADH is hydrolyzed with 74 nM NudC.

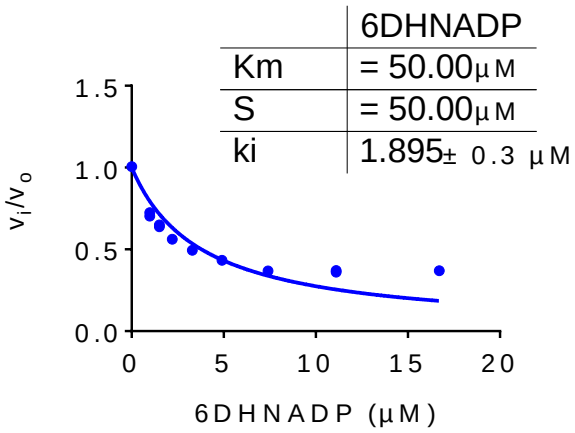

The inhibition constant K_i is a measure of the potency of an inhibitor. This assay is yet another experimental evidence that NudC has enzymatic 'housecleaning' activity on the toxic isomer of NADPH, 6DHNADP.

6.4 Discussion

This chapter discuses a novel FR-based assay developed, exploiting the fluorescence of NADH. This assay may be used extensively in the future to study either the kinetics of NADH-cleaving Nudix hydrolases on ncinRNA. ncinRNA could be *in vitro* transcribed from fluorescently labelled oligonucleotides and used in this FR-based protocol.

Chapter 7 NudC & Nudt12 Cleave NAD-capped RNA

7.1 Summary

In this chapter, we have designed and optimized an analytical approach using LC/MS to demonstrate the successful *in vitro* transcription of ncinRNAs. This protocol puts the concern as to whether NAD-capped RNAs or NAD alone is being studied to rest. Through this experiment, we confirm that the NAD moiety is indeed attached to the terminal end of the RNA transcripts through the adenine end. We also use this LC/MS-based approach to study the hydrolytic cleavage of bacterial and human Nudix hydrolases on NAD-capped RNA. This study demonstrates the activity of NAD-cleaving Nudix hydrolases on ncinRNAs, confirming that NAD-capped RNAs might be their substrate *in vivo,* and not NAD as previously thought. The protocol discussed in this chapter may be used to further study in depth the energetics of Nudix hydrolytic cleavage of ncinRNA or even study the activity of other NAD-cleaving Nudix hydrolases, such as NPY1 on ncinRNAs.

7.2 Background

The existence of covalently modified NAD^+/NADH on the terminal end of both prokaryotic (Chen et al., 2009) and eukaryotic (Julius et al., 2018) mRNAs *in vivo* is still a mystery. It has been suggested by Cahová et al. (2015) that the role of such non-canonical modifications on the 5'- end of mRNAs is to stabilize the nucleic acid transcript, similar to the role of the m^7G cap on eukaryotic RNA transcripts.

The NAD^+ is thought to be attached on the adenine side to the terminal end of the RNA transcript (Höfer et al., 2016; Grudzien-Nogalska et al. 2019). It has been hypothesized that these *in vitro* transcribed ncinRNAs undergo ribonucleolytic cleavage, after hydrolysis by NADH-

cleaving Nudix proteins. The bacterial NudC (Höfer et al., 2016) and human Nudt12 (Grudzien-Nogalska et al., 2019) hydrolyzes the phosphodiester bond in the NAD^+ moiety to yield free NMN and a 5'-monophosphorylated RNA strand. Grudzien-Nogalska et al. (2019) have demonstrated the degradation of ncinRNAs using radiolabeled NAD^+-RNA, showing the activity of NADH-cleaving Nudix proteins.

All experiments have been set up as described in Section 3.2.4.

7.3 Results

7.3.1 In vitro transcription of ncinRNA

All *in vitro* transcription reactions were set up as described in Section 3.1.5. Briefly, pET24-NudC plasmid constructed in Section 4.3.1 was miniprepped, following EZNA® Plasmid Mini Kit I- Omega Bio-tek and treated with Thermo Scientific Fermentas FastDigest HindIII at 37°C for 15 minutes. The digested vector (~ 6047 bp) was then gel extracted and consequently used as the DNA template for *in vitro* transcription reactions (Fig. 7-1)

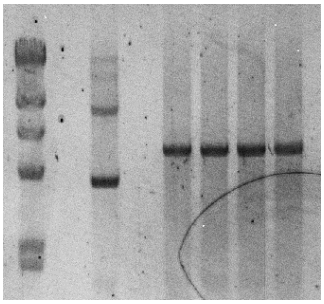

Figure 7-1| Agarose gel electrophoresis of *Hind*III digested pET24d-NudC
Lane 1: Lambda DNA/HindIII Marker, Lane 3: Miniprep of pET24d-NudC Lane 5-8: pET24d-NudC digested with HindIII. The HindIII digested bands from lane 5 through lane 8 were gel extracted and used as the DNA template for *in vitro* transcription of ncinRNA.

We used T7 RNA polymerase to synthesize RNA with non-canonical initiating nucleotides (ncin) such as NAD^+, NADH, $NADP^+$ and NADPH. The DNA template used for each ncinRNA transcription is NsiI digested pET24a vector. Five similar reactions were set up with the gel extracted DNA, ~ 2.5 mM NAD^+, ~ 2.5 mM NADH, 2.5 mM NADPH, 2.5 mM $NADP^+$ and 4

mM ARCA mix, 1-1.5 mM NTPs and T7 RNA Polymerase. Resulting *in vitro* transcribed ^{7}mG-capped and ncinRNA were run on an agarose gel (Fig. 7-2A).

Figure 7-2| Synthesis of ncinRNA by phage T7 RNA polymerase

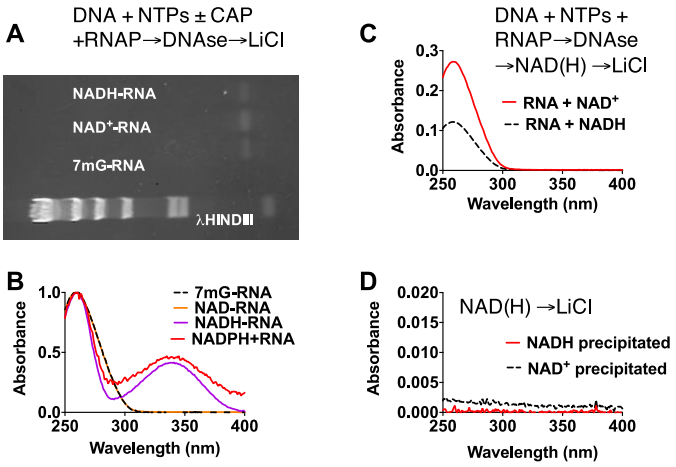

(A) T7 RNA polymerase was used to synthesize RNA initiating with 3'-O-Me m^{7}GpppA or the NCINs NAD^{+}, NADH, NADP^{+} and NADPH and purified using gel electrophoresis. (B) Absorbance spectrum of each RNA product after LiCl and gel-purification (note characteristic 340 nm absorbance of reduced nicotinamide). (C) Spectra of products produced when NADH was added after the RNAP reaction was terminated, but before purification. (D) Demonstration that neither NAD^{+} nor NADH co-purify with NADH-capped RNA.

Each *in vitro* transcribed ncinRNA was then gel extracted from a RNase free agarose gel and the absorbance of each gel-extracted ncinRNA was then observed between 250-400 nm and then normalized (Fig. 7-2B). Control reactions to confirm that free NAD^{+}/NADH is not observed in our future experiments, leftover from the transcription reaction, were carried out as well. NAD^{+} or NADH was added once the transcription reaction was completed, following DNAse treatment. Absorbance at 260 nm for *in vitro* transcribed RNA was observed, however no absorbance at 340 nm was recorded (Fig. 7-2C). Free NAD^{+} and NADH were precipitated with LiCl solution and no UV absorbance was detected, confirming that NAD alone does not precipitate with *in vitro* transcribed ncinRNA (Fig. 7-2D).

Free NADH has a 10:4 ratio of their UV absorbances at 260 nm and 340 nm, respectively. It was hypothesized that NADH-capped RNA should have a different UV absorbance ratio at the

two wavelengths, assuming that the NADH moiety has an RNA tail, which absorbs at 260 nm, attached to its terminal end.

7.3.2 Different lengths of NAD(H)-RNA run differently on the LCMS

NAD^+-capped RNA was *in vitro* transcribed from two different DNA templates, to yield a final mRNA transcript of ~ 200 bp (green) and ~ 1000 bp (purple) respectively. Also, free NAD^+ and NAD^+ and AMP solutions were used as a standard to test the elution of samples for future LC/MS experiments (Fig. 7-4).

Figure 7-3| LC/MS analysis of NAD^+, AMP, and NAD^+-capped RNA

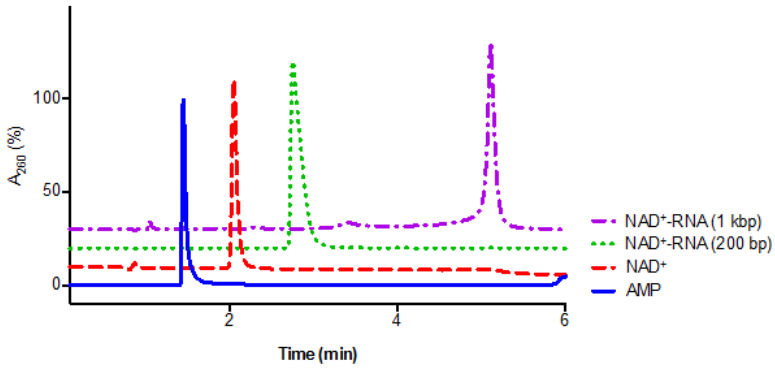

NAD^+-capped RNA was *in vitro* transcribed from two different DNA templates, to yield a final mRNA transcript of 258 bp (green) and 806 bp (purple) respectively. Each NAD^+-capped RNA was injected into the LC/MS to test the hypothesis that the RNA strand attached to the NAD^+ moiety affects its elution time on the instrument. As a control, 1 µM solutions of NAD^+ alone and AMP were run on the LC/MS under identical conditions. The shorter RNA transcript (green) elutes at 2.756 minutes while the longer RNA transcript elutes at 5.112 minutes. NAD^+ alone, being a smaller molecule than when attached to RNA, elutes at 2.052 minutes, while AMP elutes at 1.46 minutes. The normalized absorbances of each sample at 260 nm has been plotted against elution time using GraphPad Prism (v.6).

It should be noted that both the NAD^+-capped RNA transcripts tested have an elution time (2.7 to 5.1 minutes) later than free NAD^+ (2.0 minutes), further confirming our hypothesis that when NAD is attached to the terminal end of the RNA transcript. The PDA data showing absorbance between 252-271 nm is characteristic of other nucleotides present in the RNA strand, demonstrating the successful *in vitro* transcription of ncinRNA.

7.3.3 NudC and Nudt12 cleave NADH-capped RNA

1 mM NADH was treated with NAD-cleaving Nudix hydrolase at 37 °C for 15 minutes, the proteins filtered out and the elution of products was observed at both 260 nm and 340 nm. We hypothesized that when the NADH moiety is attached to the terminal end of the RNA transcript, it should have a different elution time compared to free NADH observed. *In vitro* transcribed NADH-capped RNA was run on an agarose gel under RNase free conditions, gel extracted and then injected into the LC/MS. Gel extracted NADH-capped RNA was also treated with both the bacterial NudC and human Nudt12, under similar conditions described above. The sample was treated with Tris-equilibrated phenol to precipitate the protein, then with 50:50 phenol:chloform mixture and finally with chloroform to remove any traces of phenol. This method will be referred to as the "Sevag" method, in future experiments. Removing any residual phenol was essential because phenol, being an aromatic compound, absorbs at 260 nm as well. The products of hydrolysis, NMNH has an absorbance maximum at 340 nm, and AMP has an absorbance maximum at 260 nm while the substrate NADH absorbs both at 260 nm and 340 nm.

Figure 7-4| Effect of NudC on NADH and NADH-capped RNA

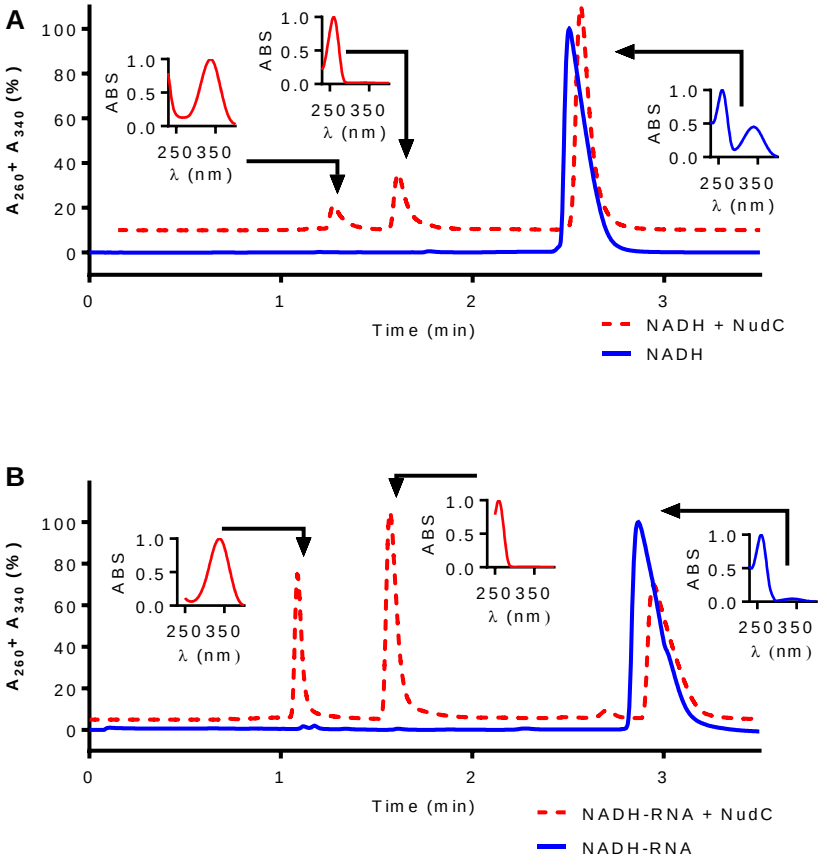

(A) 1 mM NADH alone (blue) and treated with NudC (red) at 37 °C for 15 minutes was centrifuged to remove any traces of protein then injected into the LC/MS instrument, and the elution of products were observed at 260 nm and 340 nm. The products, NMNH (red) elutes at 1.16 minutes, AMP (red) elutes at 1.42 minutes while both unhydrolyzed NADH (red) and NADH alone (blue) elutes at 2.05 minutes. The normalized PDA data of NMNH, AMP and NADH has been recorded. (B) Gel extracted NADH-capped RNA alone (blue) and treated with NudC at 37 °C for 15 minutes and subsequently Sevag treated, then injected into the LC/MS and the elution of products is observed at both 260 nm and 340 nm, with the products NMNH (red) eluting at 1.24 minutes, 5'-monophosphorylated RNA (red) eluting at 1.684 minutes, while both unhydrolyzed NADH-capped RNA and NADH-capped RNA alone elute at 3.096 minutes. The normalized Photodiode Array (PDA) data of NMNH, 5'- monophosphorylated RNA and NADH-capped RNA has been recorded.

The above data suggests that the NADH moiety is indeed attached to the terminal end of the RNA transcript, because it elutes at a later time point (3.096 minutes) when compared to free NADH which elutes at 2.42 minutes. As predicted, NMNH hydrolyzed from NADH-capped RNA

(Fig. 7-6B) elutes at a similar time point (1.24 minutes) as that off NMNH hydrolyzed from free NADH (1.16 minutes) (Fig. 7-6A), while 5'- monophosphorylated RNA elutes at a later time point (1.684 minutes) compared to free AMP (1.42 minutes) under otherwise identical conditions. The spectra of each peak (Fig. 7-6 inserts) further confirms the successful *in vitro* transcription of NADH-capped RNA, having an uncharacteristic 260:340 absorbances when compared to canonical NADH.

Figure 7-5| Effect of Nudt12 on NADH and NADH-capped RNA

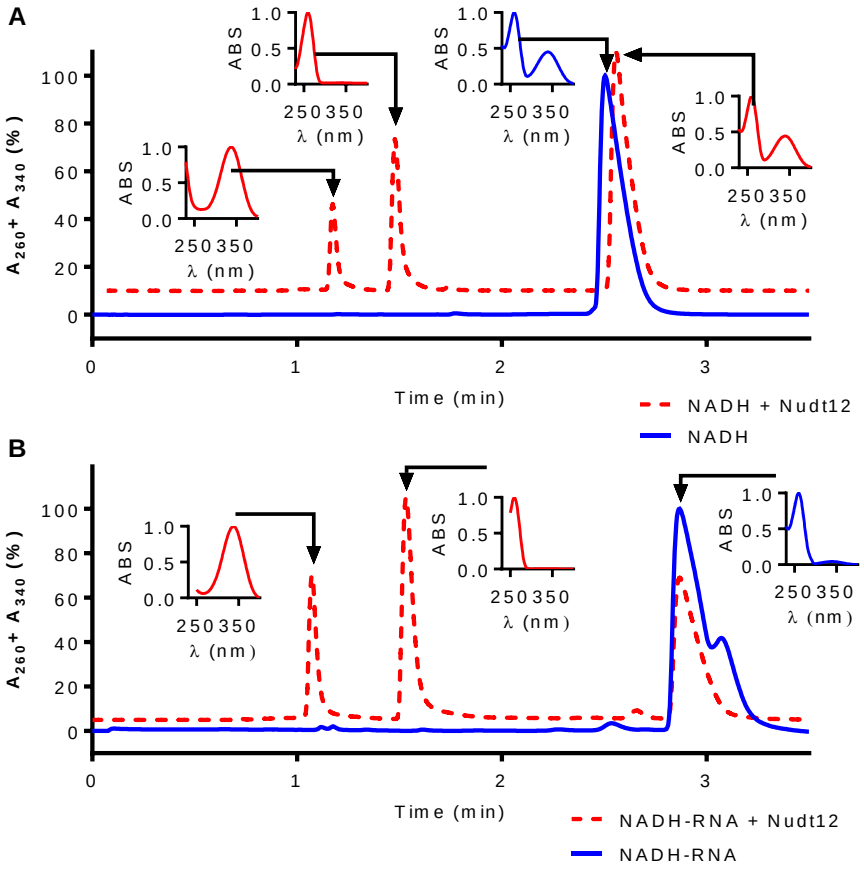

(A) 1 mM NADH alone (blue) and treated with Nudt12 (red) at 37 °C for 15 minutes was centrifuged to remove any traces of protein then injected into the LC/MS instrument, and the elution of products were observed at 260 nm and 340 nm. The products, NMNH (red) elutes at 1.16 minutes, AMP (red) elutes at 1.42 minutes while both unhydrolyzed NADH (red) and NADH alone (blue) elutes at 2.05 minutes. The normalized PDA data (absorbance spectra) of NMNH,

AMP and NADH has been recorded. (B) Gel extracted NADH-capped RNA alone (blue) and treated with Nudt12 at 37 °C for 15 minutes and subsequently Sevag treated, then injected into the LC/MS and the elution of products is observed at both 260 nm and 340 nm, with the products NMNH (red) eluting at 1.23 minutes, 5'- monophosphorylated RNA (red) eluting at 1.69 minutes, while both unhydrolyzed NADH-capped RNA and NADH-capped RNA alone elute at 3.03 minutes. The normalized Photodiode Array (PDA) data of NMNH, 5'- monophosphorylated RNA and NADH-capped RNA has been recorded.

Similar to the NudC hydrolysis of NADH-capped RNA, the above data confirms that the NADH moiety is indeed attached to the terminal end of the RNA transcript, because it elutes at a later time point (3.03 minutes) when compared to free NADH which elutes at 2.42 minutes. As predicted, NMNH hydrolyzed from NADH-capped RNA elutes at a similar time point (1.228 minutes) as that off NMNH hydrolyzed off free NADH (1.16 minutes), while 5'-monophosphorylated RNA elutes at a later time point (1.688 minutes) compared to that of free AMP (1.42 minutes), under otherwise identical conditions.

We also further analyzed the above results on the mass spectrometer (MS), which collected m/z ranging between 100 to 1000, in both positive and negative ionization mode. However, to avoid noisy MS data, we used Selected Ion Monitoring (SIM) mode to select for our expected molecules. The MS data show that NudC cleaves NADH to NMN and AMP (Fig. 7-7A), and that free AMP is not released from the hydrolysis of NADH-capped RNA, confirming that NADH is covalently attached to the terminal end of the RNA transcript (Fig. 7-7B).

Figure 7-6| LC/MS analysis of NudC reaction products

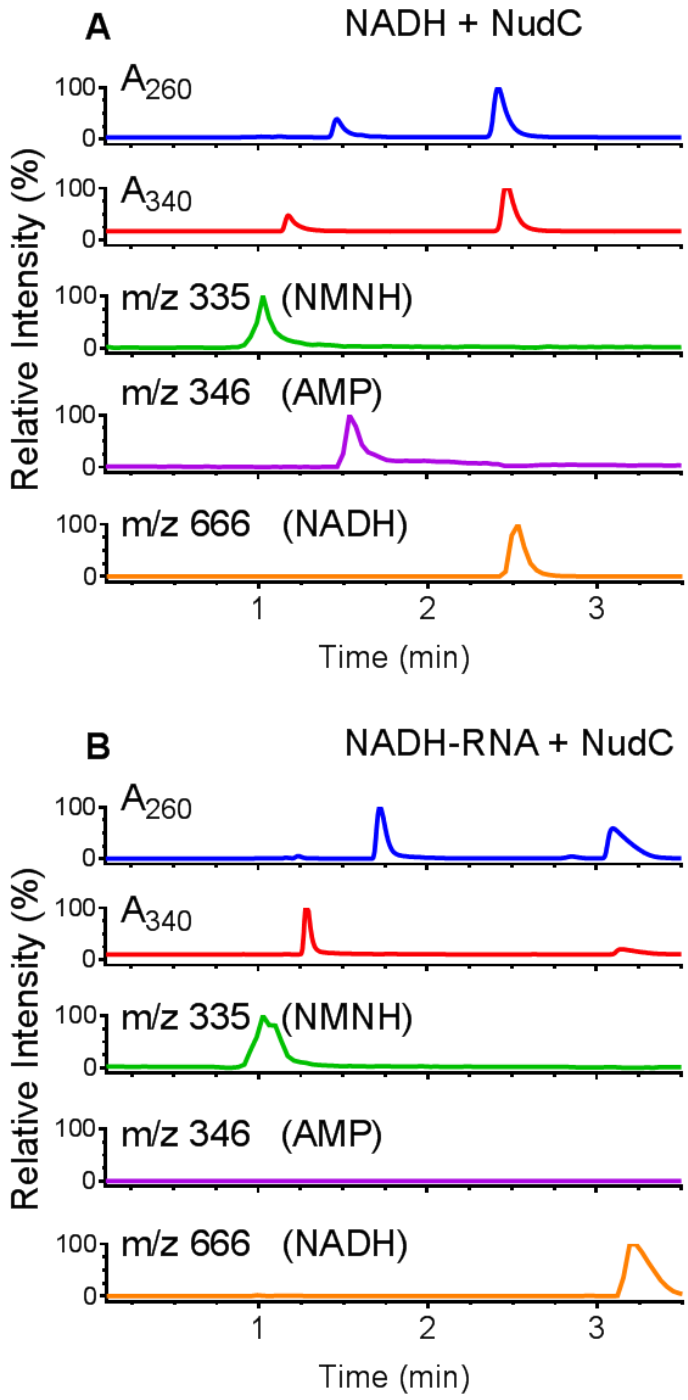

(A) 1 mM NADH treated with NudC at 37 °C for 15 minutes was injected into the LC/MS instrument and the elution of products was observed at both 260 nm (blue) and 340 nm (red). Selected Ion Monitoring (SIM) was selected for m/z= 666 (orange) for NADH, 346 (purple) for AMP and 335 (green) for NMNH in positive ionization mode and overlaid with the LC chromatogram using GraphPad Prism (v.6) (B) Gel extracted NADH-capped RNA, treated with

NudC, then Sevag treated was injected into the LC/MS instrument and the elution of the products were observed at 260 nm (blue) and 340 nm (red). SIM was selected for m/z= 666 (orange) for NADH, 346 (purple) for AMP and 335 (green) for NMNH in positive ionization mode.

The MS data overlays well with the absorbance data suggesting the NudC degradation of *in vitro* transcribed NADH-capped RNA. Identical experiments were repeated with Nudt12 and NADH (Fig. 7-8A) and NADH-capped RNA (Fig. 7-8B); 10 µl sample was injected into the LC/MS after either filtering out or removing the Nudt12 protein using the Sevag protocol.

Figure 7-7| LC/MS analysis of Nudt12 reaction products

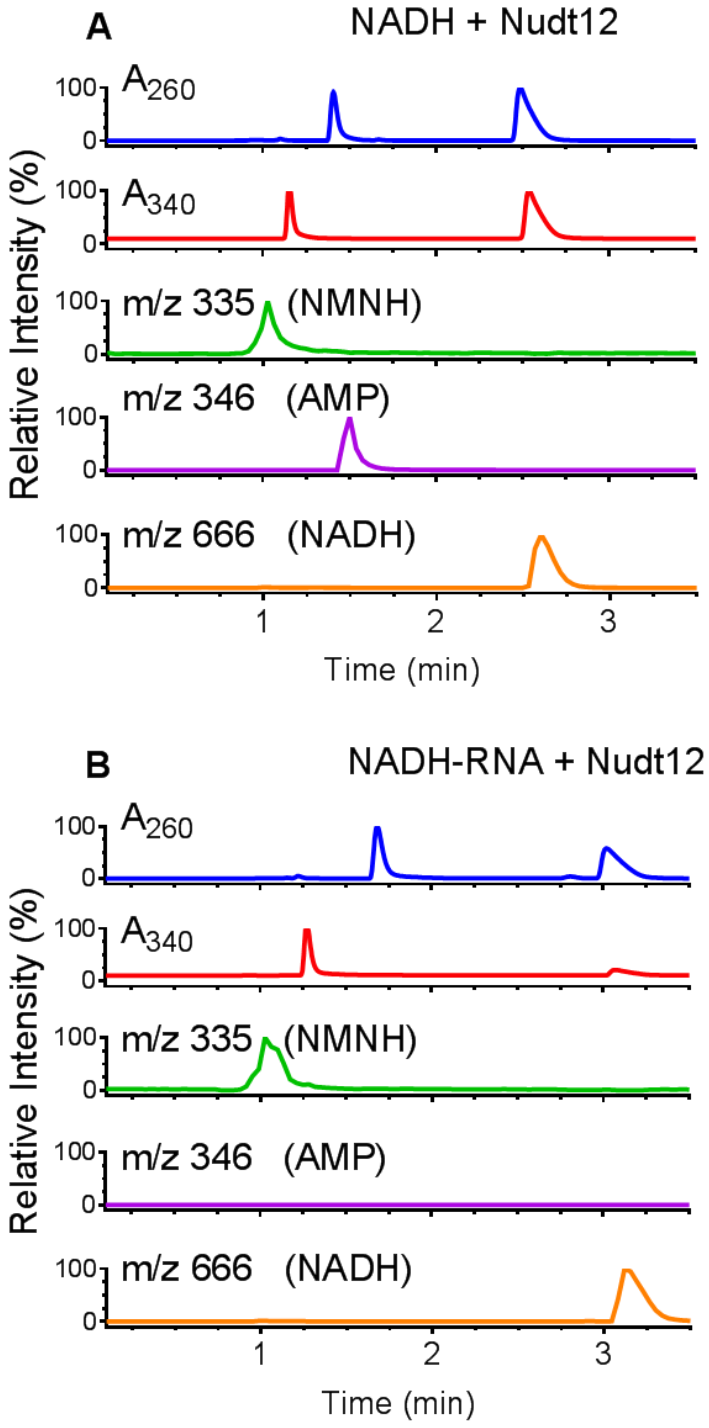

(A) 1 mM NADH treated with Nudt12 at 37 °C for 15 minutes was injected into the LC/MS instrument and the elution of products was observed at both 260 nm (blue) and 340 nm (red). Selected Ion Monitoring (SIM) was selected for m/z= 666 (orange) for NADH, 346 (purple) for AMP and 335 (green) for NMNH in positive ionization mode and overlaid with the LC chromatogram using GraphPad Prism (v.6) (B) Gel extracted NADH-capped RNA, treated with

Nudt12, then Sevag treated was injected into the LC/MS instrument and the elution of the products were observed at 260 nm (blue) and 340 nm (red). SIM was selected for m/z= 666 (orange) for NADH, 346 (purple) for AMP and 335 (green) for NMNH in positive ionization mode. The MS data shows that free AMP is not released from the hydrolysis of NADH-capped RNA, confirming that NADH is modified to the 5'- end of the RNA transcript.

7.3.4 NudC and Nudt12 cleave NAD$^+$-capped RNA

In vitro transcribed NAD$^+$-capped RNA was run on an RNase-free agarose gel, gel extracted, incubated with NudC at 37 °C for 15 minutes and then Sevag treated. 10 µl of the resulting sample was then injected into the LCMS instrument. 1 mM NAD$^+$ alone was treated under identical conditions and injected into the LCMS as well. As assumed, unhydrolyzed NAD$^+$-capped RNA eluted much later than unhydrolyzed free NAD$^+$. Products of each hydrolysis were confirmed by both LC (260 nm) and MS data, which identified the substrate NAD$^+$ (purple), and the products, AMP (green) and NMN (red) (Fig. 7-9A). However, when NAD$^+$-capped RNA was hydrolyzed with NudC, although NAD$^+$ (purple) and NMN (red) were identified, the SIM failed to recognize AMP, further confirming that the NAD modification on the 5'- end of RNA transcripts is through the adenine side. The LC chromatogram however identified three peaks at 260 nm, first for NMN, second for the hydrolyzed nucleotides form the terminal end and third for unhydrolyzed substrate, NAD$^+$-capped RNA. (Fig. 7-9B)

Figure 7-8| LC/MS analysis of NudC reaction products

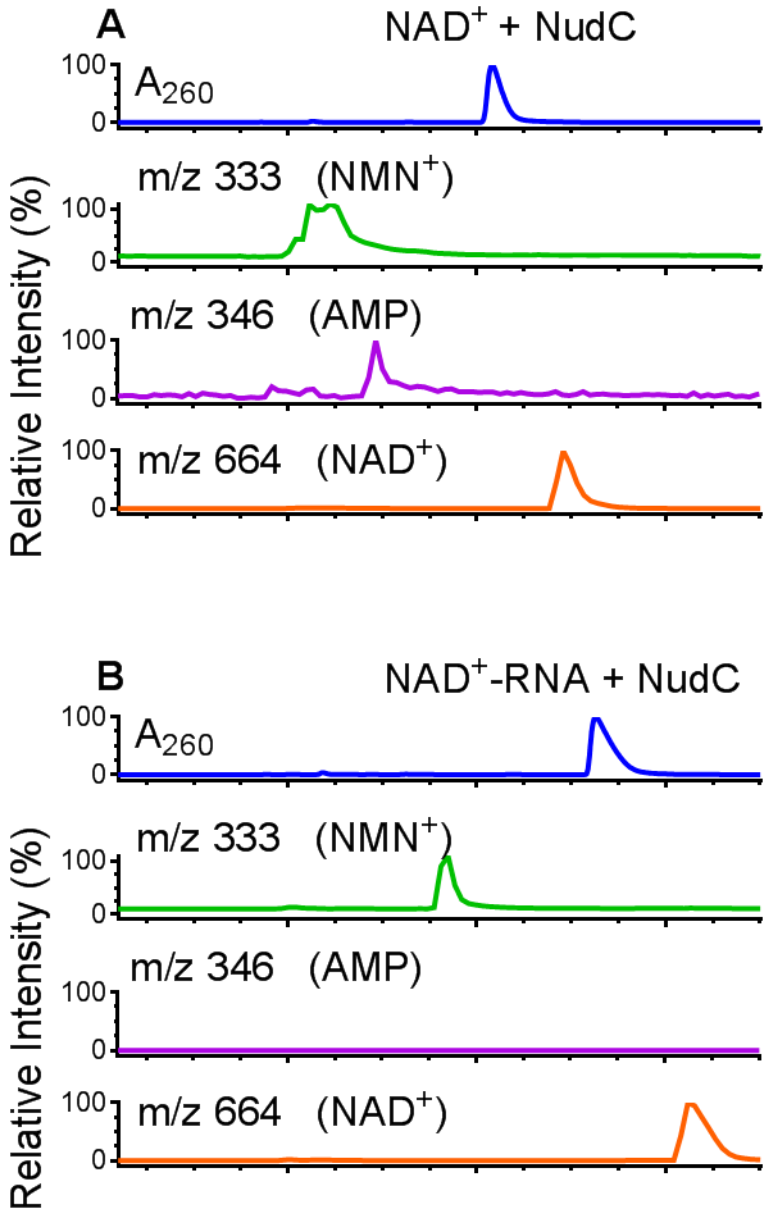

(A) 1 mM NAD^+ treated with NudC at 37 °C for 15 minutes was injected into the LC/MS instrument and the elution of products was observed at both 260 nm (blue). Selected Ion Monitoring (SIM) was selected for m/z= 664 (orange) for NAD^+, 346 (purple) for AMP and 333 (green) for NMN in positive ionization mode and overlaid with the LC chromatogram using GraphPad Prism (v.6) (B) Gel extracted NAD^+-capped RNA, treated with NudC, then Sevag treated was injected into the LC/MS instrument and the elution of the products were observed at 260 nm (blue). SIM was selected for m/z= 664 (orange) for NAD^+, 346 (purple) for AMP and 333 (green) for NMN in positive ionization mode.

A major concern our NAD^+ data however is that the MS data for m/z= 664 does not align with the peaks observed on the chromatogram at 260 nm. A control with NAD^+ hydrolyzed by NudC shows masses for both products, AMP and NMN. (Fig. 7-10A). The MS data shows that free AMP is not released from the hydrolysis of NAD^+-capped RNA, supporting the contention that NAD^+ is modified to the 5'- end of the RNA transcript (Fig. 7-10B).

Figure 7-9| LC/MS analysis of Nudt12 reaction products

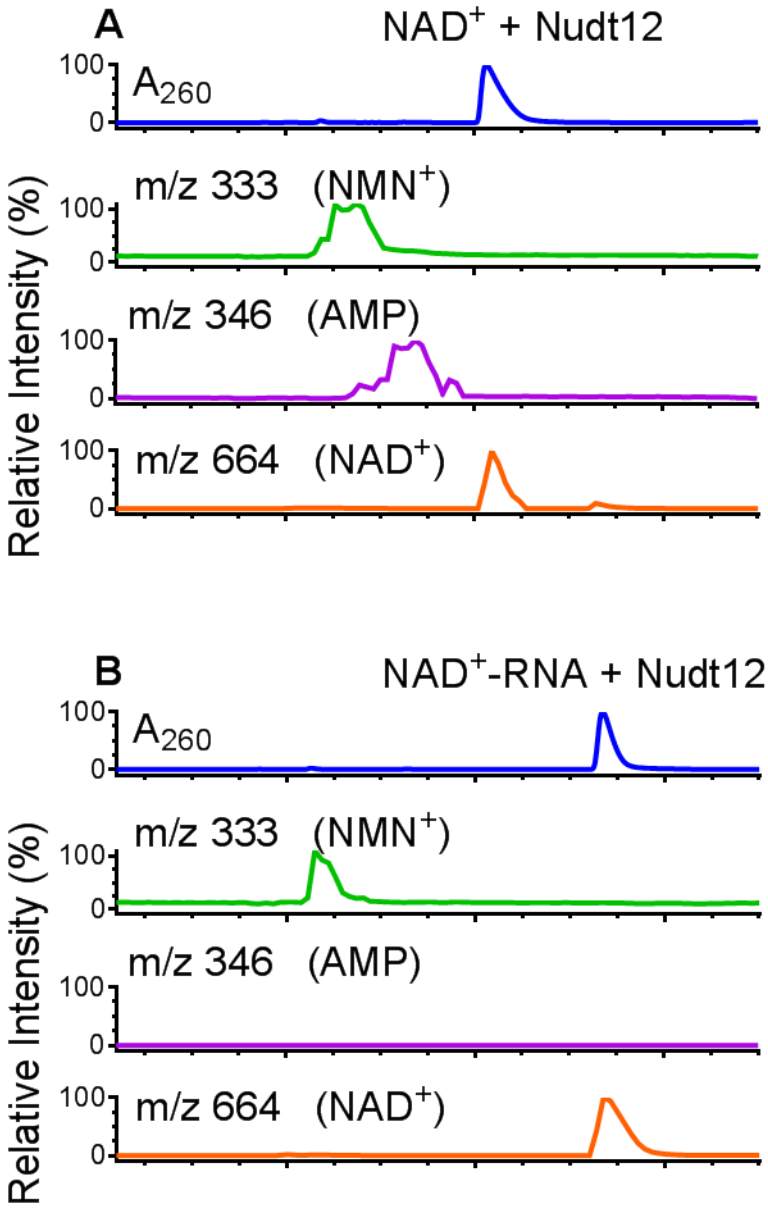

(A) 1 mM NAD^+ treated with Nudt12 at 37 °C for 15 minutes was injected into the LC/MS instrument and the elution of products was observed at 260 nm (blue). Selected Ion Monitoring (SIM) was selected for m/z= 664 (orange) for NAD^+, 346 (purple) for AMP and 333 (green) for NMN in positive ionization mode and overlaid with the LC chromatogram using GraphPad Prism (v.6) (B) Gel extracted NAD^+-capped RNA, treated with Nudt12, then Sevag treated was injected into the LC/MS instrument and the elution of the products were observed at 260 nm (blue). SIM was selected for m/z= 664 (orange) for NAD^+, 346 (purple) for AMP and 333 (green) for NMN in

positive ionization mode. The MS data shows that free AMP is not released from the hydrolysis of NAD^+-capped RNA, confirming that NAD^+ is modified to the 5'- end of the RNA transcript.

7.4 Discussion

A major concern for previous studies on *in vitro* transcribed ncinRNAs has been the confirmation that NAD is indeed attached to the terminal end of the RNA transcripts. Also, previous studies have demonstrated the Nudix hydrolysis of ncinRNA using radioactivity and gel shift assays. However, the experiments discussed in this chapter ensures that *in vitro* transcribed ncinRNA and not free NAD is being studied. Our results confirm previous studies, that NAD attaches itself through the adenine side on the terminal end of RNA transcripts. However, this LC/MS-based assay is a more analytical approach to validate the *in vitro* transcription of ncinRNAs. Our results also confirm that the biochemical role of NAD-cleaving Nudix hydrolases may be to hydrolyze ncinRNAs instead off energy-rich molecules such as NADH. This analytical approach may be used to further study the kinetics of other NAD-cleaving Nudix hydrolases among prokaryotes and eukaryotes, on ncinRNAs.

Chapter 8 Energetics of Nudix-Nucleic Acid Binding

8.1 Summary

Since the discovery of Nudix hydrolases, the superfamily has been divided into classes based on their substrate specificity (Srouji et al., 2017) having activity over a range of substrates such as deoxynucleotides, nucleotide sugars, dinucleoside polyphosphates and dinucleotide coenzymes. The *E. coli* enzyme, NudC and its functional homolog in humans, Nudt12 are members of one such subclass of the Nudix family, that cleave dinucleotides, such as NADH, NADPH, $NADP^+$, ADP-ribose and AppA to yield two nucleoside monophosphates. Since the first purification of the bacterial NudC protein (Frick et al., 1995), it was found to co-precipitate with nucleic acids. Later with the discovery of the NAD-capped RNA and the decapping function of NudC on such covalently modified RNAs, it may be hypothesized that NudC interacts with nucleic acids. Over the years, several other mammalian proteins have been reported to have mRNA decapping activity, which may be argued to be directly interacting with their nucleic acid substrates. Both the bacterial NudC and Nudt12 proteins have a Zinc-finger domain, known for interacting with nucleic acids, in their amino acid sequences. However, the energetics of the direct interaction between nucleic acids and bacterial and human nudix proteins has never been shown until now. In this chapter, our results confirm that the human Nudt12 protein specifically binds to only RNA. This surprising result has been confirmed by gel shift, fluorescence polarization and emission, and probe displacement assays. The human Nudt12 protein also has a clear preference to bind NAD^+-capped RNA over NADH-capped RNA and ^{7}mG-capped RNA, confirming that ncinRNAs might be the real substrates for Nudt12 *in vivo*. Our results demonstrate previously unknown features of the human NAD-cleaving Nud12 protein.

8.2 Background

The *E. coli* genome encodes for a mutT mutator gene, the progenitor of the family expressing the MutT pyrophosphohydrolase (NudA) protein (Treffers et al., 1954; Bhatnagar et al., 1988). The enzyme was found to catalyze the hydrolysis of canonical and mutagenic nucleoside triphosphates, most commonly the toxic form of dGTP, 8-oxo-dGTP, preventing its misincorporation during DNA replication (Maki et al., 1992). Nudt1 is its functional homologue in humans and plays a vital role in removing mutagenic dNTPs to prevent A:T to C:G transversion, by hydrolyzing the 8-oxo dGTP to 8-oxo dGMP (Nakabeppu Y, 2001). Since the early discovery of *E. coli* NudC, nucleic acids were found to co-precipitate with the protein, suggesting its interaction (Frick et al., 1995). With the recent discovery of the cofactor nicotinamide adenine dinucleotide (NAD^+) as a transcriptional modification of prokaryotic mRNA (Chen et al., 2009), it has been suggested that NudC is involved in RNA decapping, eventually triggering its decay (Cahová et al., 2014). Its functional homolog in mouse, Nudt12 has also been shown to decap both canonical capped mRNA, between the β- and γ- phosphate moieties and NAD^+-capped RNA *in vitro* (Grudzien-Nogalska et al., 2017). Although, evidence is yet to be shown for direct interaction between these decapping Nudix hydrolases and their oligonucleotide substrates.

Following the discovery of the hydrolytic activity of MutT, it was believed that the protein bound to the nucleic acid. However, it was later shown that MutT only interacted with its mutagenic nucleotide substrate, 8-oxo dGTP, holding onto the product, 8-oxo dGMP with an exceptionally high affinity (Massiah et al., 2003). In stark contrast, MutY, an *E. coli* adenine glycosylase initiates the repair of A:oxoG to C:G by removing the mismatched adenine moiety from the entire DNA backbone (Fromme et al., 2004).

The cofactor, NAD^+ at the terminal end of bacterial mRNA resembles the eukaryotic cap and has been shown to stabilize some mRNAs in *E. coli* in the same manner as the ^{7}mG cap found on eukaryotic mRNAs. This is where the Nudix phosphohydrolase NudC plays an important role to decap NAD^+-capped RNA, by cleaving the phosphoanhydride bond in the cap, thereby triggering RNA decay.

Confined to the cytoplasm, phylogenetic assignment classified Nudt3 as a DIPP (diphosphoinositol polyphosphate phosphohydrolase). Nudt3 has also been demonstrated as an mRNA decapping enzyme (McLennan et al., 2006; Song et al., 2013; Kiledjian et al., 2016). Nudt16 has been reported to be localized in the cytoplasm as well, with 5'-end U8 snoRNA decapping activity (Grzela et al., 2018). Human Nudt12 is a NADH diphosphatase, found to be localized in the peroxisome (Abdelraheim, et al., 2003). Nudt20, more commonly referred to as Dcp2 is a member of the Nudix hydrolase superfamily of enzymes and was the first eukaryotic mRNA decapping enzyme to be discovered (Wang Z et al., 2002). It removes the ^{7}mG cap from the 5'-end of eukaryotic mRNA. Similar to Nudt16, Nudt20 also hydrolyzes the α-β-phosphate bond of the mRNA cap, whereas Nudt3 can hydrolyze both α-β- and β-γ-phosphates with similar activity (Grudzien-Nogalska et al., 2017). Thus, we reasoned that for human Nudt3, Nudt12, Nudt16 and Nudt20 (Dcp2) and the bacterial NudC Nudix proteins to be active RNA decapping enzymes, there has to be direct interaction between the proteins and their nucleic acid substrates.

Supporting this hypothesis, it has been reported that Nudt20 (Dcp2) in budding yeast has an additional well conserved RNA binding channel that promotes decapping by the Dcp1/Dcp2 complex. The interactions between the protein and its ^{7}mG-capped RNA substrate have been shown using gel shift assays (Deshmukh et al., 2008). Although human Nudt3 and Nudt16 are functional RNA decapping enzymes, they do not have any domain additional to the Nudix catalytic

site. *E. coli* RNA decapping enzyme, NudC has been shown to have a positively charged area adjacent to the NAD^+ binding domain, suggesting its interaction with nucleic acids (Höfer et al., 2016). Its functional homolog in humans, Nudt12 also has an additional Ankyrin repeat domain, essential for NAD^+-capped RNA decapping activity (Grudzien-Nogalska et al., 2019). Additionally, both NudC and Nudt12 have Zinc-finger domains, suggesting yet another possible binding site for nucleic acids.

In this study, we developed and optimized a fluorescence polarization (FP) assay to quantify affinity between RNA decapping Nudix hydrolases and nucleic acids. Fluorescence polarization is a property of most fluorophores. Often times, polarization is a more preferred measurement to study ligand interactions, being less reliant on environmental changes, such as pH and temperature. Fluorescence polarization (P) is defined from fluorescence intensities of both parallel ($F_{||}$) and perpendicular ($F_{\perp}$) light with respect to the plane of linearly polarized excitation light (Eq. 5). Anisotropy (r) is also another method of detecting ligand interactions without being dependent on the concentrations of the fluorophore (Eq. 6).

$$P = \left(\frac{F_{||} - F_{\perp}}{F_{||} + F_{\perp}}\right) \quad \text{(Eq. 5)}$$

$$r = \left(\frac{F_{||} - F_{\perp}}{F_{||} + 2F_{\perp}}\right) \quad \text{(Eq. 6)}$$

where $F_{||}$ is the fluorescence intensity parallel to the linearly polarized excitation light and $F_{\perp}$ is the fluorescence intensity perpendicular to the linearly polarized excitation light.

Since the fluorescence intensities cancel each other out in the above equation for measurement of polarization, unlike the calculation of fluorescence intensities in section 3.2.6, fluorescence polarization does not depend on the concentration of fluorophore in the assay.

Surprisingly, our data shows that the human NADH-cleaving Nudix hydrolase, Nudt12 exclusively binds RNA and not DNA. We further validated these results by designing another FP assay to displace the bound protein-nucleic acid complex with either DNA or RNA. Nudt12 also has an incredibly high affinity to bind *in vitro* transcribed NAD^+-capped RNA compared to NADH-capped RNA and ^{7}mG capped RNA. This is the first study to demonstrate the kinetics of the interactions between human and bacterial RNA decapping Nudix hydrolases and nucleic acids.

8.3 Results

The Nudix proteins used to test their nucleic acid binding are the bacterial NudC and the mammalian Nudt12, Nudt1, Nudt3, Nudt16 and Nudt20 proteins (Fig. 4-16).

8.3.1 Interaction between Nudix hydrolase and fluorescently labelled DNA

A gel shift assay was designed to test the interaction between fluorescently labeled DNA and Nudix proteins (Fig. 8-1). Samples containing either [HF]DNA45 alone or with Nudt1 (MutH1), Nudt3, Nudt12, Nudt16, Nudt20 (Dcp2) and NudC were made to ta total volume of 10 µl with 50 mM TrisCl pH 8.5, incubated on ice for 20 minutes and then run on a 12% non-denaturing polyacrylamide gel at 4°C at 100 V for 60 minutes. Fluorescence was observed with a UV trans-illuminator. [HF]45 was used alone as a negative control. A ‘band shift’ was assumed to be because of a complex forming between fluorescently labeled DNA and the interacting proteins, Nudt3, Nudt16, Nudt20 (Dcp2) or4 NudC. NS3h protein, used as a positive control observed a clear band shift, while DNA interacting Nudix proteins shifted with a more smear-like appearance. Surprisingly, a ‘band shift’ was not observed with Nudt12 and Nudt1 (MutH1), which was used as a known negative control.

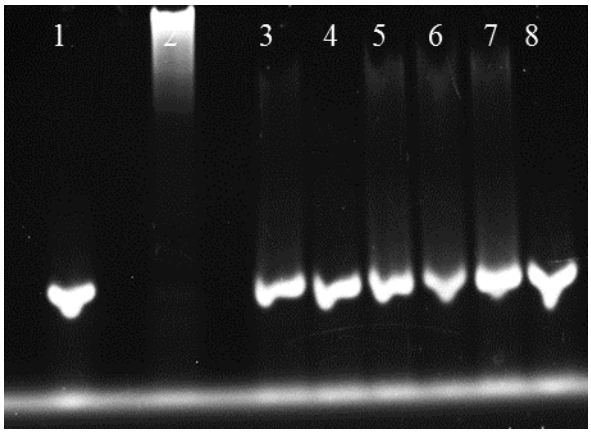

Figure 8-1| Interaction between Nudix hydrolases and [HF]DNA45 using native PAGE
Lanes 1: 1 µM [HF]DNA45, 2: [HF]DNA45 and NS3h, 3: [HF]DNA45 and NudC, 4: [HF]DNA45 and Nudt12, 5: [HF]DNA45 and Nudt20 (Dcp2), 6: [HF]DNA45 and Nudt16, 7: [HF]DNA45 and Nudt3, 8: [HF]DNA45 and Nudt1

The above non-denaturing polyacrylamide gel was then stained with coomasie blue dye solution to confirm the overlay of the Nudix proteins with each 'gel shift' (Fig. 8-2). Lane 1, containing fluorescent DNA alone did not stain with coomasie blue solution. Lane 2, containing the positive control protein, NS3h and lanes 3, 5, 6, 7 and 8 containing Nudix proteins showed a protein band or smear in accordance to where the gel shift was assumed to be. Lanes 4 and 8 containing Nudt1 and Nudt12 proteins respectively did not observe a gel shift with the DNA, but still had a band for protein in Fig. 8-2.

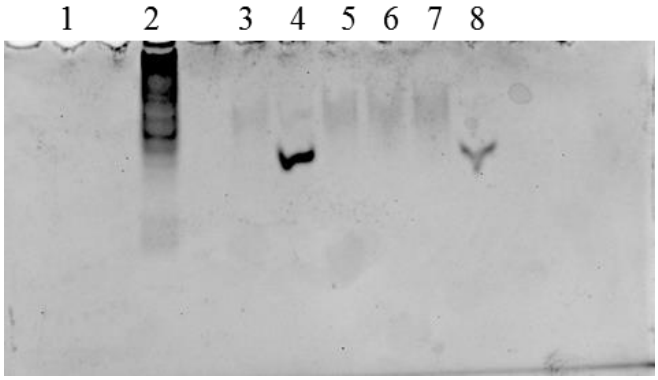

Figure 8-2| Interaction between Nudix hydrolases and [HF]DNA45 using native PAGE
The non-denaturing polyacrylamide gel was stained with Coomasie blue stain and the proteins in each lane were observed. Lanes 1: 1 µM [HF]DNA45, 2: [HF]DNA45 and NS3h, 3: [HF]DNA45 and NudC, 4: [HF]DNA45 and Nudt12, 5: [HF]DNA45 and Nudt20 (Dcp2), 6: [HF]DNA45 and Nudt16, 7: [HF]DNA45 and Nudt3, 8: [HF]DNA45 and Nudt1

Since the desired 'gel shift' results could not be replicated using numerous non-denaturing polyacrylamide gels, we proceeded to design two fluorescence-based assays. Interactions between fluorescently labelled nucleic acids and the Nudix proteins are assumed to be at equilibrium, to estimate binding affinity/dissociation constant (Lohman et al., 1992; Smolik et al., 2014).

Fluorescently labeled DNA, [FAM]DNA18 was titrated with serially diluted concentrations of Nudix proteins. The first point in each titration is the intensity of 20 nM [FAM]DNA18 alone, in the absence of any protein. If the fluorescence emission increases, then it was assumed to be because of binding between [FAM]DNA18 and the protein (Lohman et al., 2012; Hwang et al., 2014). Non-specific interaction was ruled out by the addition of Bovine serum albumin (BSA) with [FAM]DNA18. The fluorescence emission was measured on FLUOstar Omega (BMG LABTECH), with a gain= 100. The increase in fluorescence emission (Ex. wavelength= 485 nm, Em. Wavelength= 520 nm) suggests the binding of [FAM]DNA18 with Nudt3, Nudt16, Nudt20 (Dcp2) and NudC (Fig. 8-3A). However, with Nudt1(MutH1) and Nudt12, both the fluorescence emission and polarized values remain unchanged, even with the addition of protein, suggesting that there is no interaction between the oligonucleotide and protein. The fluorescence emission data were fit Eq. 1 (Section 3.2.6) to calculate the dissociation constants (K_d) (Fig. 8-3B). Similar results were obtained in repeat experiments.

Figure 8-3| Effect of Nudix hydrolases on the fluorescence intensity of [FAM]DNA18

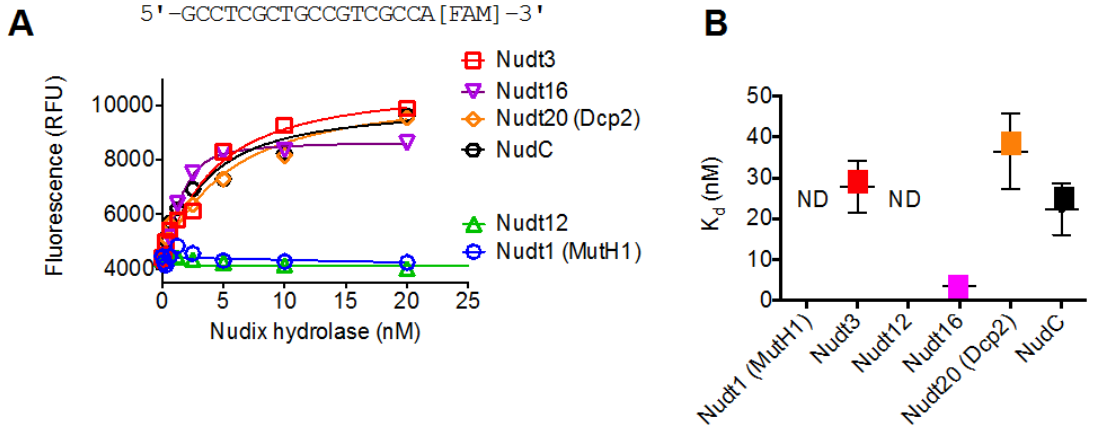

(A) 20 nM [FAM]DNA18 was titrated with various concentrations of Nudix proteins and fluorescence emission was observed at 520 nm when excited at 485 nm. The raw fluorescence data, measured on FLUOstar Omega (BMG LABTECH) were fit Eq. 1 where F_s= 230.5, F_c= 507.5 and n= 11 are shared values among all data sets. (B) A summary of the best fit dissociation

constants (K_d) determined by GraphPad Prism. K_d for Nudt1= Not defined, Nudt3= 28, Nudt12= Not defined, Nudt16= 3.5, Nudt20= 36, NudC= 22 nM.

Although the above results suggest that Nudix hydrolases bind probe DNA to enhance its fluorescence intensity, we designed a fluorescence-based polarization assay to further validate the binding between DNA or RNA and Nudix hydrolases. When a fluorophore is excited by polarized light, fluorescence polarization of the molecule is inversely proportional to its rotational speed (Lakowicz, 2006). If the polarization increased with the titration of fluorescently labeled DNA to Nudix hydrolases, then it was assumed that the fluorescently labeled DNA interacted with the protein. The increase in polarization is presumed to be because of a significantly lower rate of rotation compared to the free [FAM]DNA18. Unlike fluorescence intensity, polarization is not dependent on the concentration of fluorophore. Fluorescence polarization at 520 nm when excited at 470 nm was measured on TECAN infinite M1000. G-factor reference well was set with 1 nM Fluorescein in 0.01 M NaOH= 180, while blank well was set with 50 mM Tris pH7.5. Polarization values were data were fit Eq. 1 (Section 3.4.6) (Fig. 8-4A) to calculate the dissociation constants (K_d) (Fig. 8-4B).

Figure 8-4| Effect of Nudix hydrolases on the polarization of [FAM]DNA18

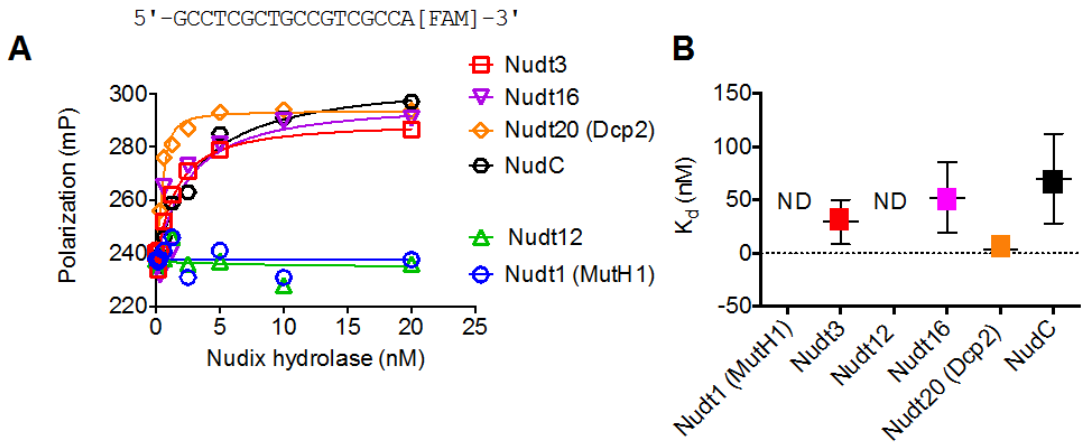

(A) 20 nM [FAM]DNA18 was titrated with each Nudix protein and polarization measured on TECAN infinite M1000, at 520 nm emission, when excited at 485 nm. The polarization values were fit Eq. 1 (Section 3.2.6), where F_s= 230, F_c= 296 and n= 25 are shared values among all data sets. (B) A summary of the best fit dissociation constants determined by GraphPad Prism. Nudt1= Not defined, Nudt3= 29, Nudt12= Not defined, Nudt16= 52, Nudt20= 3.1, NudC= 70 nM.

We also ruled out the hypothesis that the proteins may be interacting with the fluorophore alone and not the nucleic acids. However, no enhancement in fluorescence intensity or polarization (Em. 520 nm, Ex. 485 nm) was observed with the titration of 20 nM fluorescein with the Nudix hydrolases.

Next, we wanted to examine whether the interaction between Nudix proteins and nucleic acids was specific for the [FAM]-labeled probe, by using another fluorescently labeled DNA probe, Cy5 labeled dT15 and its RNA counterpart, Cy5 labeled rU15. The fluorescently labeled nucleic acid probes were titrated with each Nudix protein. The first point in each titration is the intensity of fluorescently labeled oligonucleotide alone, in the absence of any protein. If the fluorescence intensity increases with the titration of [Cy5]dT15 with the proteins, then it was assumed to be because of binding between [Cy5]dT5 and the Nudix hydrolases (Lohman et al., 2012; Hwang et al., 2014). Non-specific binding was ruled out by the addition of Bovine serum albumin (BSA) to [Cy5]dT15. The fluorescence emission was measured on FLUOstar Omega

(BMG LABTECH), with a gain= 100. The increase in fluorescence intensity (Ex. wavelength= 640 nm, Em. Wavelength= 670 nm) suggests the binding of [Cy5]dT15 with Nudt3, Nudt16, Nudt20 (Dcp2) and NudC. However, even with the addition of Nudt1(MutH1) and Nudt12, both the fluorescence intensity and polarization remain unchanged, suggesting that there is no interaction between the oligonucleotide and protein. The fluorescence intensity data (Fig. 8-5A) were fit to Eq. 1 (Section 3.4.6) to calculate the K_d (Fig. 8-5B). Similar results were obtained in repeat experiments.

Figure 8-5| Effect of Nudix hydrolases on the fluorescence intensity of [Cy5]dT15

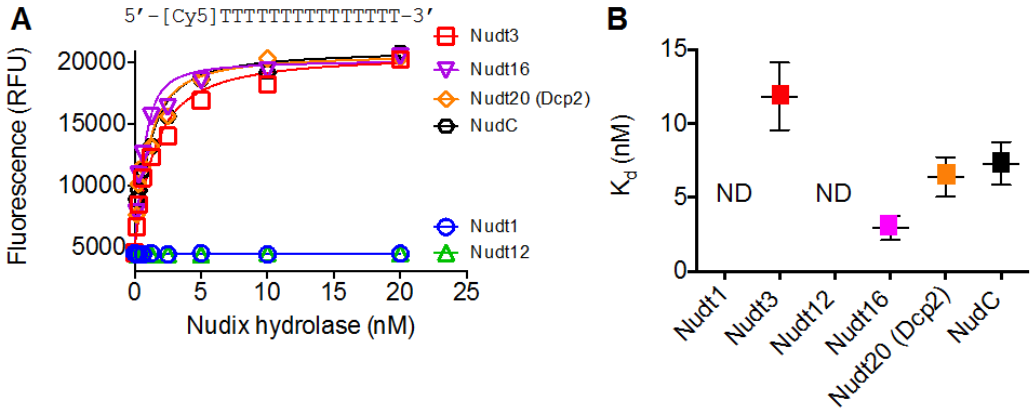

(A) Fluorescence intensity values, measured on FLUOstar Omega (BMG LABTECH), were fit to Eq. 1 (Section 3.2.6), where F_s= 461.3, F_c= 2099 and n= 11.3 are shared values among all data sets (B) A summary of the best-fit dissociation constants (K_d) obtained. K_d for Nudt1= Not defined, Nudt3= 11.841, Nudt12= Not defined, Nudt16= 2.957, Nudt20= 6.394, NudC= 7.308 nM.

The polarization of the same titration samples as described above, were measured at 520 nm when excited at 470 nm, on TECAN infinite M1000. G-factor reference well was set with 1 nM Fluorescein in 0.01 M NaOH= 180, while blank well was set with 50 mM Tris pH7.5. If the fluorescence polarization increased with the titration of [Cy5]dT15 into Nudix hydrolases, then an interaction between the DNA and the protein is confirmed. The polarization values (Fig. 8-6A) were data were fit Eq. 1 (Section 3.2.6) to calculate the dissociation constants (K_d) (Fig. 8-6B).

Figure 8-6| Effect of Nudix hydrolases on the polarization of [Cy5]dT15

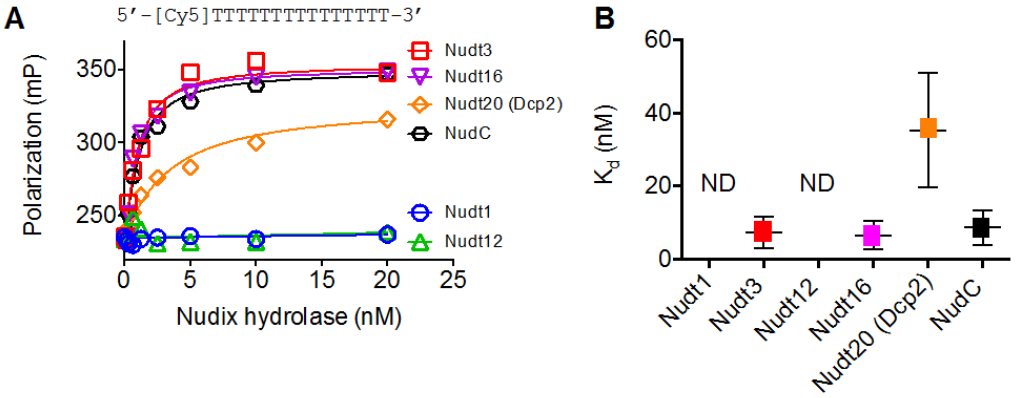

(A) The raw polarization, measured on TECAN infinite M1000, were fit to Eq. 1 (Section 3.2.6), where F_s= 23.52, F_c= 35.08 and n=11.3 are shared values among all data sets and (B) a summary of the dissociation constants (K_d) using GraphPad Prism (v.6). K_d for Nudt1= Not defined, Nudt3= 7.432, Nudt12= Not defined, Nudt16= 6.561, Nudt20= 35.328, NudC= 8.695 nM.

The fluorescence intensity and polarization experiments were conducted on two independent instruments, with both supporting the contention that some Nudix hydrolases interact with DNA. Data also suggest that the fluorophore on the oligonucleotide does not affect the interaction. Surprisingly, amongst the mammalian decapping Nudix hydrolases tested, only the human Nudt12 protein did not bind DNA.

8.3.2 Interaction between Nudix hydrolase and fluorescently-labeled RNA

Next, we wanted to study the interaction between RNA and Nudix hydrolases. Fluorescently labeled RNA probe, [FAM]RNA36 was titrated with serially diluted concentrations of Nudix proteins. The first point in each titration is the intensity of 20 nM [FAM]RNA36 alone, in the absence of any protein. If the fluorescence intensity increased with the amount of protein added to [FAM]RNA36, then it was assumed to be because of binding between [FAM]RNA36 and the Nudix hydrolases (Lohman et al., 2012; Hwang et al., 2014). Non-specific binding was ruled out by the addition of bovine serum albumin (BSA) with [FAM]RNA36. The fluorescence emission was measured on FLUOstar Omega (BMG LABTECH), with a gain= 100. The increase

in fluorescence emission (Ex. wavelength= 485 nm, Em. Wavelength= 520 nm) suggests the binding of [FAM]RNA36 with Nudt3, Nudt12, Nudt16, Nudt20 (Dcp2) and NudC (Fig. 8-7A). However, with Nudt1(MutH1), both the polarization and intensity values remain unchanged, even with the addition of protein, suggesting that there is no interaction between the oligonucleotide and protein. The fluorescence emission data were fit to Eq. 1 (Section 3.2.6) to calculate the K_d (Fig. 8-7B).

Figure 8-7| Effect of Nudix hydrolases on the fluorescence intensity of [FAM]RNA36

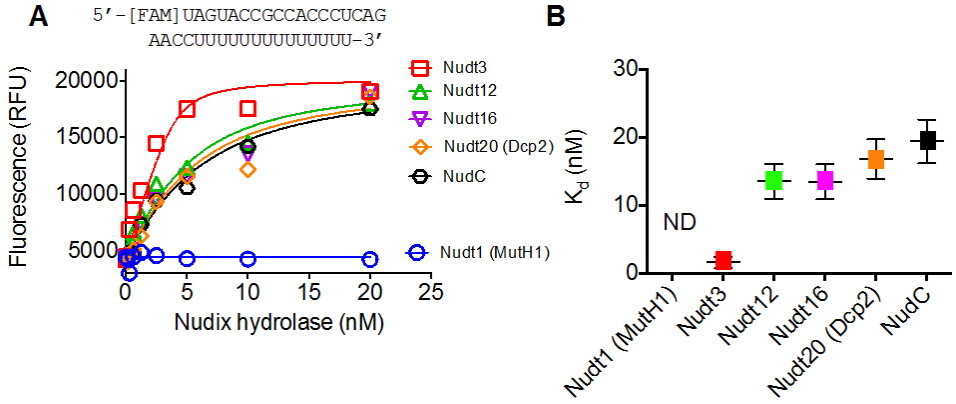

(A) The raw fluorescence intensity data, measured on FLUOstar Omega (BMG LABTECH), were fit Eq. 1 (Section 3.2.6), where F_s= 222, F_c= 979 and n= 5 are shared values among all data sets. (B) A summary of the dissociation constants (K_d). K_d for Nudt1= Not defined, Nudt3= 1.606, Nudt12= 13.528, Nudt16= 13.495, Nudt20= 16.844, NudC= 19.400 nM.

Fitting the enhancement in fluorescence emission (Em. 520 nm, Ex. 485 nm) to a binding model, confirmed the interaction between the human Nudt12 protein and RNA. Next, 20 nM, 40 nM and 80 nM [FAM]RNA 36 were titrated with serially diluted concentrations of Nudix proteins (Fig. 8-8). The first point in each titration is the fluorescence intensity of 20 nM or 40 nM [FAM]RNA36 alone, in the absence of any protein. Again, it was assumed that any increase in fluorescence emission and polarization is due to binding between [FAM]RNA36 and the protein. Non-specific binding was ruled out by the addition of Bovine serum albumin (BSA) with

[FAM]RNA36. The fluorescence emission was measured on FLUOstar Omega (BMG LABTECH), with a gain= 100. Both the fluorescence and polarization values remain unchanged, with the addition of Nudt1(MutH1) to [FAM]RNA36, suggesting that there is no interaction between the oligonucleotide and protein.

We couldn't include the fluorescence intensity data for 80 nM [FAM]RNA36 titrated with Nudix proteins, because the readings with our instrument maxed out at that particular concentration of fluorophore. However, since polarization intensity is not dependent on the concentration of fluorophore, we could replicate the desired results. The polarization intensity was measured at 520 nm when excited at 470 nm, on TECAN infinite M1000. As stated above, the G-factor reference well was set with 1 nM Fluorescein in 0.01 M NaOH= 180, while the blank well was set with 50 mM Tris pH7.5. The raw polarization values data were fit were fit Eq. 1 (Section 3.2.6) to calculate the K_d and the sites of binding (N). Both the K_d and N, assumed to be constant at equilibrium, were shared among the three data sets for each protein. Since the polarization intensity does not depend on concentration of the fluorophore, the maximum polarization of the complex between the protein and the RNA (F_c) and the initial polarization of [FAM]RNA36 alone (F_s) were shared for each protein as well.

Figure 8-8| Effect of Nudix hydrolases on the polarization of different concentrations of [FAM]RNA36

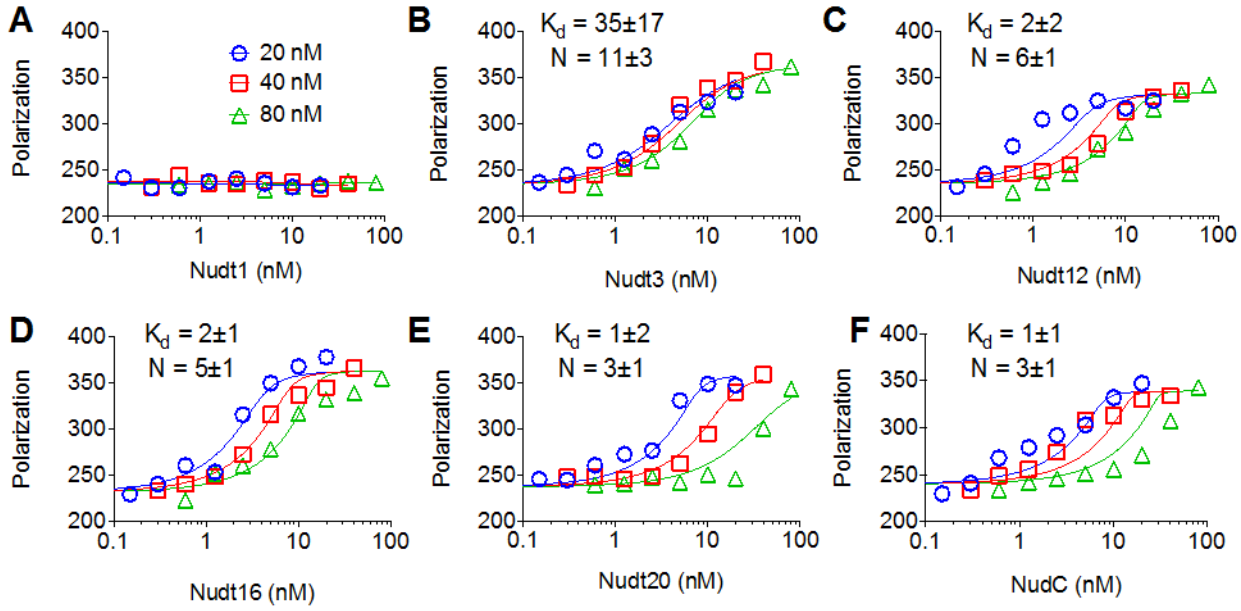

[FAM]RNA36 was titrated with various concentrations of (A) Nudt1 (MutH1) (B) Nudt3 (C) Nudt12 (D) Nudt16 (E) Nudt20 (Dcp2) and (F) NudC and an increase in polarization at 520 nm, measured on TECAN infinite M1000, was observed when excited at 485 nm. The data were fit to Eq. 1 (Section 3.2.6), where [FAM]RNA36= 20 nM (blue) or 40 nM (red) or 80 nM (green). K_d and N, assumed to be constant at equilibrium, were shared among the data sets.

We also wanted to test the hypothesis that the enhancement of fluorescence and polarization intensities observed with the titration of fluorescently labeled RNA to Nudix protein, was not depended on the fluorophore [FAM] used in previous experiments. Hence, another fluorescently labeled RNA, [Cy5]rU15 was titrated with serially diluted concentrations of Nudix proteins (Fig. 8-9). The fluorescence emission was measured on FLUOstar Omega (BMG LABTECH), with a gain= 100. If an increase in fluorescence emission (Ex. wavelength= 640 nm, Em. Wavelength= 670 nm) was observed, then binding of [Cy5]rU15 with Nudt3, Nudt12, Nudt16, Nudt20 (Dcp2) and NudC was assumed. The fluorescence emission data was then fit to Eq. 1 using GraphPad Prism (v.6) to calculate a K_d and for each protein-probe combination. However, with Nudt1(MutH1), both the polarization and fluorescence values remain unchanged,

even with the addition of protein, suggesting that there is no interaction between the oligonucleotide and protein. Similar results were obtained in repeat experiments (Fig. 8-9).

Figure 8-9| Effect of Nudix hydrolases on the fluorescence intensity of [Cy5]rU15

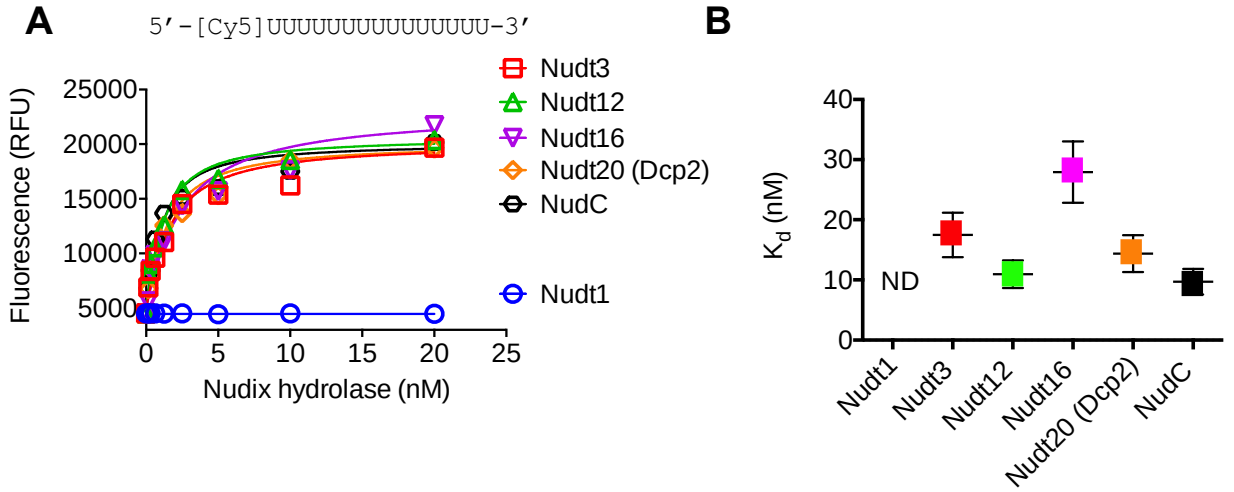

The raw fluorescence data, measured on FLUOstar Omega (BMG LABTECH), were fit to Eq. 1 (Section 3.2.6), where F_s= 474.4, F_c= 2096 and n=11.3 are shared values among all data sets and (B) a summary of the dissociation constants (K_d) using GraphPad Prism (v.6). K_d for Nudt1= Not defined, Nudt3= 17.487, Nudt12= 10.939, Nudt16= 27.925, Nudt20= 17.394, NudC= 9.718 nM.

The polarization intensity of the same titration samples as described above, were measured at 670 nm when excited at 640 nm, on TECAN infinite M1000. G-factor reference well was set with 1 nM Fluorescein in 0.01 M NaOH= 180, while blank well was set with 50 mM Tris pH7.5. The polarization emission data was fit to Eq. 1 with GraphPad Prism (v.6), to calculate the K_d for each interaction between [Cy5]rU15 and the Nudix hydrolases.

Figure 8-10| Effect of Nudix hydrolases on the polarization of [Cy5]rU15

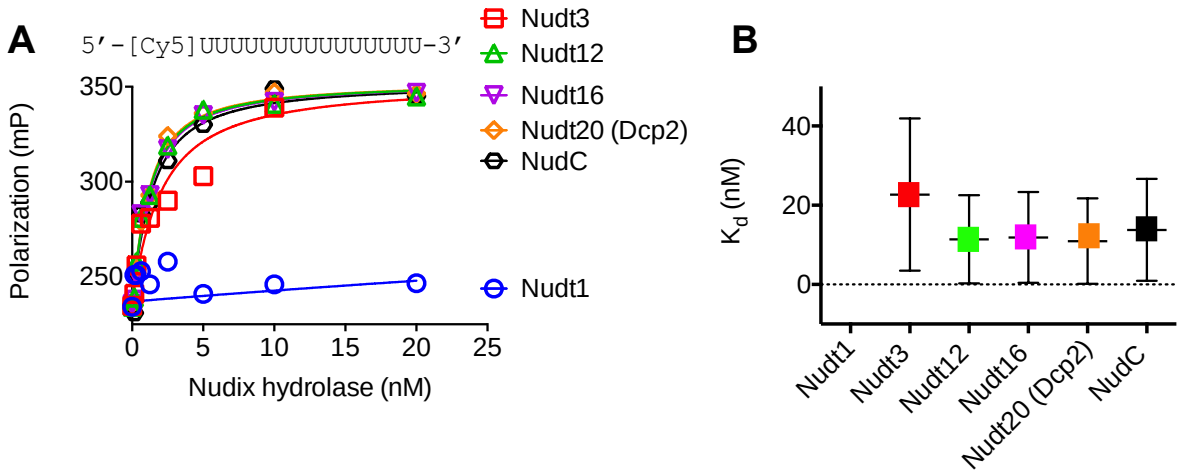

(A) The raw polarization measured on TECAN infinite M1000, were fit to Eq. 1 (Section 3.2.6), where F_s= 24, F_c= 35 and n= 13 are shared values among all data sets. (B) A summary of the dissociation constants (K_d) using GraphPad Prism (v.6). K_d for Nudt1= Not defined, Nudt3= 22, Nudt12= 11, Nudt16= 12, Nudt20= 11, NudC= 14 nM.

These initial experiments confirmed that the fluorophore does not affect the interaction between the RNA and the nudix proteins, further showing that the human Nudt12 protein specifically binds to only RNA and not DNA (Fig. 8-10).

8.3.3 A probe-displacement assay to monitor RNA/DNA binding to Nudix hydrolases

Next, a probe displacement assay was designed using unlabeled RNA, to test preferential binding between Nudix hydrolases and DNA or RNA. 20 nM [FAM]RNA36 was titrated with 5 nM Nudix hydrolases to replicate the previously observed enhanced fluorescence and polarization intensity at 520 nm, when excited at 485 nm. An increase in fluorescence emission suggested the interaction of the Nudix hydrolase with the nucleic acid. This enhanced fluorescence polarization (Fig. 8-11) and of the bound [FAM]RNA36 was displaced from various Nudix hydrolase complex using unlabeled RNAs, either RNA36 (Fig. 8-11A) or RNA18 (Fig. 8-11B). If a decrease in the fluorescence and polarization with an increasing titration of RNA36 or RNA18 was observed, then it was assumed that Nudix hydrolase interacted with the unlabeled oligonucleotides instead of the

existing [FAM]RNA36. Supportive data has been shown for NudC, Nudt3, Nudt12, Nudt16 and Nudt20 (Dcp2). However, with Nudt1 (MutH1), the fluorescence values remain unchanged, suggesting yet again that there is no interaction between RNA18 or RNA36 and the protein. The fluorescence intensity values were fit to Eq. 2 using GraphPad Prism (v.6), as described in Section 3.2.8.

Figure 8-11| Displacement of [FAM]RNA36 from Nudix hydrolases with RNA18 and RNA36

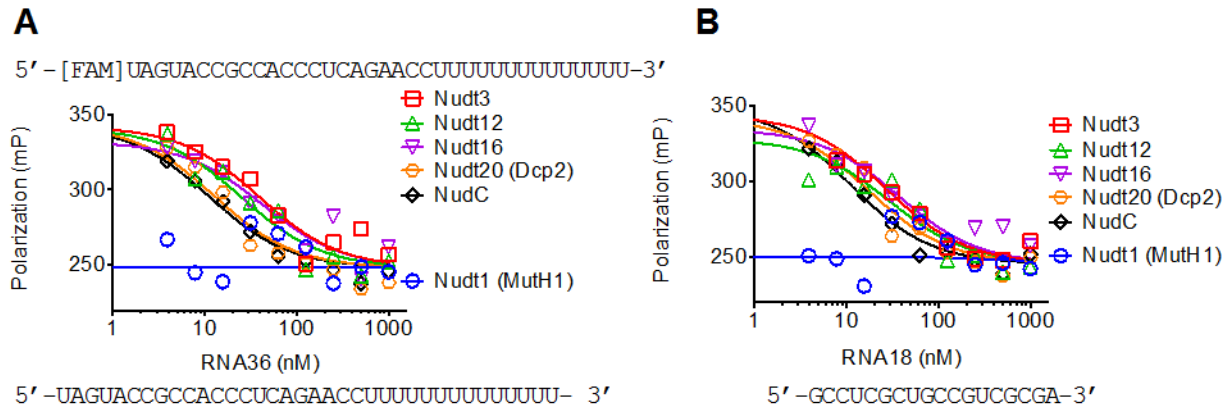

The polarization measured on TECAN infinite M1000, at 520 nm when excited at 485 nm when 20 nM [FAM]RNA36 was titrated with 5 nM Nudix hydrolase and subsequently displaced using various concentrations of (A) RNA36. The raw data were fit to Eq. 2 (Section 3.2.8) to yield IC50 values for Nudt1= Not defined, Nudt3= 39.43, Nudt12= 25.42, Nudt16= 42.60, Nudt20= 12.84, NudC= 11.21 nM. (B) RNA18. The raw data was fit to inhibition dose response curve using GraphPad Prism (v.6) to yield IC_{50} values for Nudt1= Not defined, Nudt3= 27, Nudt12= 30 Nudt16= 37, Nudt20= 18, NudC= 11 nM.

This data suggests that the length of the RNA does not affect its interaction with the proteins. Both RNA18 and RNA36 displaced the existing enhanced fluorescence emission of [FAM]RNA36-Nudix hydrolase complex, with the proteins not preferring any length of oligonucleotide more than the other. Another pair of unlabeled oligonucleotides, RNA29 and its deoxynucleotide counterpart, DNA29 were chosen to disrupt the binding between [FAM]RNA36 and Nudix hydrolases, to further validate the specificity of the human Nudt12 protein binding RNA

only, over DNA (Fig. 8-12). The fluorescence emission at 520 nm when excited at 485 nm was measured on FLUOstar Omega (BMG LABTECH), with a gain= 100. If a decrease in the fluorescence emission was observed, then it was assumed that the Nudix hydrolases bound the unlabeled oligonucleotide instead of [FAM]RNA36. The fluorescence emission data was fit to Eq. 2 using GraphPad Prism (v.6), as described in Section 3.2.8.

Figure 8-12| Displacement of [FAM]RNA36 from Nudix hydrolases with RNA29 and DNA29

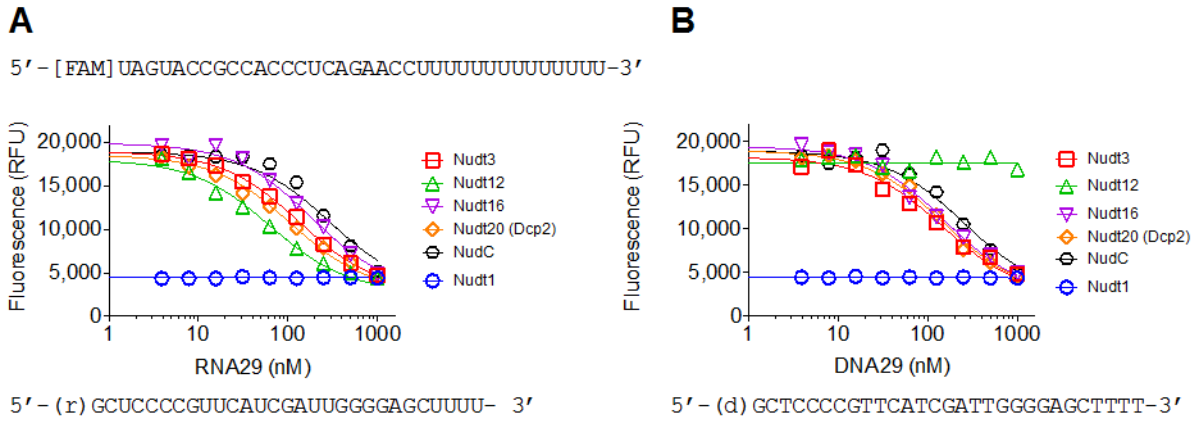

The fluorescence emission, measured on FLUOstar Omega (BMG LABTECH), at 520 nm when excited at 485 nm when 20 nM [FAM]RNA36 was titrated with 5 nM Nudix hydrolase and subsequently displaced using various concentrations of (A) RNA29. The raw data were fit to Eq. 2 (Section 3.2.8) to yield IC_{50} values for Nudt1= Not defined, Nudt3= 133, Nudt12= 63, Nudt16= 184, Nudt20= 108 and NudC= 292 nM. (B) DNA29. The raw data were fit to Eq. 2 (Section 3.2.8) to yield IC_{50} values for Nudt1= Not defined, Nudt3= 147, Nudt12= Not defined, Nudt16= 158, Nudt20= 152 and NudC= 258 nM. The DNA oligonucleotide, DNA29 fails to displace the enhanced fluorescence of [FAM]RNA36 already bound to Nudt12, further confirming that Nudt12 exclusively binds RNA and not DNA.

This experiment confirmed that irrespective of having the same sequence, the deoxynucleotide version (DNA29) failed to interact with the human Nudt12 protein, while its RNA complement, RNA29 displaced the existing interaction between [FAM]RNA36 with the Nudt12. To further test the hypothesis that Nudt12 exclusively binds RNA and not DNA, the enhanced fluorescence and polarization intensity of [FAM]RNA36 bound with Nudt12 was displaced with

unlabeled DNA nucleotides GA9, C18 and RNA nucleotides RNA18 and RNA36 under identical conditions. To test the reproducibility of the data, various concentrations of [FAM]RNA36 bound to Nudt12 were displaced with appropriate concentrations of unlabeled oligonucleotides. The fluorescence enhancement (Em. 520 nm, Ex. 485 nm) was measured on FLUOstar Omega (BMG LABTECH), with a gain= 100. If a decrease in the enhanced fluorescence emission was observed, then it was assumed that the human Nudt12 protein interacted with the unlabeled oligonucleotide titrated into the sample. The fluorescence emission data was fit to Eq. 3 (Section 3.2.8) to calculate inhibition constant (K_i).

Figure 8-13| Displacement of [FAM]RNA36 from Nudt12 with GA9, C18, RNA18 and RNA36

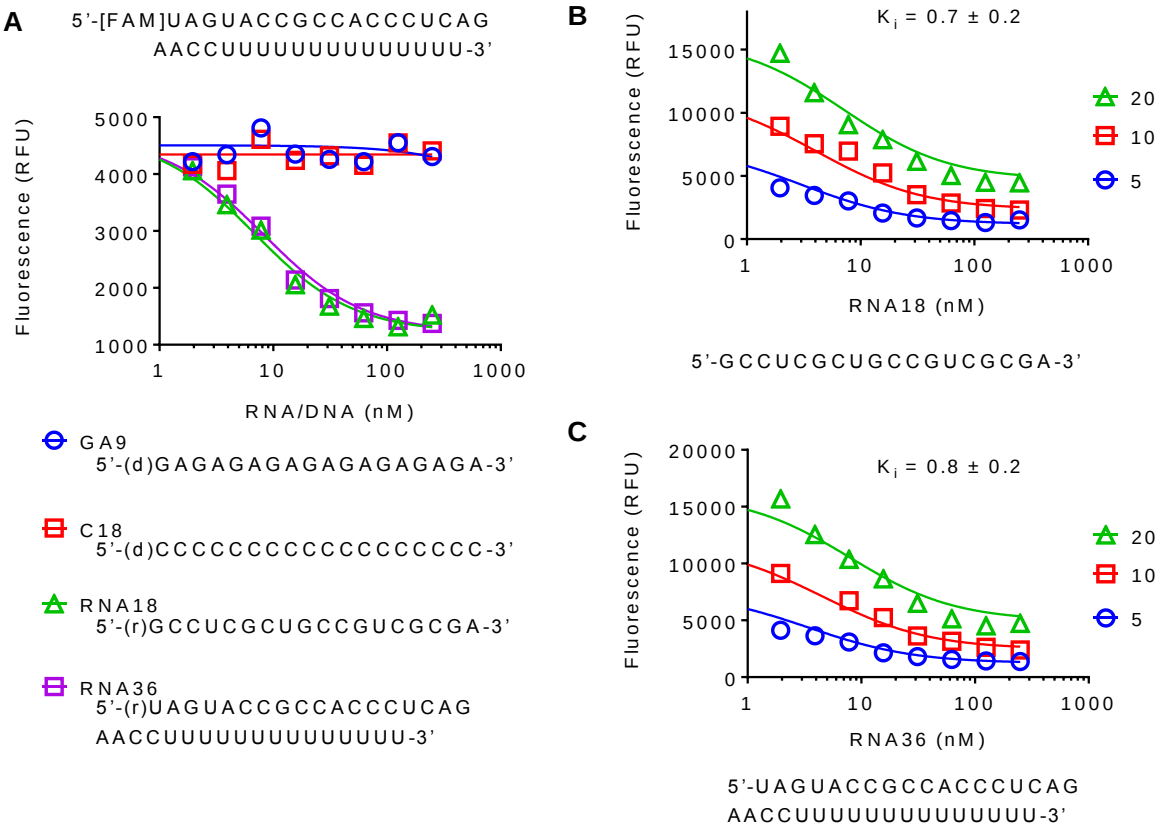

The fluorescence emission, measured on FLUOstar Omega (BMG LABTECH), at 520 nm when excited at 485 nm when (A) 5 nM [FAM]RNA36 was titrated with 1 nM Nudt12 and displaced using various concentrations of DNAs GA9 (blue), C18 (red) and RNAs RNA18 (green) and RNA36 (purple). The DNA oligonucleotides, GA9 and C18 failed to displace the enhanced fluorescence of the [FAM]RNA36 bound to Nudt12 complex. The data were fit to Eq. 2 (Section 3.2.8) to yield IC_{50} values for GA9= Not defined, C18= Not defined, RNA18= 6.8 and RNA36= 8.2 nM. Next, the enhanced fluorescence emission at 520 nm when 5 nM [FAM]RNA36 was titrated with 1 nM Nudt12 (blue), 10 nM [FAM]RNA36 was titrated with 2.5 nM Nudt12 (red) and 20 nM [FAM]RNA36 was titrated with 5 nM Nudt12 (green) and displaced using various concentrations of (B) RNA18 and (C) RNA36. In (B) and (C), the raw data was fit to Eq. 3 (Section 3.2.8)

Since the fluorescence emission is dependent on the concentration of the fluorophore titrated in each experiment, the initial fluorescence of [FAM]RNA36 titrated with Nudt12 is indicative of the concentration of [FAM]. K_i, assumed to be constant at equilibrium is shared among the three data sets for each titration of unlabeled oligonucleotide. The length of the 'competing' unlabeled oligonucleotide does not affect the interactions between the RNA and Nudt12.

8.3.4 In vitro transcription of ncinRNA

To test if Nudt12 binds to ncinRNA (non-canonical initiating nucleotide RNA), we used T7 RNA polymerase to synthesize RNA with non-canonical initiating nucleotides (ncin) such as NAD^+, NADH, $NADP^+$ and NADPH. The DNA template used for each ncinRNA transcription is NsiI digested pET24-nudC vector, obtained as described in Section 3.1.5.

Each band was excised out of the gel (Fig.7-2) and gel extracted. The gel purified NAD^+-capped RNA was phenol:chloroform treated and then injected into a LCMS-2020. Elution of each sample was observed, ions were collected for m/z ranging from 100 to 1000, and photodiode array spectra was collected between 190-700 nm.

NAD^+-capped RNA eluted at much later at 4.5 minutes, compared to free NAD^+ which eluted at 2.0 minutes under identical assay conditions (Fig. 8-14). It was assumed that since the

NAD^+ was covalently attached to the terminal end of the RNA transcript, it would elute at a later time point compared to free NAD^+.

Figure 8-14| LC of in vitro transcribed NAD^+-capped RNA

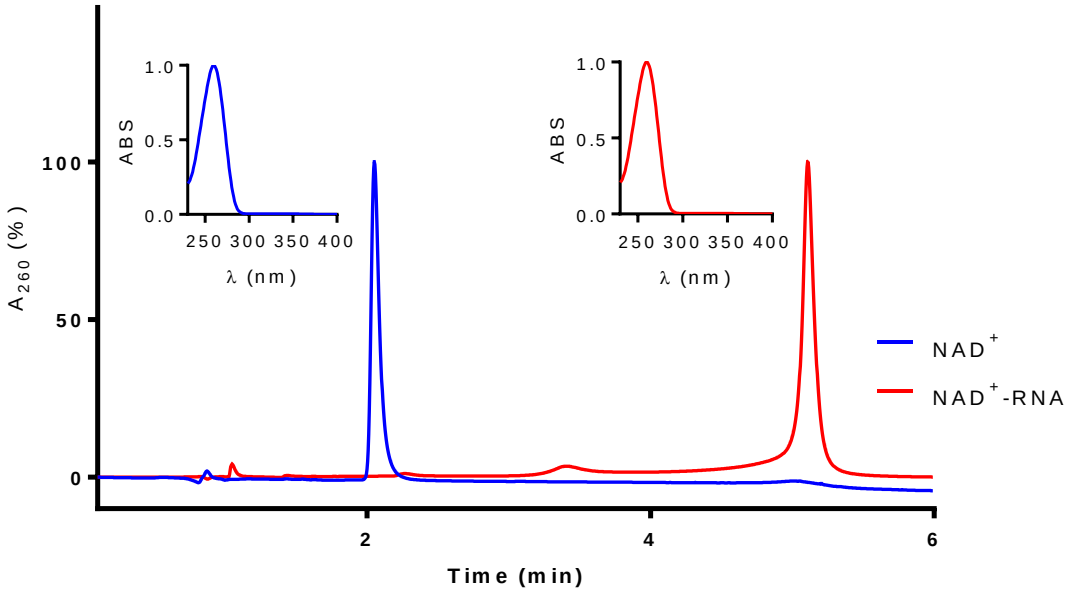

LC data (260 nm) of both free NAD^+ (blue) and NAD^+-capped RNA (red) to illustrate their different elution times on the instrument under identical conditions and the normalized PDA of both NAD^+ and NAD^+-capped RNA

Similarly, *in vitro* transcribed NADH-capped RNA was gel extracted, treated according to the Sevag protocol and injected into the LCMS instrument. As a control, NADH alone was run on the LCMS instrument under identical conditions. It was assumed again that NADH-capped RNA would elute at a much later time point on the chromatogram compared to free NADH (Fig. 8-15).

Figure 8-15| LC of in vitro transcribed NADH-capped RNA

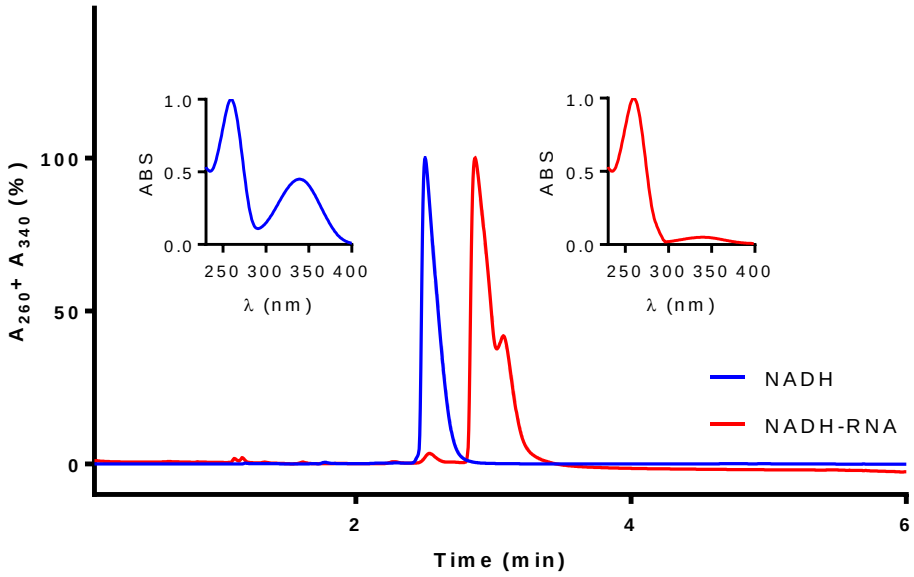

LC data (260 nm, 340 nm) of both NADH alone (blue) and NADH-capped RNA (red) to illustrate their different elution times on the instrument under identical conditions and the normalized PDA data of both samples as well.

The ratio of the absorbance at 260 nm to 340 nm of NADH-capped RNA is not characteristic of free NADH, suggesting the presence of an RNA tail attached to a NADH moiety.

8.3.5 Nudt12 prefers to bind NAD$^+$-capped RNA

To test the hypothesis whether Nudt12 binds ncinRNA, the enhanced fluorescence and polarization intensity of [FAM]RNA36 bound with Nudt12 was displaced with unlabeled ncinRNA (Fig. 8-16). Similar results were observed in repeat experiments. If the existing fluorescence emission of the [FAM]RNA36-Nudt12 complex decreased with the titration of unlabeled ncinRNA, then it was assumed that Nudt12 was interacting with ncinRNA instead of [FAM]RNA36. Concentrations of ncinRNAs were determined from their absorbance at 260 nm. Fluorescence emission was measured on FLUOstar Omega (BMG LABTECH), with a gain= 100

(Em. 520 nm, Ex. 485 nm). The fluorescence data were fit to Eq. 2 (Section 3.2.8) to yield IC_{50} values.

Figure 8-16| Displacement of [FAM]RNA36 from Nudt12 with ncinRNA (fluorescence emission)

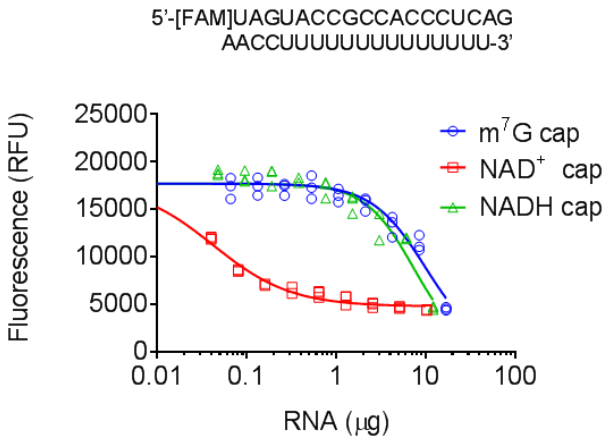

The fluorescence emission, measured on FLUOstar Omega (BMG LABTECH), at 520 nm when excited at 485 nm when 20 nM [FAM]RNA36 was titrated with 5 nM Nudt12 was displaced using various concentrations of ncinRNAs, NAD^+-capped RNA (red) and NADH-capped RNA (green). The raw data were fit to Eq. 2 (Section 3.2.8) and IC_{50} values were found to be similar for ^{7}mG and NADH capped RNA (10 µg/ml), but an impressive 300 fold lower for NAD^+-capped RNA (0.04 µg/ml).

The same experiment was repeated to observe a decrease in polarization (Em. 520 nm, Ex. 485 nm) of the [FAM]RNA36-Nudt12 complex, being displaced with *in vitro* transcribed capped RNA. The polarized intensities measured on TECAN infinite M1000 (Fig. 8-17) were fit to Eq. 2 (Section 3.2.8). G-factor reference well was set with 1 nM Fluorescein in 0.01 M NaOH= 180, while blank well was set with 50 mM Tris pH 7.5.

Figure 8-17| Displacement of [FAM]RNA36 from Nudt12 with ncinRNA (polarization).

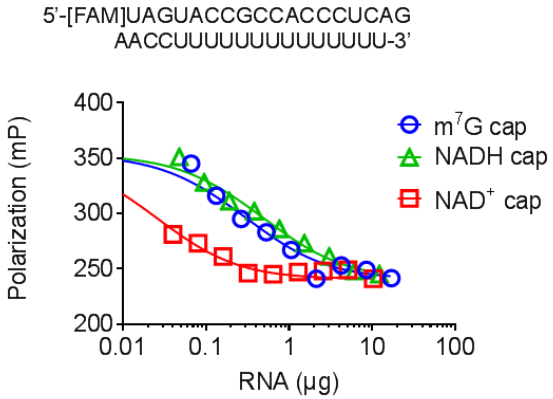

Polarization measured on TECAN infinite M1000, at 520 nm when excited at 485 nm when (A) 20 nM [FAM]RNA36 was titrated with 5 nM Nudt12 was displacement using various concentrations of ncinRNAs, NAD^+-capped RNA (red) and NADH-capped RNA (green). Data were fit to Eq. 2 (Section 3.2.8) and IC_{50} values were found to be much higher for ^{7}mG (0.2 µg) and NADH-capped RNA (~ 0.4 µg), but an impressive 100 fold lower for NAD^+-capped RNA (0.002 µg).

8.4 Discussion

Ever since the purification of the first NAD-cleaving nudix hydrolase, bacterial NudC, it has been shown to precipitate with nucleic acids. Since then, other prokaryotic and eukaryotic Nudix hydrolases have been shown to have RNA decapping activity on non-methylated, monomethylated and ncinRNAs. The crystal structure solved for NudC showed a positively charged residue adjacent to the NAD-binding pocket, for a possible site to bind nucleic acids. The sequences of both bacterial NudC and human Nudt12 shows a 110-161 amino acid residue, comprising of a zinc-finger domain, known to interact with nucleic acids. However, the direct interaction between such Nudix proteins and their nucleic acid substrates have never been studied before. This chapter for the first time, clearly demonstrates an interaction between Nudix decapping proteins and nucleic acids. Surprisingly, our results also show that the human NAD-cleaving Nudt12 protein exclusively binds to RNA, and not DNA. These results were confirmed by both gel shift assays and a more quantitative approach using fluorescence polarization and

emission assays, as wells as probe displacement assays. Our results also show that Nudt12 prefers to bind NAD^+-capped RNA strongly than either NADH-capped or ^{7}mG-capped RNA. It may be concluded from these studies that the *in vivo* substrate for NAD-cleaving Nudix hydrolases might be NAD^+-capped RNA and not NADH, as previously thought. The optimized fluorescence polarization and emission-based assays may be used to either screen a library of inhibitory compounds against the Nudix proteins or to study interactions between yeast NPY1 and nucleic acids.

Chapter 9 Lactate Dehydrogenase Reduce NAD-capped RNA

9.1 Summary

Ever since the identification of non-canonical covalent modifications on the terminal end of both prokaryotic and eukaryotic RNA transcripts, their existence *in vivo* has been a mystery. In this chapter, we test the idea that the NAD modification might not just be to stabilize the RNA transcripts but to function as an important cofactor to several metabolic enzymes. Our results demonstrate that NAD-capped RNA might not only be a cofactor to NAD-utilizing metabolic enzyme, such as LDH but also the more preferred cofactor compared to NAD alone. For the first time, the studies discussed in this chapter establishes a clear biochemical role of such ncinRNAs *in vivo*, making way for a possibly new class of ribonucleoproteins or even ribozymes.

9.2 Background

Lactate dehydrogenase (LDH) is an important enzyme in anaerobic respiration, the conversion of pyruvate into lactate in the absence oxygen. This pathway is crucial for the essential generation of ATP and the regeneration of NAD^+ from NADH. Simultaneously, during the Cori cycle, lactate dehydrogenase can reduce NAD^+ back, by transferring a hydride from lactate to pyruvate. We hypothesized that the biochemical role of the cofactors NAD^+ or NADH attached to the terminal end of *in vitro* transcribed RNAs could be instrumental in such metabolic redox reactions.

In vivo, L-lactate dehydrogenase is found in five forms of isoenzymes, each having a slightly different structure and spread over various tissues like the heart and the skeletal muscle. NADPH and $NADP^+$ were used as negative controls that do not assist the activity of L-lactate dehydrogenase. Interestingly, ncinRNA was found to be a substrate of the same enzyme. This

finding is supported further by the fact that lactate dehydrogenase is an mRNA binding enzyme, specifically found to interact with GM-CSF mRNA 3'UTR (Rigby et al., 2002).

L-lactate dehydrogenase catalyzes the conversion of pyruvate to lactate and back, by transferring a hydride between the two molecules. NADH is oxidized to NAD^+, while pyruvate is reduced to lactate, during the redox reaction. The pyridine ring of NAD^+ has a more stable configuration than NADH, making NADH absorb at both 260 nm and 340 nm, while NAD^+ only absorbs at 260 nm. Hence, this assay was designed to monitor the decay in the absorbance at 340 nm, with the reduction of pyruvate to lactate. The reverse redox reaction was studied as well, with an increase in the absorbance at 340 nm.

All experiments were set up as described in Section 3.2.8.

9.3 Results

9.3.1 Minimizing LDH assays

The recombinant bacterial lactate dehydrogenase has been cloned from chicken heart. Recombinant *E. coli* (chicken heart) L-LDH catalyzes the reduction of pyruvate to lactate, and the subsequent oxidation of NADH. Each reaction mixture containing 60 μM NADH, 4.65 nM chicken heart LDH was made to a final volume of either 1 ml (Fig 9-2A) or 0.05 ml (Fig 9-2B) with 220 mM Tris Cl pH 7.3. Each reaction was then initiated with various concentrations of pyruvate to observe a decay in the absorbance at 340 nm, as NAD^+ was produced from NADH.

Figure 9-1| Initiating the LDH reactions with pyruvate

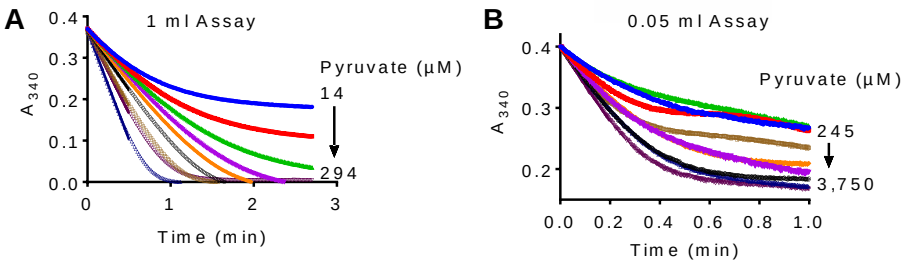

220 mM Tris pH 7.3, 4.65 nM chicken heart lactate dehydrogenase, containing either ~ 60 µM NADH was initiated with varying concentrations of a 30 mM sodium pyruvate stock solution, either in a (A) 1 ml or (B) 0.05 ml cuvette. The decay in absorbance at 340 nm was recorded for 3 minutes. Initial rates were observed to be dependent on substrate concentration which were and plotted using GraphPad Prism (v.6).

In vitro transcription yields only 50 µl of ncinRNA product. Hence, the replication of the LDH assay in a much smaller volume (50 µl) was essential to test the activity of such ncinRNAs in similar redox reactions.

9.3.2 NADH-capped RNA is a substrate of recombinant E. coli lactate dehydrogenase

We tested the hypothesis that *in vitro* transcribed ncinRNA may be a substrate for L-lactate dehydrogenase. Identical reactions containing 220 mM Tris Cl pH 7.3, 1 mM Sodium pyruvate, 20 µM substrate (NADH or NADH-capped RNA and NADPH or NADPH-capped RNA) was initiated with 4.65 nM of lactate dehydrogenase and the absorbance at 340 nm, 25°C was collected every 0.1 seconds on Varian Cary 50 UV-Vis Spectrophotometer for 3 minutes. The concentration of the chicken heart LDH used in each assay was calculated using its molecular weight (43 kDa). NADPH was chosen as a negative control because it has previously been reported to be inactive in aiding redox reactions catalyzed by L-lactate dehydrogenase (Holmberg et al., 1999, Zhu et al., 2015).

Figure 9-2| NAD-capped RNA is a substrate of recombinant E. coli lactate dehydrogenase
Reaction mixtures containing 220 mM Tris Cl pH 7.3, 1 mM Sodium pyruvate was initiated with 4.65 nM of chicken heart lactate dehydrogenase for NADH (blue), NADH-capped RNA (purple), NADPH (green) and NADPH-capped RNA (red) and a decay in absorbance at 340 nm was observed. However, the absorbance remained constant for both NADPH and NADPH-capped RNA, even with the addition of enzyme. Raw UV absorbance data was plotted using GraphPad Prism (v.6).

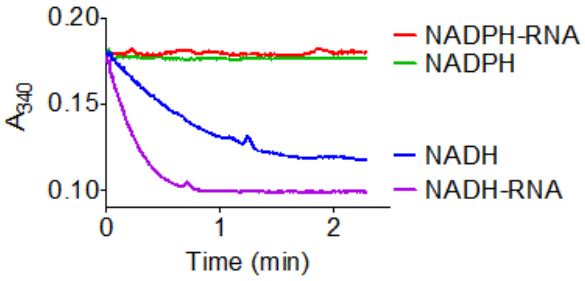

Surprisingly, the NADH-capped RNA was found to be a substrate of the recombinant bacterial lactate dehydrogenase and the initial rate was found to be 10 times faster than when NADH alone as a cofactor. Since this was the first study to establish a clear biochemical role of ncinRNAs, we proceeded to further study the kinetic parameters of ncinRNAs involved in redox metabolic reactions (Fig. 9-1).

Reaction mixture containing 220 mM Tris pH 7.3, 150 µM NADH, 4.65 nM chicken heart lactate dehydrogenase was initiated with varying concentrations of sodium pyruvate. With the simultaneous reduction of pyruvate to lactate, and the oxidation of NADH to NAD^+, a decay in the absorbance at 340 nm was recorded every 0.25 seconds on Varian Cary 50 UV-Vis Spectrophotometer for 3 minutes. Each reaction containing NADH and enzyme was made to a total volume of 1 ml with 220 mM Tris pH 7.3, then initiated with varying volumes of a 30 mM Sodium pyruvate solution.

To test the hypothesis that NADH-capped RNA may be a substrate for chicken heart lactate dehydrogenase, similar experiments as described above were repeated with 45 µM NADH-capped RNA. Each reaction containing NADH-capped RNA and enzyme was made to a total volume of 60 µl with 220 mM Tris pH 7.3, then initiated with varying volumes of a 30 mM Sodium pyruvate solution. Each reaction was carried out in a 50 µl quartz cuvette.

The rates for each reaction was fit to a substrate inhibition curve (Eq. 7) using GraphPad Prism (v.6).

$$v = \frac{V_{max}S}{(K_m + S(1 + {}^{S}/_{K_i})} \quad \text{(Eq. 7)}$$

Where v= Enzyme activity in A_{340} min^{-1}

S= Substrate concentration (µM)

V_{max}= Maximum enzyme activity in A_{340} min^{-1}

K_m= Michaelis-Menten constant (µM)

Figure 9-3| Initiating the recombinant *E. coli* LDH reaction with pyruvate

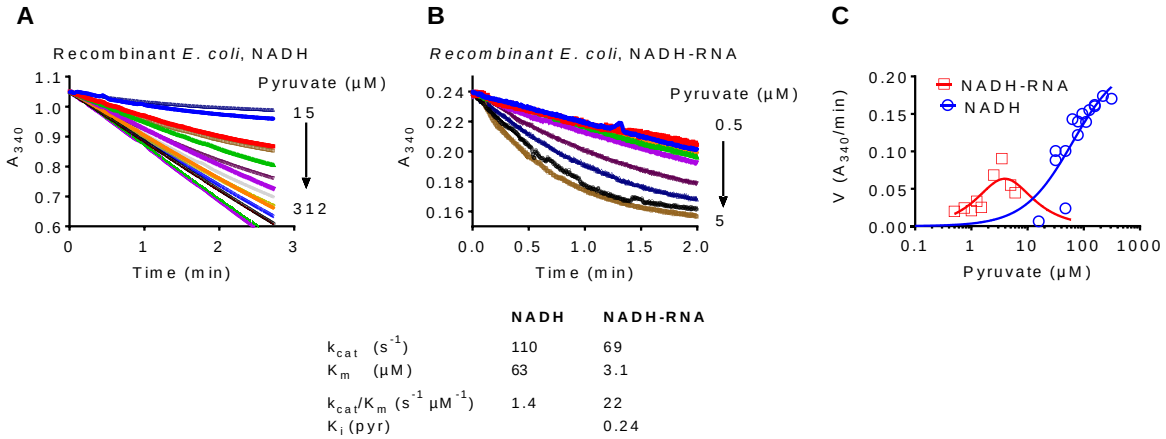

	NADH	NADH-RNA
k_{cat} (s^{-1})	110	69
K_m (µM)	63	3.1
k_{cat}/K_m (s^{-1} $µM^{-1}$)	1.4	22
K_i (pyr)		0.24

220 mM Tris pH 7.3, 4.65 nM recombinant bacterial (chicken heart) lactate dehydrogenase, containing either (A) 175 µM NADH or (B) 30 µM NADH-capped RNA was initiated with varying concentrations of a 30 mM sodium pyruvate stock solution. The decay in absorbance at 340 nm was collected at an interval of 0.5 seconds on Varian Cary 50 UV-Vis Spectrophotometer for 3 minutes. Initial rates were (C) plotted against pyruvate concentration and fit to substrate inhibition model (Eq. 7) using GraphPad Prism (v.6) to yield a ~ 20 fold lower K_m value for NADH-capped RNA (red) compared to NADH (blue) and a ~ 20 fold higher catalytic efficiency (22 $s^{-1}µM^{-1}$) for the ncinRNA compared to free NADH (1.4 $s^{-1}µM^{-1}$). Surprisingly, NADH-capped RNA was found to experience more substrate inhibition compared to NADH.

Turnover number (k_{cat}) is a measure of lactate that is converted to pyruvate per second, by each active site on LDH and was calculated by dividing the v_{max} by the total LDH concentration in each assay. Surprisingly, not only was the NADH moiety of NADH-capped RNA found to be a

substrate for chicken heart LDH, but it had 20 times lower K_m compared to that of NADH, and a higher catalytic efficiency (k_{cat}/K_m) as well. Also, a more pronounced substrate inhibition is observed when NADH-capped RNA catalyzes the redox reaction, compared to free NADH.

9.3.3 NADH-capped RNA is a substrate of bovine heart lactate dehydrogenase

The subunits of lactate dehydrogenase can be divided between M (muscle type) or H (heart type) encoded by two distinct genes LDH-A and LDH-B, respectively (Alegre E et al., 2015). So, we tested the hypothesis that *in vitro* transcribed ncinRNA may be a substrate for both subunits of mammalian L-lactate dehydrogenase, from these two different sources: heart and muscle. Identical reactions containing 220 mM Tris Cl pH 7.3, 1 mM Sodium pyruvate, ~ 50 µM substrate (NADH or NADH-capped RNA and NADPH or NADPH-capped RNA) was initiated with 506 pM heart lactate dehydrogenase and the absorbance at 340 nm, 25°C was collected every 0.1 seconds on Varian Cary 50 UV-Vis Spectrophotometer for 3 minutes. NADPH was chosen as a negative control because it has previously been reported to be inactive in aiding redox reactions catalyzed by L-lactate dehydrogenase (Holmberg et al., 1999, Zhu et al., 2015). The bovine heart lactate dehydrogenase was purchased from Sigma-Aldrich (L2625).

Reaction mixture containing 220 mM Tris pH 7.3, ~50 µM NADH, 506 pM bovine heart lactate dehydrogenase was initiated with varying concentrations of sodium pyruvate. With the simultaneous reduction of pyruvate to lactate, and the oxidation of NADH to NAD^+, a decay in the absorbance at 340 nm was recorded every 0.1 seconds on Varian Cary 50 UV-Vis Spectrophotometer for 3 minutes. The concentration of the mammalian heart LDH used in each assay was calculated using its molecular weight (36.4 kDa). Each reaction, containing the NADH and enzyme was made to a total volume of 60 µl with 220 mM Tris pH 7.3, then initiated by adding varying concentrations of sodium pyruvate.

Figure 9-4| Initiating the heart LDH reaction with pyruvate

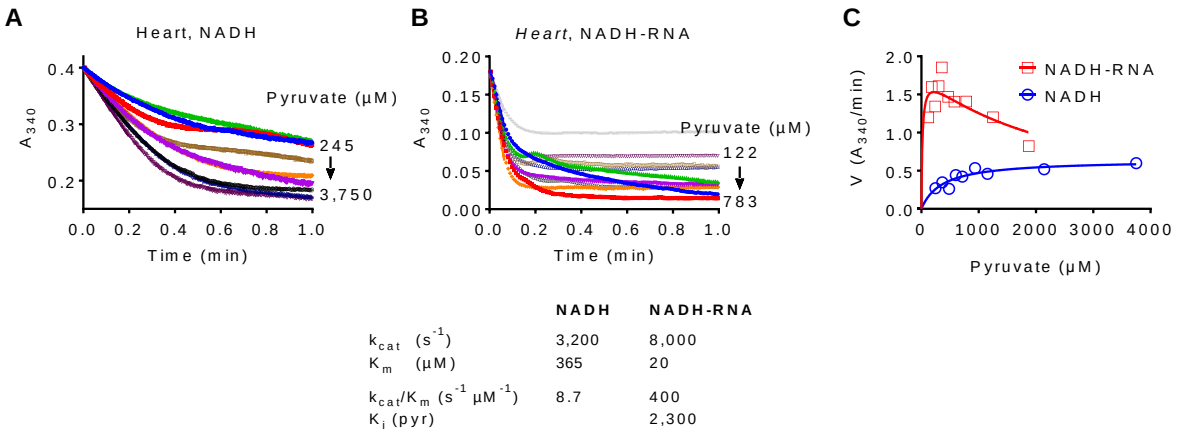

	NADH	NADH-RNA
k_{cat} (s^{-1})	3,200	8,000
K_m (µM)	365	20
k_{cat}/K_m (s^{-1} μM^{-1})	8.7	400
K_i (pyr)		2,300

220 mM Tris pH 7.3, 506 pM bovine heart lactate dehydrogenase, containing either (A) 50 µM NADH or (B) 30 µM NADH-capped RNA was initiated with varying concentrations of a 30 mM sodium pyruvate stock solution. The decay in absorbance at 340 nm was collected at an interval of 0.5 seconds on Varian Cary 50 UV-Vis Spectrophotometer for 3 minutes. Initial rates were (C) plotted against pyruvate concentration and fit to substrate inhibition model (Eq. 7) using GraphPad Prism (v.6) to yield a significantly (~ 20 folds) lower K_m and a higher (~ 50 folds) higher k_{cat}/K_m for ncinRNA compared to free NADH.

Surprisingly, not only was the NADH moiety of NADH-capped RNA found to be a substrate for mammalian heart lactate dehydrogenase, but it was a more preferred cofactor compared to that of NADH, with an almost 20 folds lower K_m and ~ 50 folds higher catalytic efficiency for ncinRNA. A similar trend in substrate inhibition to that experienced by recombinant bacterial LDH is observed in this case as well. It is important to note that both enzymes used are the heart isozymes of L-lactate dehydrogenase.

9.3.4 NADH-capped RNA is a substrate of rabbit muscle lactate dehydrogenase

Similar to experiments described in section 9.3.2, we tested the hypothesis that ncinRNA may be a substrate for the muscle subunit of L-lactate dehydrogenase, as well. Identical reactions containing 220 mM Tris Cl pH 7.3, 1 mM Sodium pyruvate, 50 µM substrate (NADH or NADH-capped RNA and NADPH or NADPH-capped RNA) was initiated with 0.963 pM muscle lactate dehydrogenase and the absorbance at 340 nm, 25°C was collected every 0.1 seconds on Varian

Cary 50 UV-Vis Spectrophotometer for 3 minutes. The muscle subunit lactate dehydrogenase was sourced from Sigma-Aldrich (L2500-5KU).

Reaction mixture containing 220 mM Tris pH 7.3, ~50 µM NADH, 0.963 pM rabbit muscle lactate dehydrogenase was initiated with varying concentrations of sodium pyruvate. With the simultaneous reduction of pyruvate to lactate, and the oxidation of NADH to NAD^+, a decay in the absorbance at 340 nm was recorded every 0.1 seconds on Varian Cary 50 UV-Vis Spectrophotometer for 3 minutes. The concentration of the mammalian muscle LDH used in each assay was calculated using its molecular weight (35 kDa). Each reaction, containing the NADH or NADH-capped RNA and enzyme was made to a total volume of 60 µl with 220 mM Tris pH7.3, then initiated with varying volumes of a 15 mM sodium pyruvate solution.

Figure 9-5| Initiating the muscle LDH reaction with pyruvate

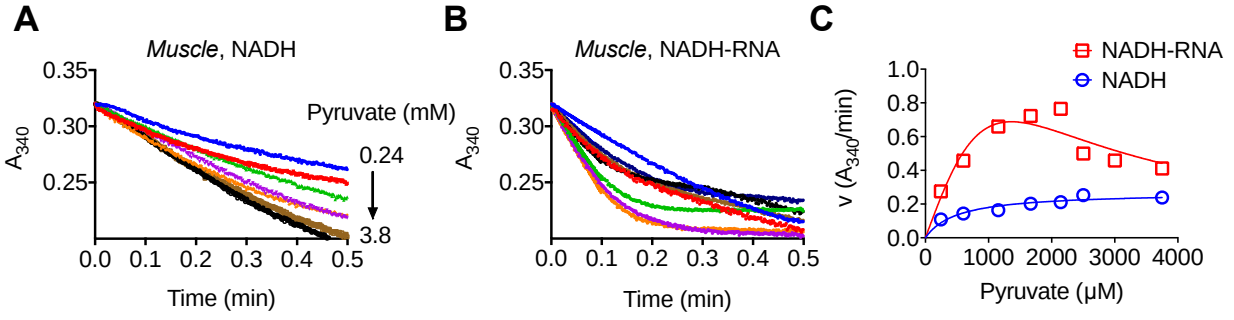

	NADH	NADH-RNA
k_{cat} (s^{-1})	750	2,800
K_m (µM)	500	680
k_{cat}/K_m (s^{-1} $µM^{-1}$)	1.5	4.0

220 mM Tris pH 7.3, 0.963 pM rabbit muscle lactate dehydrogenase, containing either (A) 50 µM NADH or (B) 50 µM NADH-capped RNA was initiated with varying concentrations of a 30 mM sodium pyruvate stock solution. The decay in absorbance at 340 nm was collected at an interval of 0.5 seconds on Varian Cary 50 UV-Vis Spectrophotometer for 3 minutes. Initial rates were (C) plotted against pyruvate concentration and fit to substrate inhibition model (Eq. 7) using GraphPad Prism (v.6) to yield similar K_m values, however a much higher catalytic efficiency for NADH-capped RNA (4.0 $s^{-1}µM^{-1}$) compared to free NADH (1.5 $s^{-1}µM^{-1}$).

Thus, NADH-capped RNA not only is a substrate for the muscle subunit of lactate dehydrogenase as well but has a more than 2 folds higher catalytic efficiency for ncinRNA compared to free NADH. For the first time, our results demonstrate that the NADH moiety of NADH-capped RNA may be involved in cellular redox reactions, catalyzed by both isozymes of mammalian metabolic dehydrogenases.

From our experiments, it may be concluded that the NADH-capped RNAs, when used as a cofactor for anaerobic reaction catalyzed by LDH-H, exhibits a more pronounced substrate inhibition compared to NADH alone. This led to the velocity curves of NADH-capped RNAs to escalate to a maximum velocity and then decline as the pyruvate concentration continued to increase. However similar substrate inhibition is not observed with LDH-M catalyzing the anaerobic redox reaction.

9.3.5 NAD^+-capped RNA is a substrate of E. coli lactate dehydrogenase

Reaction mixture containing 220 mM Tris pH9, ~ 40 μM NAD^+, 4.65 nM chicken heart lactate dehydrogenase was initiated with varying concentrations of lactate. With the simultaneous oxidation of lactate to pyruvate, and the regeneration of NADH from NAD^+, the increase in the absorbance at 340 nm was recorded every 0.25 seconds on Varian Cary 50 UV-Vis Spectrophotometer for 5 minutes. Reaction samples containing NAD^+ and enzyme were made to a final volume of 60 μl, then initiated with varying volumes of a 30 mM lactic acid solution, sourced from Dot Scientific Inc (DSL17500-500). Initial rates were found to be dependent on substrate concentration.

To test the hypothesis that NAD^+-capped RNA is a substrate for chicken heart lactate dehydrogenase, identical experiments as described above were repeated with ~ 40 μM NAD^+-

RNA. Surprisingly enough, the NAD^+ moiety of NAD^+-capped RNA was found to be a substrate for lactate dehydrogenase, even with an oligonucleotide 'tail'.

Figure 9-6| Initiating the recombinant *E. coli* LDH reaction with lactate

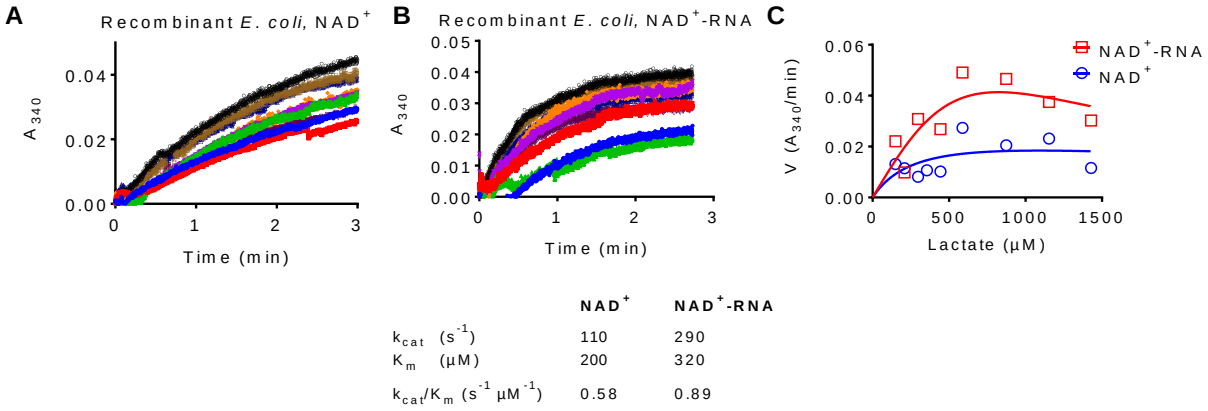

	NAD^+	NAD^+-RNA
k_{cat} (s^{-1})	110	290
K_m (µM)	200	320
k_{cat}/K_m (s^{-1} μM^{-1})	0.58	0.89

(A) Reaction mixtures containing 220 mM Tris pH9, ~10 µM NAD^+, 4.65 nM recombinant bacterial (chicken heart) lactate dehydrogenase was initiated with varying concentrations of a 30 mM lactate stock concentration. The increase in absorbance at 340 nm was collected at an interval of 0.5 seconds. Each reaction was carried out in a 50 µl quartz cuvette (B) Initial rates, observed to be dependent on substrate concentration were plotted against lactate concentration and fit to a substrate inhibition model (Eq. 7) using GraphPad Prism (v.6) to yield similar K_m values, however a higher catalytic efficiency for NAD^+-capped RNA (~ 1 $s^{-1}\mu M^{-1}$) compared to free NAD^+ (~ 0.5 $s^{-1}\mu M^{-1}$).

Not only was the NAD^+ moiety of NAD^+-capped RNA found to be a substrate for LDH, but it had a significantly higher catalytic efficiency (k_{cat}/K_m) as well.

9.3.6 NAD^+-capped RNA is a substrate of bovine heart lactate dehydrogenase

Initial experiments demonstrated that NADH-capped RNA is a substrate of mammalian heart lactate dehydrogenase. Next, we tested the hypothesis whether the reverse oxidation of lactate may also be catalyzed by NAD^+-capped RNA. Reaction mixture containing 220 mM Tris pH9, 40 µM NAD^+, 506 pM lactate dehydrogenase was initiated with varying concentrations of lactate. With the simultaneous oxidation of lactate to pyruvate, and the regeneration of NADH from NAD^+, the increase in the absorbance at 340 nm was recorded every 0.25 seconds on Varian

Cary 50 UV-Vis Spectrophotometer for 5 minutes. Reaction samples containing NAD^+ and enzyme were made to a final volume of 60 µl, then initiated with varying volumes of a 30 mM lactic acid solution, sourced from Dot Scientific Inc (DSL17500-500). Initial rates were found to be dependent on substrate concentration.

To test the hypothesis that NAD^+-capped RNA is a substrate for bovine heart lactate dehydrogenase, identical experiments as described above were repeated with 40 µM NAD^+-capped RNA. Surprisingly enough, the NAD^+ moiety of NAD^+-capped RNA was found to be a substrate for lactate dehydrogenase, even with an oligonucleotide 'tail'.

Figure 9-7| Initiating the heart LDH reaction with lactate

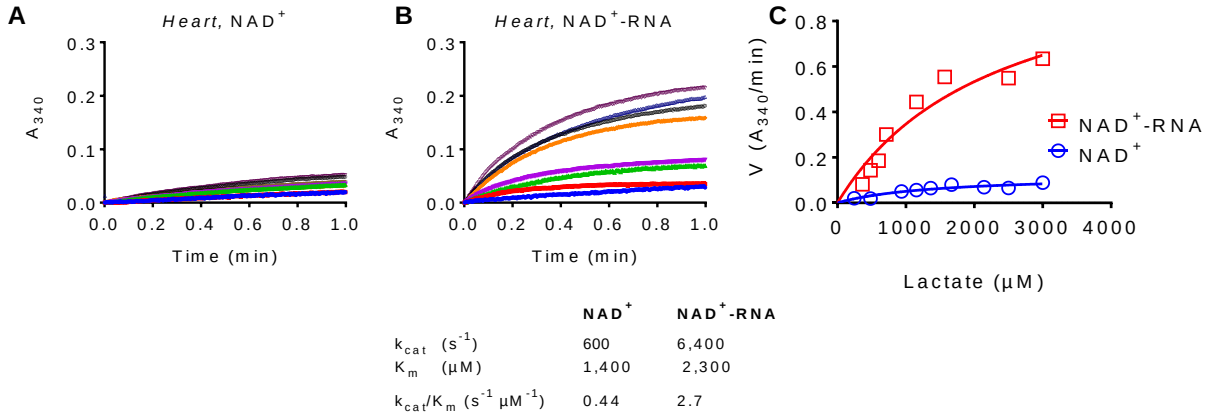

	NAD$^+$	NAD$^+$-RNA
k_{cat} (s^{-1})	600	6,400
K_m (µM)	1,400	2,300
k_{cat}/K_m (s^{-1} μM^{-1})	0.44	2.7

220 mM Tris pH 9, 506 pM bovine heart lactate dehydrogenase, containing either (A) 50 µM NAD^+ or (B) 50 µM NAD^+-capped RNA was initiated with varying concentrations of a 30 mM lactate stock solution. The increase in absorbance at 340 nm as NADH was regenerated was collected at an interval of 0.5 seconds on Varian Cary 50 UV-Vis Spectrophotometer for 3 minutes. Initial rates were observed to be dependent on substrate concentration which were (C) plotted against lactate concentration and fit to a substrate inhibition model (Eq. 7) using GraphPad Prism (v.6) to yield a greater than six-folds higher catalytic efficiency for NAD^+-capped RNA (~ 3 $s^{-1}\mu M^{-1}$) compared to free NAD^+ (~ 0.5 $s^{-1}\mu M^{-1}$).

Our results demonstrate that NAD^+-capped RNA is a substrate for mammalian heart LDH, having a considerably higher catalytic efficiency (k_{cat}/K_m) compared to free NAD^+.

9.3.7 NAD^+-capped RNA is a substrate of rabbit muscle lactate dehydrogenase

Experiments described in section 9.3.4 showed that NADH-capped RNA is a substrate of rabbit muscle lactate dehydrogenase. So, we tested the hypothesis whether the reverse oxidation of lactate may also be catalyzed by NAD^+-capped RNA. Reaction mixture containing 220 mM Tris pH9, ~ 40 μM NAD^+, 0.963 pM lactate dehydrogenase was initiated with varying concentrations of lactate. With the simultaneous oxidation of lactate to pyruvate, and the regeneration of NADH from NAD^+, the increase in the absorbance at 340 nm was recorded every 0.25 seconds on Varian Cary 50 UV-Vis Spectrophotometer for 5 minutes. Reaction samples containing NAD^+ and enzyme were made to a final volume of 60 μl, then initiated with varying volumes of a 30 mM lactic acid solution. Initial rates were found to be dependent on substrate concentration.

To test the hypothesis that NAD^+-capped RNA is a substrate for rabbit muscle lactate dehydrogenase, identical experiments as described above were repeated with ~ 40 μM NAD^+-capped RNA. Surprisingly enough, the NAD^+ moiety of NAD^+-capped RNA was found to be a substrate for lactate dehydrogenase, even with an oligonucleotide ‘tail’.

Figure 9-8| Initiating the muscle LDH reaction with lactate

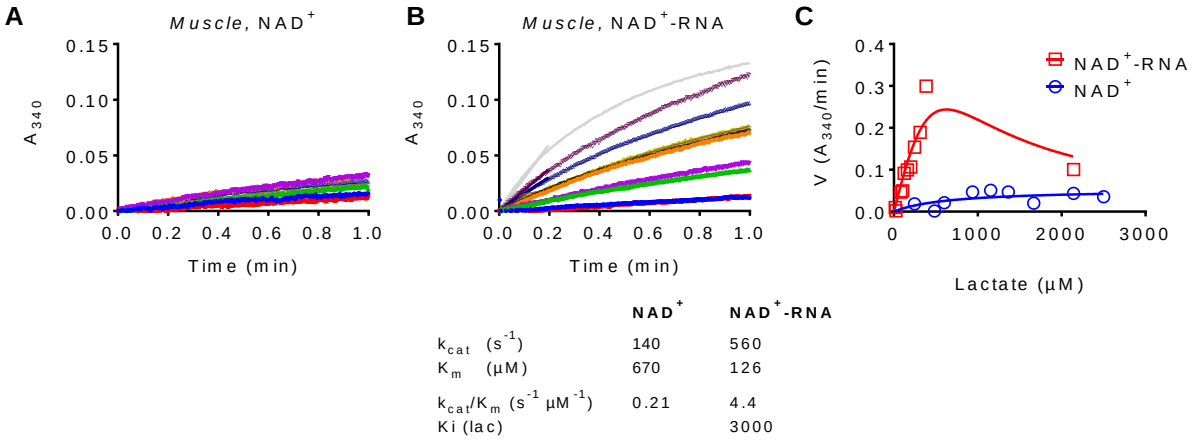

	NAD$^+$	NAD$^+$-RNA
k_{cat} (s^{-1})	140	560
K_m (µM)	670	126
k_{cat}/K_m (s^{-1} μM^{-1})	0.21	4.4
Ki (lac)		3000

220 mM Tris pH 9, 0.963 pM rabbit muscle lactate dehydrogenase, containing either (A) 50 µM NAD$^+$ or (B) 50 µM NAD$^+$-capped RNA was initiated with varying concentrations of a 30 mM sodium pyruvate stock solution. The decay in absorbance at 340 nm was collected at an interval of 0.5 seconds on Varian Cary 50 UV-Vis Spectrophotometer for 3 minutes. Initial rates were (C) plotted against lactate concentration and fit to a substrate inhibition model (Eq. 7) using GraphPad Prism (v.6) to yield a lower K_m for NAD$^+$-capped RNA (126 µM) compared to free free NAD$^+$ (670 µM). A 20-folds higher catalytic efficiency for NAD$^+$-capped RNA was also observed compared to free NAD$^+$.

Our experiments illustrate that NAD$^+$-capped RNA significantly inhibits the activity of LDH compared to free NAD$^+$, with a significantly higher catalytic efficiency (k_{cat}/K_m) compared to free NAD$^+$. A more pronounced substrate inhibition was observed with the muscle isozyme of lactate dehydrogenase, when catalyzing the aerobic reaction.

9.4 Discussion

Ever since the discovery of NAD-capped RNAs in booth prokaryotes and eukaryotes, their function *in vivo* has been a concern. It has been hypothesized that similar to the methylated cap on eukaryotic mRNA transcripts, the NAD cap may stabilize its prokaryotic RNA substrates. However, evidence for this role is yet to be demonstrated. The results in this chapter confirm that NAD-capped RNA not only functions as a cofactor to eukaryotic metabolic dehydrogenases, but the enzyme LDH seems to prefer NAD-capped RNA over NAD alone. This is the first report to

show a clear biochemical role for ncinRNAs, suggesting that ncinRNAs might be participants in cellular redox reactions. The activity of ncinRNAs as a viable cofactor has been confirmed with mammalian lactate dehydrogenases, as well as both its subunits (muscle and heart). *In vivo*, NAD-capped RNAs might therefore form a new class of key ribonucleoproteins or even ribozymes capable of catalyzing redox reactions. Several metabolic enzymes have also been reported to be RNA binding enzymes (Table 9-1), especially at 5'-UTR site where the covalent modification of ncinRNA is believed to occur as well.

Another interesting find from this chapter was the substrate inhibition observed for the two different isozymes of L-lactate dehydrogenase tested. A more pronounced substrate inhibition was observed for the aerobic conversion of lactate to pyruvate when the muscle isozyme of the enzyme uses NAD^+-capped RNA as a cofactor, whereas a similar inhibitory effect is observed when NADH-capped RNA utilizes LDH for the reverse anaerobic reduction. The same is true for the recombinant *E. coli* LDH, where the LDH gene sequence was cloned from chicken heart.

We would further like to test the activity of ncinRNAs for other RNA binding NAD-using metabolic enzymes. Using the stopped-flow technique could also give us a better understanding of the kinetics in such redox reactions.

Table 9-1|RNA binding metabolic enzymes

Pathway	Enzyme	RNA(s)
Glycolysis	GAPDH	tRNA, rRNA, ribozymes, RNA virus UTRs (Rigby WF et al., 1995; Garcin ED et al., 2016; Klug G et al., 2002; Garcin ED et al., 2015; Garcin ED 2019; Alexander GJ et al., 1999)
Glycolysis (anaerobic)	LDH	GM-CSF mRNA 3'UTR (Rigby WF et al., 2002)
TCA entry	PDH	Not known

TCA	IDH	Mitochondrial mRNA 5'UTR (Grivell LA et al., 1993)
	α-KDH	Not Known
	MDH	Not Known
Pentose Phosphate	G6PDH	GLUT1 mRNA 3'UTR (Pekala PH et al., 1996)
Amino Acid TCA entry	GDH	mRNA, gRNA, 3'oligo (U) (Lightowlers RN et al., 1993; Simpson L et al., 1997)
Nucleotide Synthesis	DHFR	DHFR mRNA (Bertino JR et al., 1997)

Chapter 10 Conclusions and Perspectives

Since the discovery of NADH-cleaving Nudix proteins, *E. coli* NudC, the progenitor of this subfamily of Nudix hydrolases, its exact biochemical role has been unclear. Despite, the cell spending energy to synthesize each molecule of NADH, bacterial NudC and human Nudt12 cleave this energy rich molecule to yield NMN and AMP. The exact reason for this hydrolytic cleavage reaction is yet to be completely understood. This thesis entirely focuses on studying the role of this class of enzymes.

Following the discovery of Nudt1 (MutH1) in as early as 1994, hydrolyzing mutagenic nucleotide pools to prevent its misincorporation into DNA, chapter 4 concentrated on a similar hypothesis. We confirmed that both bacterial NudC and human Nudt12 Nudix hydrolases has catalytic activity on the toxic isomeric forms of NADH, using HPLC. Experiments described in this thesis indicate that the human Nudix protein Nudt12 prefers to hydrolyze 6DHNAD over the nascent NADH by almost five-fold (Figure 5-7). However, additional research is required to confirm this hypothesis for both bacterial and human NADH-cleaving Nudix hydrolases. Furthermore, it would be interesting to see the effect of knocking out this particular subclass of Nudix proteins might affect the levels of 6DHNAD *in vivo.*

A novel fluorescence assay was designed in Chapter 6 to bypass the limitations of previously described colorimetric assays. A fluorescence-based assay to monitor the continuous hydrolysis of NAD-cleaving Nudix proteins on its substrates was designed. This assay confirmed that the toxic isomer of NADPH, 6DHNADP is a substrate of the bacterial Nudix hydrolase, NudC.

Results demonstrate the ongoing hydrolysis of NADH by NudC is further inhibited by the addition of the 'competing' substrate, 6DHNADP. This novel assay could be used in the future to study the activity of NADH-cleaving Nudix hydrolases, bacterial NudC, yeast NPY1 and human Nudt12 on ncinRNAs.

Chapter 8 is the first study to show the direct interaction between human and bacterial RNA decapping Nudix hydrolases and their nucleic acid substrates. Since the early discovery of NudC (Frick & Bessman, 1995), it has been demonstrated to co-purify with nucleic acids. Additionally, both NudC and its human functional homolog, Nudt12 have Zinc-finger domains, suggesting yet another possible binding site for nucleic acids. Nudt3 (McLennan et al., 2006; Song et al., 2013; Kiledjia et al., 2016), Nudt16 (Grzela et al., 2018) and Nudt20, more commonly referred to as Dcp2 (Wang et al., 2002) have all been demonstrated to have mRNA decapping activity. However, interactions between DNA or RNA and these RNA decapping Nudix hydrolases have not been studied before. In this chapter, we developed and optimized a fluorescence polarization (FP) assay to quantify affinity between RNA decapping Nudix hydrolases and nucleic acids. Surprisingly, our data shows that the human Nudt12 protein exclusively binds RNA and not DNA. We further validated these results by designing another FP assay to displace the bound RNA-protein complex with either unlabeled DNA or unlabeled RNA. We also show that Nudt12 has an incredibly high affinity to bind *in vitro* transcribed NAD^+-capped RNA compared to NADH-capped RNA and ^{7}mG capped RNA. Future work would include repeating similar FP assay using ncinRNAs transcribed using fluorescently modified nucleotides, to study the energetics of direct interaction between both bacterial and human RNA decapping Nudix proteins and fluorescently labeled ncinRNAs.

Previous studies have demonstrated that NudC (Cahová et al., 2015) and Nudt12 (Grudzien-Nogalska et al., 2019) have deNADding activity on NAD^+-RNA, using radiolabeled *in vitro* transcribed ncinRNA. Both these Nudix proteins cleave the phosphodiester bonds in the NAD^+ moiety to yield free NMN and 5'- monophosphorylated RNA. In Chapter 7, we *in vitro* synthesized ncinRNAs, NAD^+-RNA and NADH-RNA and optimized a more quantitative analytical approach using LC/MS to study the hydrolytic activity of NudC and Nudt12 on their substrates. Zhang et al. (2016) showed similar results, although this technique can be replicated to study the energetics of deNADding by the functional homolog of these proteins in yeast, Npy1.

Since the identification of NAD^+ as a covalent modification on the terminal end of RNA transcripts in bacteria (Chen et al., 2009; Cahova et al., 2015), yeast (Walters et al., 2017) and humans (Jiao, et al., 2017), its significance has been questioned. It has been hypothesized by Cahova et al. (2015), that the NAD^+ cap might play a similar role in stabilizing bacterial RNA transcripts as the m^7G cap does to eukaryotic mRNA transcripts. In Chapter 9, we hypothesized that ncinRNAs might be participants in cellular redox reactions. To test this hypothesis, two isoforms of lactate dehydrogenase: recombinant *E. coli* L-lactate dehydrogenase, rabbit muscle L-lactate dehydrogenase and bovine heart L-lactate dehydrogenase were used to test its redox activity on both pyruvate and lactate using either NADH or NADH-RNA and NAD^+ or NAD^+-RNA respectively. To our surprise, we found that not only can ncinRNAs assist in redox metabolic reactions, but they might be better cofactors compared to their free NAD^+ or NADH forms. This is the first study to demonstrate a clear biochemical role for ncinRNAs. We think that NAD^+-capped RNAs might therefore form a new class of key ribonucleoproteins or even ribozymes capable of catalyzing redox reactions, *in vivo*. Additionally, several metabolic enzymes including lactate dehydrogenase, used as an example in this thesis, have also been reported to be RNA

binding enzymes, especially at 5'-UTR site where the covalent modification of ncinRNA is believed to occur as well. It would be exciting to test the aiding effect of ncinRNAs in redox reactions catalyzed by other RNA binding metabolic enzymes mentioned in Table 9-1.

References

AbdelRaheim SR, Cartwright JL, Gasmi L, McLennan AG. The NADH diphosphatase encoded by the saccharomyces cerevisiae NPY1 nudix hydrolase gene is located in peroxisomes. Arch Biochem Biophys. 2001;388(1):18-24.

Abdelraheim SR, Spiller DG, McLennan AG. Mouse Nudt13 is a mitochondrial nudix hydrolase with NAD(P)H pyrophosphohydrolase activity. Protein J. 2017;36(5):425-432.

Abdelraheim SR, Spiller DG, McLennan AG. Mammalian NADH diphosphatases of the nudix family: Cloning and characterization of the human peroxisomal NUDT12 protein. Biochem J. 2003;374(Pt 2):329-335.

Abeygunawardana C, Weber DJ, Gittis AG, et al. Solution structure of the MutT enzyme, a nucleoside triphosphate pyrophosphohydrolase. Biochemistry. 1995;34(46):14997-15005.

Anadon C, van Tetering G, Ferreira HJ, et al. Epigenetic loss of the RNA decapping enzyme NUDT16 mediates C-MYC activation in T-cell acute lymphoblastic leukemia. Leukemia. 2017;31(7):1622-1625.

Anderson KA, Madsen AS, Olsen CA, Hirschey MD. Metabolic control by sirtuins and other enzymes that sense NAD(+), NADH, or their ratio. Biochim Biophys Acta Bioenerg. 2017;1858(12):991-998.

Bao F, Yan H, Sun H, Yang P, Liu G, Zhou X. Hydrolysis of by-product adenosine diphosphate from 3'-phosphoadenosine-5'-phosphosulfate preparation using nudix hydrolase NudJ. Appl Microbiol Biotechnol. 2015;99(24):10771-10778.

Beaupre BA, Carmichael BR, Hoag MR, Shah DD, Moran GR. Renalase is an alpha-NAD(P)H oxidase/anomerase. J Am Chem Soc. 2013;135(37):13980-13987.

Beaupre BA, Hoag MR, Carmichael BR, Moran GR. Kinetics and equilibria of the reductive and oxidative half-reactions of human renalase with alpha-NADPH. Biochemistry. 2013;52(49):8929-8937.

Beaupre BA, Hoag MR, Moran GR. Renalase does not catalyze the oxidation of catecholamines. Arch Biochem Biophys. 2015;579:62-66.

Beaupre BA, Hoag MR, Roman J, Forsterling FH, Moran GR. Metabolic function for human renalase: Oxidation of isomeric forms of beta-NAD(P)H that are inhibitory to primary metabolism. Biochemistry. 2015;54(3):795-806.

Beaupre BA, Roman JV, Hoag MR, et al. Ligand binding phenomena that pertain to the metabolic function of renalase. Arch Biochem Biophys. 2016;612:46-56.

Belenky P, Bogan KL, Brenner C. NAD^+ metabolism in health and disease. Trends Biochem Sci. 2007;32(1):12-19.

Bessman MJ, Frick DN, O'Handley SF. The MutT proteins or "nudix" hydrolases, a family of versatile, widely distributed, "housecleaning" enzymes. J Biol Chem. 1996;271(41):25059-25062.

Bessman MJ, Walsh JD, Dunn CA, Swaminathan J, Weldon JE, Shen J. The gene ygdP, associated with the invasiveness of escherichia coli K1, designates a nudix hydrolase, Orf176, active on adenosine (5')-pentaphospho-(5')-adenosine (Ap5A). J Biol Chem. 2001;276(41):37834-37838.

Bilan DS, Matlashov ME, Gorokhovatsky AY, Schultz C, Enikolopov G, Belousov VV. Genetically encoded fluorescent indicator for imaging NAD(+)/NADH ratio changes in different cellular compartments. Biochim Biophys Acta. 2014;1840(3):951-957.

Bird JG, Basu U, Kuster D, et al. Highly efficient 5' capping of mitochondrial RNA with NAD(+) and NADH by yeast and human mitochondrial RNA polymerase. Elife. 2018;7:10.7554/eLife.42179.

Bird JG, Nickels BE, Ebright RH. RNA capping by transcription initiation with non-canonical initiating nucleotides (NCINs): Determination of relative efficiencies of transcription initiation with NCINs and NTPs. Bio Protoc. 2017;7(12):10.21769/BioProtoc.2336.

Bird JG, Zhang Y, Tian Y, et al. The mechanism of RNA 5' capping with NAD+, NADH and desphospho-CoA. Nature. 2016;535(7612):444-447.

Brune M, Hunter JL, Howell SA, et al. Mechanism of inorganic phosphate interaction with phosphate binding protein from escherichia coli. Biochemistry. 1998;37(29):10370-10380.

Bullions LC, Mejean V, Claverys JP, Bessman MJ. Purification of the MutX protein of streptococcus pneumoniae, a homologue of escherichia coli MutT. identification of a novel catalytic domain for nucleoside triphosphate pyrophosphohydrolase activity. J Biol Chem. 1994;269(16):12339-12344.

Cahova H, Winz ML, Hofer K, Nubel G, Jaschke A. NAD captureSeq indicates NAD as a bacterial cap for a subset of regulatory RNAs. Nature. 2015;519(7543):374-377.

Carloto A, Costas MJ, Cameselle JC, McLennan AG, Ribeiro JM. The specific, submicromolar-km ADP-ribose pyrophosphatase purified from human placenta is enzymically indistinguishable from recombinant NUDT9 protein, including a selectivity for Mn2+ as activating cation and increase in km for ADP-ribose, both elicited by H2O2. Biochim Biophys Acta. 2006;1760(10):1545-1551.

Carreras-Puigvert J, Zitnik M, Jemth AS, et al. A comprehensive structural, biochemical and biological profiling of the human NUDIX hydrolase family. Nat Commun. 2017;8(1):1541-017-01642-w.

Carter SG, Karl DW. Inorganic phosphate assay with malachite green: An improvement and evaluation. J Biochem Biophys Methods. 1982;7(1):7-13.

Celesnik H, Deana A, Belasco JG. PABLO analysis of RNA: 5'-phosphorylation state and 5'-end mapping. Methods Enzymol. 2008;447:83-98.

Charenton C, Taverniti V, Gaudon-Plesse C, Back R, Seraphin B, Graille M. Structure of the active form of Dcp1-Dcp2 decapping enzyme bound to m(7)GDP and its Edc3 activator. Nat Struct Mol Biol. 2016;23(11):982-986.

Chen LY, Chen TH, Wen PY, et al. Differential expression of NUDT9 at different phases of the menstrual cycle and in different components of normal and neoplastic human endometrium. Taiwan J Obstet Gynecol. 2009;48(2):96-107.

Chen YG, Kowtoniuk WE, Agarwal I, Shen Y, Liu DR. LC/MS analysis of cellular RNA reveals NAD-linked RNA. Nat Chem Biol. 2009;5(12):879-881.

Ciesla J. Metabolic enzymes that bind RNA: Yet another level of cellular regulatory network? Acta Biochim Pol. 2006;53(1):11-32.

Cohen LS, Mikhli C, Jiao X, Kiledjian M, Kunkel G, Davis RE. Dcp2 decaps m2,2,7GpppN-capped RNAs, and its activity is sequence and context dependent. Mol Cell Biol. 2005;25(20):8779-8791.

Conyers GB, Bessman MJ. The gene, ialA, associated with the invasion of human erythrocytes by bartonella bacilliformis, designates a nudix hydrolase active on dinucleoside 5'-polyphosphates. J Biol Chem. 1999;274(3):1203-1206.

Daniels CM, Thirawatananond P, Ong SE, Gabelli SB, Leung AK. Nudix hydrolases degrade protein-conjugated ADP-ribose. Sci Rep. 2015;5:18271.

De Jong DW, Woodlief WG. Fluorimetric assay of tobacco leaf dehydrogenases with resazurin. Biochim Biophys Acta. 1977;484(2):249-259.

Deana A, Celesnik H, Belasco JG. The bacterial enzyme RppH triggers messenger RNA degradation by 5' pyrophosphate removal. Nature. 2008;451(7176):355-358.

Deana A, Celesnik H, Belasco JG. The bacterial enzyme RppH triggers messenger RNA degradation by 5' pyrophosphate removal. Nature. 2008;451(7176):355-358.

Deshmukh MV, Jones BN, Quang-Dang DU, et al. mRNA decapping is promoted by an RNA-binding channel in Dcp2. Mol Cell. 2008;29(3):324-336.

Desir GV, Wang L, Peixoto AJ. Human renalase: A review of its biology, function, and implications for hypertension. J Am Soc Hypertens. 2012;6(6):417-426.

Dunckley T, Parker R. The DCP2 protein is required for mRNA decapping in saccharomyces cerevisiae and contains a functional MutT motif. EMBO J. 1999;18(19):5411-5422.

Dunn CA, O'Handley SF, Frick DN, Bessman MJ. Studies on the ADP-ribose pyrophosphatase subfamily of the nudix hydrolases and tentative identification of trgB, a gene associated with tellurite resistance. J Biol Chem. 1999;274(45):32318-32324.

Emerson PM, Wilkinson JH. Urea and oxalate inhibition of the serum lactate dehydrogenase. J Clin Pathol. 1965;18(6):803-807.

Emerson PM, Wilkinson JH, Withycombe WA. Effect of oxalate on the activity of lactate dehydrogenase isoenzymes. Nature. 1964;202:1337-1338.

Evguenieva-Hackenberg E, Schiltz E, Klug G. Dehydrogenases from all three domains of life cleave RNA. J Biol Chem. 2002;277(48):46145-46150.

Fillman C, Lykke-Andersen J. RNA decapping inside and outside of processing bodies. Curr Opin Cell Biol. 2005;17(3):326-331.

Foley PL, Hsieh PK, Luciano DJ, Belasco JG. Specificity and evolutionary conservation of the escherichia coli RNA pyrophosphohydrolase RppH. J Biol Chem. 2015;290(15):9478-9486.

Frick DN, Bessman MJ. Cloning, purification, and properties of a novel NADH pyrophosphatase. evidence for a nucleotide pyrophosphatase catalytic domain in MutT-like enzymes. J Biol Chem. 1995;270(4):1529-1534.

Frick DN, Townsend BD, Bessman MJ. A novel GDP-mannose mannosyl hydrolase shares homology with the MutT family of enzymes. J Biol Chem. 1995;270(41):24086-24091.

Frindert J, Zhang Y, Nubel G, et al. Identification, biosynthesis, and decapping of NAD-capped RNAs in B. subtilis. Cell Rep. 2018;24(7):1890-1901.e8.

Frindert J, Zhang Y, Nubel G, et al. Identification, biosynthesis, and decapping of NAD-capped RNAs in B. subtilis. Cell Rep. 2018;24(7):1890-1901.e8.

Gabelli SB, Bianchet MA, Ohnishi Y, Ichikawa Y, Bessman MJ, Amzel LM. Mechanism of the escherichia coli ADP-ribose pyrophosphatase, a nudix hydrolase. Biochemistry. 2002;41(30):9279-9285.

Gad H, Koolmeister T, Jemth AS, et al. MTH1 inhibition eradicates cancer by preventing sanitation of the dNTP pool. Nature. 2014;508(7495):215-221.

Garcin ED. GAPDH as a model non-canonical AU-rich RNA binding protein. Semin Cell Dev Biol. 2019;86:162-173.

Gasmi L, McLennan AG. The mouse Nudt7 gene encodes a peroxisomal nudix hydrolase specific for coenzyme A and its derivatives. Biochem J. 2001;357(Pt 1):33-38.

Gasser A, Bruhn S, Guse AH. Second messenger function of nicotinic acid adenine dinucleotide phosphate revealed by an improved enzymatic cycling assay. J Biol Chem. 2006;281(25):16906-16913.

Gaviraghi M, Vivori C, Pareja Sanchez Y, et al. Tumor suppressor PNRC1 blocks rRNA maturation by recruiting the decapping complex to the nucleolus. EMBO J. 2018;37(23):10.15252/embj.201899179. Epub 2018 Oct 29.

Geisler S, Lojek L, Khalil AM, Baker KE, Coller J. Decapping of long noncoding RNAs regulates inducible genes. Mol Cell. 2012;45(3):279-291.

Gibon Y, Larher F. Cycling assay for nicotinamide adenine dinucleotides: NaCl precipitation and ethanol solubilization of the reduced tetrazolium. Anal Biochem. 1997;251(2):153-157.

Goody MF, Henry CA. A need for NAD+ in muscle development, homeostasis, and aging. Skelet Muscle. 2018;8(1):9-018-0154-1.

Griffin JH, Criddle RS. Substrate-inhibited lactate dehydrogenase. reaction mechanism and essential role of dissociated subunits. Biochemistry. 1970;9(5):1195-1205.

Grudzien-Nogalska E, Bird JG, Nickels BE, Kiledjian M. "NAD-capQ" detection and quantitation of NAD caps. RNA. 2018;24(10):1418-1425.

Grudzien-Nogalska E, Jiao X, Song MG, Hart RP, Kiledjian M. Nudt3 is an mRNA decapping enzyme that modulates cell migration. RNA. 2016;22(5):773-781.

Grudzien-Nogalska E, Kiledjian M. New insights into decapping enzymes and selective mRNA decay. Wiley Interdiscip Rev RNA. 2017;8(1):10.1002/wrna.1379. Epub 2016 Jul 17.

Grudzien-Nogalska E, Wu Y, Jiao X, et al. Structural and mechanistic basis of mammalian Nudt12 RNA deNADding. Nat Chem Biol. 2019;15(6):575-582.

Grzela R, Nasilowska K, Lukaszewicz M, et al. Hydrolytic activity of human Nudt16 enzyme on dinucleotide cap analogs and short capped oligonucleotides. RNA. 2018;24(5):633-642.

Hand NJ, Silhavy TJ. Null mutations in a nudix gene, ygdP, implicate an alarmone response in a novel suppression of hybrid jamming. J Bacteriol. 2003;185(22):6530-6539.

Heinonen JK, Honkasalo SH, Kukko EI. A method for the concentration and for the colorimetric determination of nanomoles of inorganic pyrophosphate. Anal Biochem. 1981;117(2):293-300.

Hoag MR, Roman J, Beaupre BA, Silvaggi NR, Moran GR. Bacterial renalase: Structure and kinetics of an enzyme with 2- and 6-dihydro-beta-NAD(P) oxidase activity from pseudomonas phaseolicola. Biochemistry. 2015;54(24):3791-3802.

Hofer K, Abele F, Schlotthauer J, Jaschke A. Synthesis of 5'-NAD-capped RNA. Bioconjug Chem. 2016;27(4):874-877.

Hofer K, Jaschke A. Epitranscriptomics: RNA modifications in bacteria and archaea. Microbiol Spectr. 2018;6(3):10.1128/microbiolspec.RWR-0015-2017.

Hofer K, Jaschke A. Molecular biology: A surprise beginning for RNA. Nature. 2016;535(7612):359-360.

Hofer K, Li S, Abele F, et al. Structure and function of the bacterial decapping enzyme NudC. Nat Chem Biol. 2016;12(9):730-734.

Houtkooper RH, Canto C, Wanders RJ, Auwerx J. The secret life of NAD+: An old metabolite controlling new metabolic signaling pathways. Endocr Rev. 2010;31(2):194-223.

Huang F. Efficient incorporation of CoA, NAD and FAD into RNA by in vitro transcription. Nucleic Acids Res. 2003;31(3):e8.

Huang N, Sorci L, Zhang X, et al. Bifunctional NMN adenylyltransferase/ADP-ribose pyrophosphatase: Structure and function in bacterial NAD metabolism. Structure. 2008;16(2):196-209.

Huang Y, Winkler PA, Sun W, Lu W, Du J. Architecture of the TRPM2 channel and its activation mechanism by ADP-ribose and calcium. Nature. 2018;562(7725):145-149.

Hudson WH, Ortlund EA. The structure, function and evolution of proteins that bind DNA and RNA. Nat Rev Mol Cell Biol. 2014;15(11):749-760.

Imai S, Guarente L. NAD+ and sirtuins in aging and disease. Trends Cell Biol. 2014;24(8):464-471.

Itaya K, Ui M. A new micromethod for the colorimetric determination of inorganic phosphate. Clin Chim Acta. 1966;14(3):361-366.

Jenkins WT, Marshall MM. A modified direct phosphate assay for studying ATPases. Anal Biochem. 1984;141(1):155-160.

Julius C, Riaz-Bradley A, Yuzenkova Y. RNA capping by mitochondrial and multi-subunit RNA polymerases. Transcription. 2018;9(5):292-297.

Julius C, Yuzenkova Y. Noncanonical RNA-capping: Discovery, mechanism, and physiological role debate. Wiley Interdiscip Rev RNA. 2019;10(2):e1512.

Julius C, Yuzenkova Y. Bacterial RNA polymerase caps RNA with various cofactors and cell wall precursors. Nucleic Acids Res. 2017;45(14):8282-8290.

Katsyuba E, Auwerx J. Modulating NAD(+) metabolism, from bench to bedside. EMBO J. 2017;36(18):2670-2683.

Kettle JG, Alwan H, Bista M, et al. Potent and selective inhibitors of MTH1 probe its role in cancer cell survival. J Med Chem. 2016;59(6):2346-2361.

Kiledjian M. Eukaryotic RNA 5'-end NAD(+) capping and DeNADding. Trends Cell Biol. 2018;28(6):454-464.

Kiledjian M, Zhou M, Jiao X. Normal and aberrantly capped mRNA decapping. Enzymes. 2012;31:165-180.

Koonin EV. A highly conserved sequence motif defining the family of MutT-related proteins from eubacteria, eukaryotes and viruses. Nucleic Acids Res. 1993;21(20):4847.

Kramer S, McLennan AG. The complex enzymology of mRNA decapping: Enzymes of four classes cleave pyrophosphate bonds. Wiley Interdiscip Rev RNA. 2019;10(1):e1511.

Kraszewska E. The plant nudix hydrolase family. Acta Biochim Pol. 2008;55(4):663-671.

Lauhon CT, Szostak JW. RNA aptamers that bind flavin and nicotinamide redox cofactors. J Am Chem Soc. 1995;117(4):1246-1257.

Legler PM, Lee HC, Peisach J, Mildvan AS. Kinetic and magnetic resonance studies of the role of metal ions in the mechanism of escherichia coli GDP-mannose mannosyl hydrolase, an unusual nudix enzyme. Biochemistry. 2002;41(14):4655-4668.

Legler PM, Massiah MA, Bessman MJ, Mildvan AS. GDP-mannose mannosyl hydrolase catalyzes nucleophilic substitution at carbon, unlike all other nudix hydrolases. Biochemistry. 2000;39(29):8603-8608.

Legler PM, Massiah MA, Mildvan AS. Mutational, kinetic, and NMR studies of the mechanism of E. coli GDP-mannose mannosyl hydrolase, an unusual nudix enzyme. Biochemistry. 2002;41(35):10834-10848.

Li J, Bonkowski MS, Moniot S, et al. A conserved NAD(+) binding pocket that regulates protein-protein interactions during aging. Science. 2017;355(6331):1312-1317.

Li K, Li T, Yang SS, et al. Deletion of nudB causes increased susceptibility to antifolates in escherichia coli and salmonella enterica. Antimicrob Agents Chemother. 2017;61(5):10.1128/AAC.02378-16. Print 2017 May.

Lim YT, Prabhu N, Dai L, et al. An efficient proteome-wide strategy for discovery and characterization of cellular nucleotide-protein interactions. PLoS One. 2018;13(12):e0208273.

Lin S, Gasmi L, Xie Y, et al. Cloning, expression and characterisation of a human nudix hydrolase specific for adenosine 5'-diphosphoribose (ADP-ribose). Biochim Biophys Acta. 2002;1594(1):127-135.

Liu H, Kiledjian M. Decapping the message: A beginning or an end. Biochem Soc Trans. 2006;34(Pt 1):35-38.

Long A, Klimova N, Kristian T. Mitochondrial NUDIX hydrolases: A metabolic link between NAD catabolism, GTP and mitochondrial dynamics. Neurochem Int. 2017;109:193-201.

Luciano DJ, Belasco JG. NAD in RNA: Unconventional headgear. Trends Biochem Sci. 2015;40(5):245-247.

Luciano DJ, Vasilyev N, Richards J, Serganov A, Belasco JG. Importance of a diphosphorylated intermediate for RppH-dependent RNA degradation. RNA Biol. 2018;15(6):703-706.

Luciano DJ, Vasilyev N, Richards J, Serganov A, Belasco JG. A novel RNA phosphorylation state enables 5' end-dependent degradation in escherichia coli. Mol Cell. 2017;67(1):44-54.e6.

Massiah MA, Saraswat V, Azurmendi HF, Mildvan AS. Solution structure and NH exchange studies of the MutT pyrophosphohydrolase complexed with mg(2+) and 8-oxo-dGMP, a tightly bound product. Biochemistry. 2003;42(34):10140-10154.

McLennan AG. Substrate ambiguity among the nudix hydrolases: Biologically significant, evolutionary remnant, or both? Cell Mol Life Sci. 2013;70(3):373-385.

McLennan AG. Decapitation: Poxvirus makes RNA lose its head. Trends Biochem Sci. 2007;32(7):297-299.

McLennan AG. The nudix hydrolase superfamily. Cell Mol Life Sci. 2006;63(2):123-143.

McLennan AG. The MutT motif family of nucleotide phosphohydrolases in man and human pathogens (review). Int J Mol Med. 1999;4(1):79-89.

Mejean V, Salles C, Bullions LC, Bessman MJ, Claverys JP. Characterization of the mutX gene of streptococcus pneumoniae as a homologue of escherichia coli mutT, and tentative definition of a catalytic domain of the dGTP pyrophosphohydrolases. Mol Microbiol. 1994;11(2):323-330.

Messing SA, Gabelli SB, Liu Q, et al. Structure and biological function of the RNA pyrophosphohydrolase BdRppH from bdellovibrio bacteriovorus. Structure. 2009;17(3):472-481.

Mildvan AS, Xia Z, Azurmendi HF, et al. Structures and mechanisms of nudix hydrolases. Arch Biochem Biophys. 2005;433(1):129-143.

Modzelan M, Kujawa M, Glabski K, Jagura-Burdzy G, Kraszewska E. NudC nudix hydrolase from pseudomonas syringae, but not its counterpart from pseudomonas aeruginosa, is a novel regulator

of intracellular redox balance required for growth, motility and biofilm formation. Mol Microbiol. 2014;93(5):867-882.

Moran GR. The catalytic function of renalase: A decade of phantoms. Biochim Biophys Acta. 2016;1864(1):177-186.

Moran GR, Hoag MR. The enzyme: Renalase. Arch Biochem Biophys. 2017;632:66-76.

Mugridge JS, Tibble RW, Ziemniak M, Jemielity J, Gross JD. Structure of the activated Edc1-Dcp1-Dcp2-Edc3 mRNA decapping complex with substrate analog poised for catalysis. Nat Commun. 2018;9(1):1152-018-03536-x.

Mugridge JS, Ziemniak M, Jemielity J, Gross JD. Structural basis of mRNA-cap recognition by Dcp1-Dcp2. Nat Struct Mol Biol. 2016;23(11):987-994.

Nagy E, Rigby WF. Glyceraldehyde-3-phosphate dehydrogenase selectively binds AU-rich RNA in the NAD(+)-binding region (rossmann fold). J Biol Chem. 1995;270(6):2755-2763.

Nubel G, Sorgenfrei FA, Jaschke A. Boronate affinity electrophoresis for the purification and analysis of cofactor-modified RNAs. Methods. 2017;117:14-20.

Ogasawara Y, Funakoshi M, Ishii K. Determination of reduced nicotinamide adenine dinucleotide phosphate concentration using high-performance liquid chromatography with fluorescence detection: Ratio of the reduced form as a biomarker of oxidative stress. Biol Pharm Bull. 2009;32(11):1819-1823.

O'Handley SF, Dunn CA, Bessman MJ. Orf135 from escherichia coli is a nudix hydrolase specific for CTP, dCTP, and 5-methyl-dCTP. J Biol Chem. 2001;276(8):5421-5426.

O'Handley SF, Dunn CA, Bessman MJ. Orf135 from escherichia coli is a nudix hydrolase specific for CTP, dCTP, and 5-methyl-dCTP. J Biol Chem. 2001;276(8):5421-5426.

O'Handley SF, Frick DN, Bullions LC, Mildvan AS, Bessman MJ. Escherichia coli orf17 codes for a nucleoside triphosphate pyrophosphohydrolase member of the MutT family of proteins. cloning, purification, and characterization of the enzyme. J Biol Chem. 1996;271(40):24649-24654.

O'Handley SF, Frick DN, Dunn CA, Bessman MJ. Orf186 represents a new member of the nudix hydrolases, active on adenosine(5')triphospho(5')adenosine, ADP-ribose, and NADH. J Biol Chem. 1998;273(6):3192-3197.

Opitz CA, Heiland I. Dynamics of NAD-metabolism: Everything but constant. Biochem Soc Trans. 2015;43(6):1127-1132.

Peculis BA, Reynolds K, Cleland M. Metal determines efficiency and substrate specificity of the nuclear NUDIX decapping proteins X29 and H29K (Nudt16). J Biol Chem. 2007;282(34):24792-24805.

Penney CL. A simple micro-assay for inorganic phosphate. Anal Biochem. 1976;75(1):201-210.

Perraud AL, Fleig A, Dunn CA, et al. ADP-ribose gating of the calcium-permeable LTRPC2 channel revealed by nudix motif homology. Nature. 2001;411(6837):595-599.

Perraud AL, Shen B, Dunn CA, et al. NUDT9, a member of the nudix hydrolase family, is an evolutionarily conserved mitochondrial ADP-ribose pyrophosphatase. J Biol Chem. 2003;278(3):1794-1801.

Petitou M, Tuy F, Rosenfeld C. A simplified procedure for organic phosphorus determination from phospholipids. Anal Biochem. 1978;91(1):350-353.

Pioli PA, Hamilton BJ, Connolly JE, Brewer G, Rigby WF. Lactate dehydrogenase is an AU-rich element-binding protein that directly interacts with AUF1. J Biol Chem. 2002;277(38):35738-35745.

Piton J, Larue V, Thillier Y, et al. Bacillus subtilis RNA deprotection enzyme RppH recognizes guanosine in the second position of its substrates. Proc Natl Acad Sci U S A. 2013;110(22):8858-8863.

Ribeiro JM, Carloto A, Costas MJ, Cameselle JC. Human placenta hydrolases active on free ADP-ribose: An ADP-sugar pyrophosphatase and a specific ADP-ribose pyrophosphatase. Biochim Biophys Acta. 2001;1526(1):86-94.

Saraswat V, Massiah MA, Lopez G, Amzel LM, Mildvan AS. Interactions of the products, 8-oxo-dGMP, dGMP, and pyrophosphate with the MutT nucleoside triphosphate pyrophosphohydrolase. Biochemistry. 2002;41(52):15566-15577.

She M, Decker CJ, Svergun DI, et al. Structural basis of dcp2 recognition and activation by dcp1. Mol Cell. 2008;29(3):337-349.

Sheth U, Parker R. Decapping and decay of messenger RNA occur in cytoplasmic processing bodies. Science. 2003;300(5620):805-808.

Shumar SA, Fagone P, Alfonso-Pecchio A, et al. Induction of neuron-specific degradation of coenzyme A models pantothenate kinase-associated neurodegeneration by reducing motor coordination in mice. PLoS One. 2015;10(6):e0130013.

Song MG, Bail S, Kiledjian M. Multiple nudix family proteins possess mRNA decapping activity. RNA. 2013;19(3):390-399.

Sriskanda V, Moyer RW, Shuman S. NAD+-dependent DNA ligase encoded by a eukaryotic virus. J Biol Chem. 2001;276(39):36100-36109.

Sriskanda V, Shuman S. A second NAD(+)-dependent DNA ligase (LigB) in escherichia coli. Nucleic Acids Res. 2001;29(24):4930-4934.

Srouji JR, Xu A, Park A, Kirsch JF, Brenner SE. The evolution of function within the nudix homology clan. Proteins. 2017;85(5):775-811.

Tabor S. DNA ligases. Curr Protoc Mol Biol. 2001;Chapter 3:Unit3.14.

Taniguchi M, Hayashi T, Nii M, et al. Fine mapping of quantitative trait loci for meat color on sus scrofa chromosome 6: Analysis of the swine NUDT7 gene. J Anim Sci. 2010;88(1):23-31.

Taylor MJ, Peculis BA. Evolutionary conservation supports ancient origin for Nudt16, a nuclear-localized, RNA-binding, RNA-decapping enzyme. Nucleic Acids Res. 2008;36(18):6021-6034.

Topisirovic I, Svitkin YV, Sonenberg N, Shatkin AJ. Cap and cap-binding proteins in the control of gene expression. Wiley Interdiscip Rev RNA. 2011;2(2):277-298.

Toth B, Iordanov I, Csanady L. Ruling out pyridine dinucleotides as true TRPM2 channel activators reveals novel direct agonist ADP-ribose-2'-phosphate. J Gen Physiol. 2015;145(5):419-430.

Trapp J, Jung M. The role of NAD+ dependent histone deacetylases (sirtuins) in ageing. Curr Drug Targets. 2006;7(11):1553-1560.

Tsukiji S, Pattnaik SB, Suga H. Reduction of an aldehyde by a NADH/Zn2+ -dependent redox active ribozyme. J Am Chem Soc. 2004;126(16):5044-5045.

Tsukiji S, Pattnaik SB, Suga H. An alcohol dehydrogenase ribozyme. Nat Struct Biol. 2003;10(9):713-717.

Valkov E, Muthukumar S, Chang CT, Jonas S, Weichenrieder O, Izaurralde E. Structure of the Dcp2-Dcp1 mRNA-decapping complex in the activated conformation. Nat Struct Mol Biol. 2016;23(6):574-579.

van Dijk E, Cougot N, Meyer S, Babajko S, Wahle E, Seraphin B. Human Dcp2: A catalytically active mRNA decapping enzyme located in specific cytoplasmic structures. EMBO J. 2002;21(24):6915-6924.

van Nues RW, Castro-Roa D, Yuzenkova Y, Zenkin N. Ribonucleoprotein particles of bacterial small non-coding RNA IsrA (IS61 or McaS) and its interaction with RNA polymerase core may link transcription to mRNA fate. Nucleic Acids Res. 2016;44(6):2577-2592.

Vasilyev N, Serganov A. Structures of RNA complexes with the escherichia coli RNA pyrophosphohydrolase RppH unveil the basis for specific 5'-end-dependent mRNA decay. J Biol Chem. 2015;290(15):9487-9499.

Verdin E. NAD(+) in aging, metabolism, and neurodegeneration. Science. 2015;350(6265):1208-1213.

Vvedenskaya IO, Bird JG, Zhang Y, et al. CapZyme-seq comprehensively defines promoter-sequence determinants for RNA 5' capping with NAD. Mol Cell. 2018;70(3):553-564.e9.

Wang L, Fu TM, Zhou Y, Xia S, Greka A, Wu H. Structures and gating mechanism of human TRPM2. Science. 2018;362(6421):10.1126/science.aav4809. Epub 2018 Nov 22.

Wang Y, Li S, Zhao Y, et al. NAD(+)-capped RNAs are widespread in the arabidopsis transcriptome and can probably be translated. Proc Natl Acad Sci U S A. 2019;116(24):12094-12102.

Wang Z, Jiao X, Carr-Schmid A, Kiledjian M. The hDcp2 protein is a mammalian mRNA decapping enzyme. Proc Natl Acad Sci U S A. 2002;99(20):12663-12668.

Weinberg Z, Lunse CE, Corbino KA, et al. Detection of 224 candidate structured RNAs by comparative analysis of specific subsets of intergenic regions. Nucleic Acids Res. 2017;45(18):10811-10823.

White MR, Garcin ED. The sweet side of RNA regulation: Glyceraldehyde-3-phosphate dehydrogenase as a noncanonical RNA-binding protein. Wiley Interdiscip Rev RNA. 2016;7(1):53-70.

White MR, Khan MM, Deredge D, et al. A dimer interface mutation in glyceraldehyde 3-phosphate dehydrogenase regulates its binding to AU-rich RNA. J Biol Chem. 2015;290(7):4129.

Wilkinson A, Day J, Bowater R. Bacterial DNA ligases. Mol Microbiol. 2001;40(6):1241-1248.

Wilson TJ, Lilley DM. RNA catalysis--is that it? RNA. 2015;21(4):534-537.

Wilton DC. The mechanism of adduct formation between NAD+ and pyruvate bound to pig heart lactate dehydrogenase. Biochem J. 1979;177(3):951-957.

Winz ML, Cahova H, Nubel G, Frindert J, Hofer K, Jaschke A. Capture and sequencing of NAD-capped RNA sequences with NAD captureSeq. Nat Protoc. 2017;12(1):122-149.

Xiao W, Wang RS, Handy DE, Loscalzo J. NADH and NADPH redox couples and cellular energy metabolism. Antioxid Redox Signal. 2018;28(3):251-272.

Xu A, Desai AM, Brenner SE, Kirsch JF. A continuous fluorescence assay for the characterization of nudix hydrolases. Anal Biochem. 2013;437(2):178-184.

Xu W, Dunn CA, Bessman MJ. Cloning and characterization of the NADH pyrophosphatases from caenorhabditis elegans and saccharomyces cerevisiae, members of a nudix hydrolase subfamily. Biochem Biophys Res Commun. 2000;273(2):753-758.

Xu W, Dunn CA, O'handley SF, Smith DL, Bessman MJ. Three new nudix hydrolases from escherichia coli. J Biol Chem. 2006;281(32):22794-22798.

Xu W, Gauss P, Shen J, Dunn CA, Bessman MJ. The gene e.1 (nudE.1) of T4 bacteriophage designates a new member of the nudix hydrolase superfamily active on flavin adenine dinucleotide, adenosine 5'-triphospho-5'-adenosine, and ADP-ribose. J Biol Chem. 2002;277(26):23181-23185.

Yoon B, Yang EG, Kim SY. The ADP-ribose reactive NUDIX hydrolase isoforms can modulate HIF-1alpha in cancer cells. Biochem Biophys Res Commun. 2018;504(1):321-327.

Yoon B, Yang EG, Kim SY. The ADP-ribose reactive NUDIX hydrolase isoforms can modulate HIF-1alpha in cancer cells. Biochem Biophys Res Commun. 2018;504(1):321-327.

Yoshimura K, Shigeoka S. Versatile physiological functions of the nudix hydrolase family in arabidopsis. Biosci Biotechnol Biochem. 2015;79(3):354-366.

Yoshino J, Baur JA, Imai SI. NAD(+) intermediates: The biology and therapeutic potential of NMN and NR. Cell Metab. 2018;27(3):513-528.

Yu P, Xue X, Zhang J, et al. Identification of the ADPR binding pocket in the NUDT9 homology domain of TRPM2. J Gen Physiol. 2017;149(2):219-235.

Zewe V, Fromm HJ. Kinetic studies of rabbit muscle lactate dehydrogenase. J Biol Chem. 1962;237:1668-1675.

Zhang D, Liu Y, Wang Q, et al. Structural basis of prokaryotic NAD-RNA decapping by NudC. Cell Res. 2016;26(9):1062-1066.

Zhang Y, Zbornikova E, Rejman D, Gerdes K. Novel (p)ppGpp binding and metabolizing proteins of escherichia coli. MBio. 2018;9(2):10.1128/mBio.02188-17.

Ziemniak M, Mugridge JS, Kowalska J, Rhoads RE, Gross JD, Jemielity J. Two-headed tetraphosphate cap analogs are inhibitors of the Dcp1/2 RNA decapping complex. RNA. 2016;22(4):518-529.

Curriculum Vitae

Atreyei Ray, B Tech (Biotechnology), PhD (Biochemistry)

SUMMARY

PhD trained in molecular biology and biochemistry with ability to work independently or as part of a team, and with strong interpersonal and communication skills. Areas of interest include:

- Molecular cloning
- Protein purification
- Designing novel enzyme kinetic assays
- Analytical techniques such as LC-MS, HPLC

EDUCATION

University of Wisconsin-Milwaukee Milwaukee, WI
Ph.D., Biochemistry **2014-2019**
Supervised by Dr. David N. Frick, Due for submission December 2019

Heritage Institute of Technology Kolkata, India
B. Tech, Biotechnology **2010-2014**

RESEARCH EXPERIENCE

University of Wisconsin-Milwaukee

- Developed expression system for bacterial and human Nudix proteins
- Designed novel fluorescence-based assay to study enzyme kinetics
- Experience with analytical techniques such as HPLC, LC-MS
- Experience with *in vitro* transcription of non-canonical initiating nucleotide RNA (ncinRNA)
- Experience with studying novel protein:nucleic acid interactions using both biology technique and fluorescence
- Research centered on a never studied before biochemical role of ncinRNAs

Heritage Institute of Technology

- Designed experiments for the commercialization of the protein, dextranase in the use against dental plaque
- Identified novel method from *Tinospora cordifolia*
- Experience with DNSA (3,5-dinitrosalicylic acid) assays to investigate enzymatic activity

TECHNICAL SKILLS

Molecular biology techniques: Plasmid DNA Isolation, PCR, Gel Electrophoresis, Molecular cloning, Protein expression and purification, *in vitro* RNA transcription

Immunological techniques: Western Blotting, ELISA, Flow cytometry

Analytical techniques: High Pressure Liquid Chromatography (HPLC), Liquid Chromatography-Mass Spectrometry (LC-MS), Gas Chromatography (GC), Inductively coupled plasma mass spectrometry (ICP-MS), Fluorescence Spectroscopy, Fluorescence Polarization assays, Colorimetric assays

---

LEADERSHIP EXPERIENCE

Graduate Teaching Assistant **2014-2019**

- Prepared lectures and classroom activities for undergraduate (CHM 100, 101, 102, 103, 104) and graduate (CHM 603) level courses
- Used active learning techniques as part of classroom discussions
- Designed laboratory experiments for students to conceptualize classroom material
- Mentored undergraduate students in the lab

Lab Safety Officer **2014-2019**

- Enforced safety protocols for undergraduates and graduates working in the lab
- Maintained MSDS for chemicals stored in the lab
- Fostered safe working environment for lab users

ACADEMIC AWARDS

Best Undergraduate Poster Award **2014**
UWM Chancellor's Graduate Student Award **2014-2019**

PUBLICATIONS AND CONFERENCE PRESENTATIONS

Cloning and Purification of E. coli and Human Nudix hydrolases NudC and NUDT12 in a bacterial expression system, *Midwest Enzyme Chemistry Conference 2016*

The E. coli and Human Nudix hydrolases NudC and NUDT12 cleave damaged NADH, *The FASEB Journal, Volume 31, Apr 2017*

New assays to analyze the thermodynamics of RNA binding to enzymes that remove RNA caps, *Midwest Enzyme Chemistry Conference 2018*

The human nudix hydrolase NudT12 specifically binds RNA and remove 5'-NAD(H) caps, *LXXXXIV Cold Spring Harbor Lab 84th Symposium: RNA Control & Regulation 2019*

Energetics of the human Nudix protein interaction with nucleic acids: The Nudt12 protein preferentially binds the NAD^+-capped RNA, *Manuscript in preparation*